

# Characterization of Urbix Resources Natural Flake Graphite Material for Nuclear Applications



Austin Schumacher  
Michael Trammell  
Thomas Watkins  
Artem Trofimov  
Hsin Wang

**CRADA Final Report**

**February 2020**

Approved for public release.

## DOCUMENT AVAILABILITY

Reports produced after January 1, 1996, are generally available free via US Department of Energy (DOE) SciTech Connect.

**Website** [www.osti.gov](http://www.osti.gov)

Reports produced before January 1, 1996, may be purchased by members of the public from the following source:

National Technical Information Service  
5285 Port Royal Road  
Springfield, VA 22161  
**Telephone** 703-605-6000 (1-800-553-6847)  
**TDD** 703-487-4639  
**Fax** 703-605-6900  
**E-mail** [info@ntis.gov](mailto:info@ntis.gov)  
**Website** <http://classic.ntis.gov/>

Reports are available to DOE employees, DOE contractors, Energy Technology Data Exchange representatives, and International Nuclear Information System representatives from the following source:

Office of Scientific and Technical Information  
PO Box 62  
Oak Ridge, TN 37831  
**Telephone** 865-576-8401  
**Fax** 865-576-5728  
**E-mail** [reports@osti.gov](mailto:reports@osti.gov)  
**Website** <http://www.osti.gov/contact.html>

This report was prepared as an account of work sponsored by an agency of the United States Government. Neither the United States Government nor any agency thereof, nor any of their employees, makes any warranty, express or implied, or assumes any legal liability or responsibility for the accuracy, completeness, or usefulness of any information, apparatus, product, or process disclosed, or represents that its use would not infringe privately owned rights. Reference herein to any specific commercial product, process, or service by trade name, trademark, manufacturer, or otherwise, does not necessarily constitute or imply its endorsement, recommendation, or favoring by the United States Government or any agency thereof. The views and opinions of authors expressed herein do not necessarily state or reflect those of the United States Government or any agency thereof.

**ORNL/SPR-2020/1436  
CRADA/NFE-18-07340**

Reactor & Nuclear Systems Division

Gateway for Accelerated Innovation in Nuclear (GAIN) Program

**Characterization of Urbix Resources Natural Flake Graphite  
Material for Nuclear Applications**

Austin Schumacher  
Michael Trammell  
Thomas Watkins  
Artem Trofimov  
Hsin Wang

Date Published: February 19, 2020

Prepared by  
OAK RIDGE NATIONAL LABORATORY  
Oak Ridge, TN 37831-6283  
managed by  
UT-BATTELLE, LLC  
for the  
US DEPARTMENT OF ENERGY  
under contract DE-AC05-00OR22725

## TABLE OF CONTENTS

TABLE OF CONTENTS .....	ii
LIST OF FIGURES .....	iii
LIST OF TABLES .....	vi
ACRONYMS .....	vii
ACKNOWLEDGEMENTS .....	vii
EXECUTIVE SUMMARY .....	1
STATEMENT OF OBJECTIVES .....	1
BENEFIT TO THE FUNDING DOE OFFICE’S MISSION .....	2
TECHNICAL DISCUSSION .....	2
1. Graphite Feedstock Characterization and Heat Treatment .....	2
1.1 Powder Treatment .....	2
1.2 Scanning Electron Microscopy .....	3
1.3 Glow Discharge Mass Spectroscopy .....	3
1.4 Tap Density .....	5
1.5 Compressibility Testing .....	6
1.6 Strength After Compaction .....	7
1.7 X-Ray Diffraction .....	8
1.8 Particle Size Distribution .....	10
1.9 Surface Area Analysis .....	11
2. Fuel Body Fabrication and Characterization .....	11
2.1 Resinated Graphite Production .....	11
2.2 Resinated Graphite Compaction .....	12
2.3 Heat Treatment of Fuel Bodies .....	14
2.4 Ultimate Compressive Strength .....	14
2.5 Density and Porosity Measurements .....	15
2.6 Coefficient of Thermal Expansion .....	16
2.7 Thermal Conductivity .....	17
3. Conclusions .....	21
REFERENCES .....	22
APPENDIX A .....	A-1

## LIST OF FIGURES

Figure 1. Glow discharge mass spectroscopy results for URBIX-NHT, URBIX-HT, and Asbury 13371. Elements with concentrations below the detectable limit for GDMS are not included.....	4
Figure 2. Shows the initial and final tap density results averaged over three tests for each graphite lot tested. ....	5
Figure 3. Relationship between uniaxial compression pressure and density for Urbix and Asbury graphite powders (note that the y-axis starts at 1.75 g/cm <sup>3</sup> ). ....	7
Figure 4. Average compressive strength of each graphite compact formed at four different uniaxial compression pressures.....	8
Figure 5. Cross section of a graphite puck (a), and cross section of a puck face (b). ....	10
Figure 6. Density for each compact and the peak compaction force used to obtain that density value.....	12
Figure 7. Uniaxially pressed graphite matrix compacts created using milled Urbix powder. ....	13
Figure 8. A polymer mold used to densify graphite matrix specimens in an isostatic press. ....	13
Figure 9. Graphite matrix rods formed by isostatic pressing. Testing specimens were machined from these rods for use in characterizing isostatically pressed Urbix matrix. ....	13
Figure 10. Percent of dimensional change for Urbix and AGR compacts resulting from heat treatment. ....	14
Figure 11. Ultimate compressive strength of several graphite matrix compacts created using two types of natural graphite powders and two compaction methods (Urbix and Asbury 13371). ....	15
Figure 12. T <sub>α</sub> values for each type of graphite compact calculated as a function of temperature. ....	17
Figure 13. Specific heat capacities of AGR and Urbix matrix compacts as a function of temperature. ....	18
Figure 14. Relationship between thermal diffusivity and temperature for Urbix (uniaxially and isostatically pressed) and AGR compacts. ....	19
Figure 15. Variation in thermal conductivity over a range of temperatures for three graphite matrix recipes.....	20
Figure 16. SEM images of the as-received Urbix graphite powder. ....	A-1
Figure 17. SEM images of the as-received Urbix graphite powder. ....	A-2
Figure 18. SEM images of the as-received Urbix graphite powder. ....	A-3
Figure 19. SEM images of the as-received Urbix graphite powder. ....	A-4
Figure 20. SEM images of heat-treated Urbix graphite powder. ....	A-5
Figure 21. SEM images of heat-treated Urbix graphite powder. ....	A-6
Figure 22. SEM images of heat-treated Urbix graphite powder. ....	A-7
Figure 23. SEM images of heat-treated Urbix graphite powder. ....	A-8
Figure 24. SEM images of Asbury 13371 natural graphite powder.....	A-9
Figure 25. SEM images of Asbury 13371 natural graphite powder.....	A-10
Figure 26. SEM images of Asbury 13371 natural graphite powder.....	A-11
Figure 27. SEM images of Asbury 13371 natural graphite powder.....	A-12
Figure 28. X-ray diffraction patterns of the NIST SRM 640c silicon powder. The small peak at ~26° 2θ is the (111) Si Cu kβ reflection. ....	A-21
Figure 29. The FWHMs from Figure 28 as a function of Bragg Angle for the NIST SRM 640c silicon powder. The fitted curve used for instrumental broadening correction is shown. ....	A-21
Figure 30. X-ray diffraction pattern of Carbowax resin. ....	A-22

Figure 31. X-ray diffraction pattern of the cross section of the URBIX-HT#1 puck showing the presence of both hexagonal and rhombohedral graphite. Peaks 1–5 originate from the 5 wt% Carbowax resin. ....	A-22
Figure 32. X-ray diffraction pattern of the cross section of the URBIX-NHT#1 puck showing the presence of both hexagonal and rhombohedral graphite. Peaks 1–5 originate from the 5 wt% Carbowax resin. Sharp peaks 6 and 7 likely originate from a contaminant phase from either the cross sectioning process or picked up in the XRD lab. ....	A-22
Figure 33. X-ray diffraction pattern of the cross section of the Asbury 1 puck showing the presence of both hexagonal and rhombohedral graphite. Peaks 1–5 originate from the 5 wt% Carbowax resin. ....	A-23
Figure 34. X-ray diffraction pattern of the puck face of the URBIX-HT#1 puck showing the presence of both hexagonal and rhombohedral graphite. Peaks —5 are the graphite H(002)/R(111) reflection from $WL\gamma_1$ , $WL\beta_2$ , $WL\beta_1$ , $CuK\beta$ , and $WL\alpha_2$ radiation, respectively. Peak 6 is the graphite H(004)/R(222) reflection from $CuK\beta$ radiation. Peak 7 is presumed to originate from the 5 wt% Carbowax resin. ....	A-23
Figure 35. X-ray diffraction pattern of the puck face of the URBIX-NHT#1 puck showing the presence of both hexagonal and rhombohedral graphite. Peaks 1–5 are the graphite H(002)/R(111) reflection from $WL\gamma_1$ , $WL\beta_2$ , $WL\beta_1$ , $CuK\beta$ , and $WL\alpha_2$ radiation, respectively. The feature at 6 is due to the absorption edge of the Ni filter. Peak 7 is unidentified. Peak 8 is the graphite H(004)/R(222) reflection from $CuK\beta$ radiation. Peak 9 is presumed to originate from the 5 wt% Carbowax resin. ....	A-24
Figure 36. X-ray diffraction pattern of the puck face of the Asbury 1 puck showing the presence of both hexagonal and rhombohedral graphite. Peaks 1–5 are the graphite H(002)/R(111) reflection from $WL\gamma_1$ , $WL\beta_2$ , $WL\beta_1$ , $CuK\beta$ , and $WL\alpha_2$ radiation, respectively. Peak 6 is the graphite H(004)/R(222) reflection from $CuK\beta$ radiation. Peak 7 is presumed to originate from the 5 wt% Carbowax resin. ....	A-24
Figure 37. Particle size distribution results for the as-received Urbix graphite powder. ....	A-27
Figure 38. Particle size distribution results for the heat-treated Urbix graphite powder. ....	A-28
Figure 39. Particle size distribution results for Asbury 13371 graphite powder. ....	A-29
Figure 40. Particle size distribution results for the milled Urbix graphite powder. ....	A-30
Figure 41. Surface area analysis results for the as-received Urbix graphite powder. ....	A-31
Figure 42. Surface area analysis results for the heat-treated Urbix graphite powder. ....	A-32
Figure 43. Surface area analysis results for Asbury 13371 graphite powder. ....	A-33
Figure 44. Helium pycnometry test results for uniaxially pressed graphite matrix created using Urbix powder. ....	A-35
Figure 45. Helium pycnometry test results for graphite matrix created using the AGR blend of materials (using Asbury powder). ....	A-36
Figure 46. Helium pycnometry test results for isostatically pressed graphite matrix created using Urbix powder. ....	A-37
Figure 47. Results from tungsten verification run for coefficient of thermal expansion testing. ....	A-38
Figure 48. Plots from Runs 1 (top) and 2 (bottom) of Sample 1, a uniaxially pressed Urbix matrix compact, showing the relationship between temperature and specific heat capacity. ....	A-42
Figure 49. Plots from Runs 1 (top) and 2 (bottom) of Sample 2, a uniaxially pressed Urbix matrix compact, showing the relationship between temperature and specific heat capacity. ....	A-43
Figure 50. Plots from Runs 1 (top) and 2 (bottom) of Sample 1, a compact made using the AGR blend of materials for graphite matrix, showing the relationship between temperature and specific heat capacity. ....	A-44
Figure 51. Plots from Runs 1 (top) and 2 (bottom) of Sample 2 for a compact made using the AGR blend of materials for graphite matrix showing the relationship between temperature and specific heat capacity. ....	A-45

Figure 52. Plots from Samples 1 (top) and 2 (bottom) for an isostatically pressed Urbix matrix compact showing the relationship between temperature and specific heat capacity. .... A-46

## LIST OF TABLES

Table 1. Summary of particle size analysis results from laser diffraction testing four separate graphite powder lots.....	11
Table 2. A table of the results found by way of performing helium pycnometry tests on two different graphite matrix compacts .....	16
Table 3. Glow discharge mass spectroscopy results for the as-received Urbix graphite powder .....	A-13
Table 4. Glow discharge mass spectroscopy results for the heat-treated Urbix graphite powder .....	A-14
Table 5. Glow discharge mass spectroscopy results for Asbury 13371 graphite powder.....	A-15
Table 6. Tap density results for Urbix and Asbury 13371 graphite powders are shown. The initial unpacked density and the final tapped density are recorded. Each set of testing conditions was performed three times.....	A-16
Table 7. The density of graphite powders compacted at 12,500 and 25,000 psi .....	A-17
Table 8. Density of graphite powders compacted at 37,500 and 50,000 psi.....	A-18
Table 9. Ultimate compressive strength of as-received Urbix powder pressed at four different pressures and tested three times for each pressure.....	A-19
Table 10. Ultimate compressive strength of heat-treated Urbix powder pressed at four different pressures and tested three times for each pressure.....	A-19
Table 11. Ultimate compressive strength of milled Urbix powder pressed at four different pressures and tested three times for each pressure.....	A-20
Table 12. Ultimate compressive strength of Asbury 13371 powder pressed at four different pressures and tested three times for each pressure.....	A-20
Table 13. Crystallite sizes for various reflections present in the URBIX-HT#1 sample .....	A-25
Table 14. Crystallite sizes for various reflections present in the URBIX-NHT#1 sample .....	A-25
Table 15. Crystallite sizes for various reflections present in the Asbury 1 sample .....	A-26
Table 16. Results from ultimate compressive strength testing of all graphite matrix compacts.....	A-34
Table 17. Relationship between temperature and mean coefficient of thermal expansion ( $T.\alpha$ ) for the three types of graphite matrix compacts measured at 50 °C increments .....	A-39
Table 18. Relationship between temperature and instantaneous coefficient of thermal expansion ( $\alpha$ ) for the three types of graphite matrix compacts measured at 50 °C increments .....	A-40
Table 19. Specific heat capacity for all of the graphite compact samples at 50 °C increments up to 950 °C; measurements taken within 0.1 °C of the stated temperature.....	A-41
Table 20. Thermal diffusivity results for three uniaxially pressed Urbix matrix specimens; thermal diffusivity was measured three times at each given temperature for each specimen, and temperature and diffusivity results shown are averages of those three readings.....	A-47
Table 21. Thermal diffusivity results for three uniaxially pressed AGR matrix specimens; thermal diffusivity was measured three times at each given temperature for each specimen, and temperature and diffusivity results shown are averages of those three readings .....	A-48
Table 22. Thermal diffusivity results for two isostatically pressed Urbix matrix specimens; thermal diffusivity was measured three times at each given temperature for each specimen, and temperature and diffusivity results shown are averages of those three readings.....	A-49
Table 23. Values used to calculate thermal conductivity for each type of graphite matrix used in this study (Diffusivity was measured on the average temperature shown; values for heat capacity and CTE were measured to the nearest temperature reading (typically within 0.1 °C of the temperature listed.).....	A-50

## ACRONYMS

AGR	Advanced Gas-cooled Reactor
ASTM	American Society for Testing and Materials
BET	Brunauer-Emmett-Teller
CRADA	Cooperative Research and Development Agreement
CTE	Coefficient of Thermal Expansion
DOE	US Department of Energy
EBC	Equivalent Boron Content
FWHM	Full Width Half Maximum
HTGR	High-Temperature Graphite Reactor
ICDD	International Centre for Diffraction Data
ISO	International Organization for Standardization
LFA	Laser Flash Apparatus
MIL	milled
NHT	not heat treated
NIST	National Institute of Standards and Technology
ORNL	Oak Ridge National Laboratory
SEM	Scanning Electron Microscopy
SRM	Standard Reference Material
URBIX-ISO	isostatically pressed Urbix specimen
URBIX-UNI	uniaxially pressed Urbix specimen
XRD	X-Ray Diffraction

## ACKNOWLEDGEMENTS

This work was sponsored by the U.S. Department of Energy, Office of Nuclear Energy, through the Gateway for Accelerated Innovation in Nuclear (GAIN) Voucher program.

## EXECUTIVE SUMMARY

Urbix Resources is a company specializing in graphite powder processing and purification. Urbix is looking to become the first domestic supplier of nuclear-grade graphite in the United States. This has led to a Cooperative Research and Development Agreement (CRADA) being established between the Oak Ridge National Laboratory (ORNL) and Urbix Resources, with the goal of characterizing a purified graphite feedstock supplied by Urbix Resources. The resulting data will then be used to determine the viability of a large-scale nuclear graphite production and qualification campaign. These characterization methods have been performed on the as-received graphite feedstock, a heat-treated batch of the feedstock, a milled batch of the feedstock, and a nuclear-grade graphite powder historically used in fuel production. The data from the heat-treated and milled feedstock will determine how different processing methods affect the powder's physical properties, whereas the data from the nuclear grade graphite will provide information about the characteristics of a graphite previously accepted for nuclear applications. All of these powders have been characterized individually and as part of a resin-graphite blend (herein referred to as *matrix*) that has been used in past fuel experiments. The results of these experiments show that the Urbix powder and nuclear-grade graphite powder display notably different properties from one another in many cases, but this discrepancy may have been the result of the typical particle size of each powder. This hypothesis is supported by tests conducted on the milled powder, which showed a closer resemblance in properties to the nuclear-grade graphite than the as-received powder. The method for pressing the graphite matrix also had a noticeable effect on the measured properties.

## STATEMENT OF OBJECTIVES

The primary objective of the project was to conduct a series of graphite-specific processing and characterization tests to aid in the potential launch of a domestic supplier of graphite feedstock materials for high-temperature graphite reactors (HTGRs). In support of this objective, a series of experiments was conducted, including raw material characterization, post-heat-treatment characterization, fabrication of resinated graphite material (i.e., *matrix*), consolidation of matrix into relative fuel body geometries, and characterization of the resulting fuel bodies.

## **BENEFIT TO THE FUNDING DOE OFFICE'S MISSION**

The US Department of Energy (DOE) has long been involved in the development, demonstration, qualification, and licensing of HTGRs for domestic nuclear power production [1]. These reactors rely on structural graphite and graphite feedstock powder to produce fuel forms. The proliferation of graphite reactors depends heavily on a readily available and growing supply of feedstock material to produce these components. Specifically, natural flake graphite is crucial for the design, fabrication, and performance of the fuel bodies for HTGR designs such as the Advanced Gas-Cooled Reactor (AGR) concept [2]. The fuel developed for this program consisted of tristructural isotropic coated fuel particles embedded in graphite matrix. The graphite matrix consisted of a combination of natural and synthetic graphite mixed with a carbon-producing resin binder that held the fuel particles together to create a solid fuel body [3].

Currently there is no domestic nuclear graphite supplier available in the United States providing these materials. Urbix intends to fill this need by offering a new nuclear-grade graphite powder feedstock to be manufactured in the United States to produce nuclear graphite and graphite-based fuel forms for nuclear applications. This goal requires a long series of activities involving graphite powder processing, purification, consolidation into billets, characterization, and data generation from neutron irradiation testing and post-irradiation examination. Under this project, purified natural flake graphite powder was received and characterized, and representative fuel forms were fabricated and tested for properties determination. This detailed report on the processing and analysis was generated to provide Urbix access to valuable information to help them assess the viability of launching a large nuclear graphite production and qualification project. This effort is intended to support Urbix in the endeavor to become a domestic supplier of this strategic material.

## **TECHNICAL DISCUSSION**

### **1. GRAPHITE FEEDSTOCK CHARACTERIZATION AND HEAT TREATMENT**

#### **1.1 POWDER TREATMENT**

Natural flake graphite powder was received from Urbix for characterization and analysis. This material (batch pBM3B-DOE) was purified by Urbix using a propriety process. Once the material was received at ORNL, it was separated into three equal lots for further characterization and processing. The first lot remained as received for baseline characterization, the second lot was designated for an additional high-temperature heat treatment purification process, and the third lot remained as received but was milled to a finer particle size. These methods for treating the powder were used to determine how heat treatment and milling affect the physical properties of the as-received graphite. Asbury 13371 graphite powder was characterized alongside the three Urbix powder lots as a reference material that has been used in past fuel experiments [4], but it was only characterized in its as-received condition, as that is how it was traditionally used for matrix production. Characterization included morphology analysis by scanning electron microscopy (SEM), impurities determination, tap density analysis, compressibility analysis to determine the bonding strength of the flake graphite without binder, crystallinity analysis by x-ray diffraction (XRD), particle size analysis, and Brunauer-Emmett-Teller (BET) surface area analysis. The results from this suite of characterization can provide insight into how the natural flake graphite material may perform in specific applications.

A 700 g lot of as-received Urbix graphite powder was weighed out and taken for heat treatment. Heat treatment of the graphite was performed by heating the material up to 1,700 °C in a flowing nitrogen environment, switching to an argon sweep environment up to 2,800 °C, and holding for approximately 20 minutes. This heat-treated lot of powder was designated *URBIX-HT* (heat treated) for testing purposes, while the as-received Urbix powder was designated *URBIX-NHT* (not heat treated).

Once the laser diffraction results were analyzed for the as-received Urbix and Asbury powders, a tremendous discrepancy between each lot's mean particle size was discovered. The graphite flakes supplied by Urbix were found to have a mean particle size of approximately 300 μm, but the Asbury 13371 measured 7 μm on average (exact measurement values are listed in Section 1.8). To discern whether particle size is a factor in other physical properties of the powders, another 700 g lot of the as-received Urbix powder was weighed out for milling to a smaller mean particle size. This lot was fed through a pulverizer twice, lowering its mean particle size to approximately 100 μm in diameter. This lot of milled powder was designated *URBIX-MIL* (milled).

## 1.2 SCANNING ELECTRON MICROSCOPY

SEM images were taken of samples from *URBIX-NHT*, *URBIX-HT*, and Asbury 13371 by EAG Laboratories to discern the varying morphologies of each powder. Double-sided carbon tape was used to hold the powders in place for imaging, and the samples were sputtered with iridium to increase their conductivity. Imaging was performed using an FEI Quanta 600 SEM at varying magnifications.

In the images produced by SEM, the *URBIX-HT* and *URBIX-NHT* powders display nearly identical morphologies between their plate-like geometries and relatively large particle size. However, both are visually distinct from the Asbury flakes, which are notably smaller, often measuring under 10 μm in diameter. All SEM images taken of these graphite powders can be found in APPENDIX A, Figure 16 through Figure 27.

## 1.3 GLOW DISCHARGE MASS SPECTROSCOPY

Glow discharge mass spectroscopy (GDMS) analysis was used to determine equivalent boron content (EBC), overall purity, and full scan impurity concentrations detected in *URBIX-NHT* and *URBIX-HT* graphite material. The goal of this analysis was to determine the effect of a high-temperature heat treatment process on the purity of the natural flake graphite. The as-received material had a purity of 99.85% and an EBC of 1.69 ppm. The high-temperature heat-treated material had a purity of 99.98% and an EBC of 1.69 ppm. The reference material, Asbury 13371, had a purity of 99.95% and an EBC of 1.74 ppm. The purity was calculated by subtracting the summation of all impurities from 100%. The estimated EBC was determined per ASTM C1233 [5] by multiplying the EBC factor of each impurity by the concentration (μg/g) of that impurity as determined by GDMS analysis. The total EBC is a summation of the EBC for all impurities in the sample. For both the purity and EBC calculations, if the values were below the detectable limit, then the value of the lower limit was used per ASTM C1233 to provide the worst-case value. It is also important to note that in both cases, the GDMS values used in these calculations were gathered from a single random sample from a large batch. Since the impurities can sometimes vary throughout a batch of materials, additional sampling would be necessary to assess a more accurate statistical average.

Impurity analysis of feedstock materials used in the production of nuclear fuel bodies is important to ensure that the final fuel element meets or exceeds the design fuel specification. Depending on the end use of the material, this specification will determine allowable limits to certain impurities. Limiting those impurities in the feedstock material reduces the risk of exceeding fuel specification limits. Since there is no fuel specification under this project, the data are simply conveyed here. However, a typical fuel specification for a fuel body may include elements such as Al, Ca, Ti, V, Cr, Mn, Fe, Co, and Ni. Figure 1 provides GDMS impurity concentrations for both URBIX-NHT (not heat treated) and URBIX-HT (heat-treated) material, along with Asbury grade 13371 as a reference. For clarity, elements with concentrations below the detectable limit for GDMS are not included. The analysis indicates that the as-received material has very low values for these elements and shows good agreement with the reference natural graphite material. However, this batch did have elevated levels of Si and Fe. Analysis of the material after the high-temperature heat treatment showed a significant decrease in nearly all detectable elements. An extended list of the GDMS results can be found in APPENDIX A, Table 3 through Table 5.

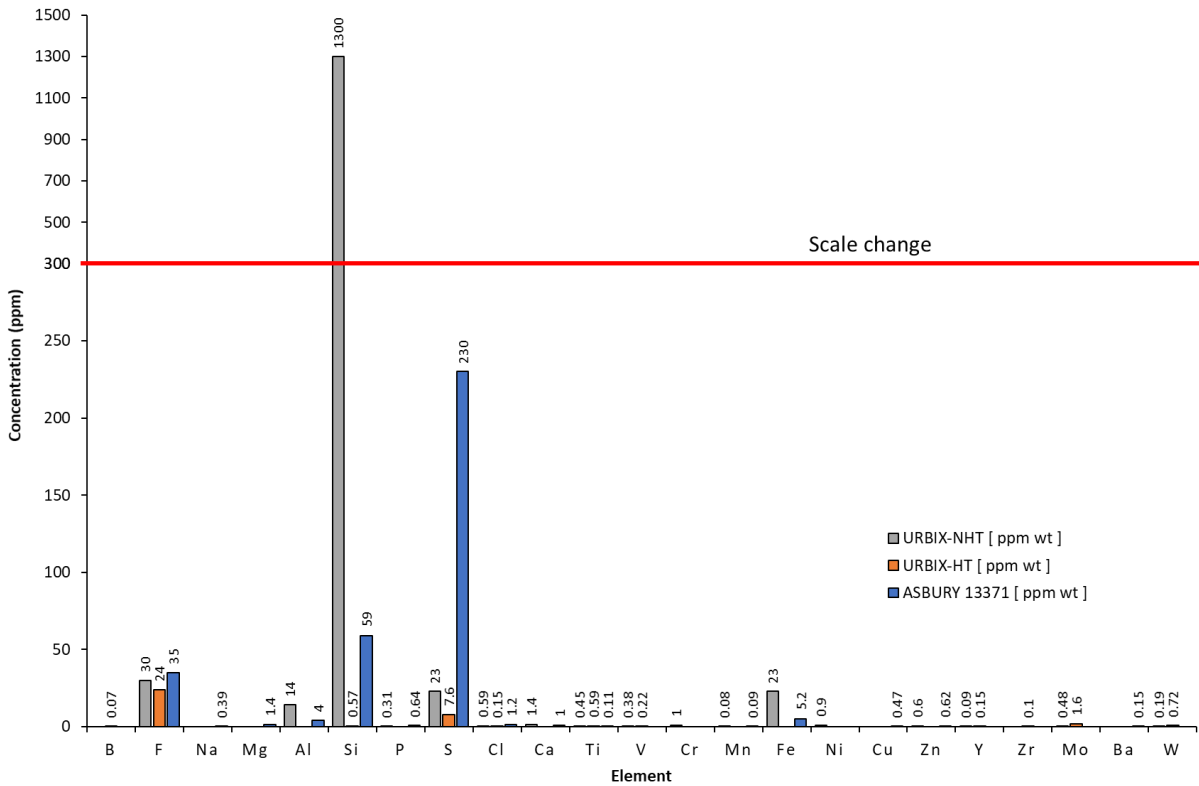


**Figure 1. Glow discharge mass spectroscopy results for URBIX-NHT, URBIX-HT, and Asbury 13371. Elements with concentrations below the detectable limit for GDMS are not included.**

## 1.4 TAP DENSITY

Tap density tests were performed on URBIX-NHT, URBIX-HT, URBIX-MIL, and Asbury 13371 to determine the packing density of each powder. All tap density tests were performed in accordance with ASTM standard D7481-18 [6]. Asbury 13371 was fed through a No. 12 sieve to break apart any agglomerates that formed, as the relatively small particle size would result in their formation. Each powder was then loaded into a 100 mL graduated cylinder up to the 100 mL mark and leveled, taking care to prevent disturbing the powder to allow for the measurement of loose bulk density. The total mass of powder was then measured by subtracting the mass of the cylinder from the mass of the cylinder loaded with powder. The graduated cylinders were then placed on the tapping apparatus for testing. All tap tests were performed on a Quantachrome Autotap and performed for a specified number of taps based on ASTM D7481-18. At each interval, the volume of the powder was measured to the nearest milliliter, and once the difference in volume from the last measurement was below 2%, the test was deemed complete. The mass of powder and final volume measurement allowed for the measurement of tapped bulk density for each powder. This test was performed three times for each powder, and the results were averaged.

The graph shown in Figure 2 displays the results for the tap density tests. Each value is averaged over the three tests performed for each powder. Each powder densified during testing to varying degrees and to notably different final densities. The as-received and heat-treated Urbix powders showed similar tap densities at  $0.879 \text{ g/cm}^3$  and  $0.913 \text{ g/cm}^3$ , respectively. However, the heat-treated powder had a consistently higher tap density in all tests. This indicates that the heat treatment likely had some effect on how the particles interact with one another. On the other hand, the Asbury powder showed a much lower tap density relative to the Urbix powders tested, measuring  $0.328 \text{ g/cm}^3$ . The smaller particle size of the Asbury powder, which is discussed in Section 1.2, is likely to be a key factor in the discrepancy between the two powders, since testing the milled Urbix powder resulted in a tap density much closer to that of the Asbury powder, measuring  $0.577 \text{ g/cm}^3$ . All measurements taken for the tap density testing can be found in APPENDIX A, Table 6.

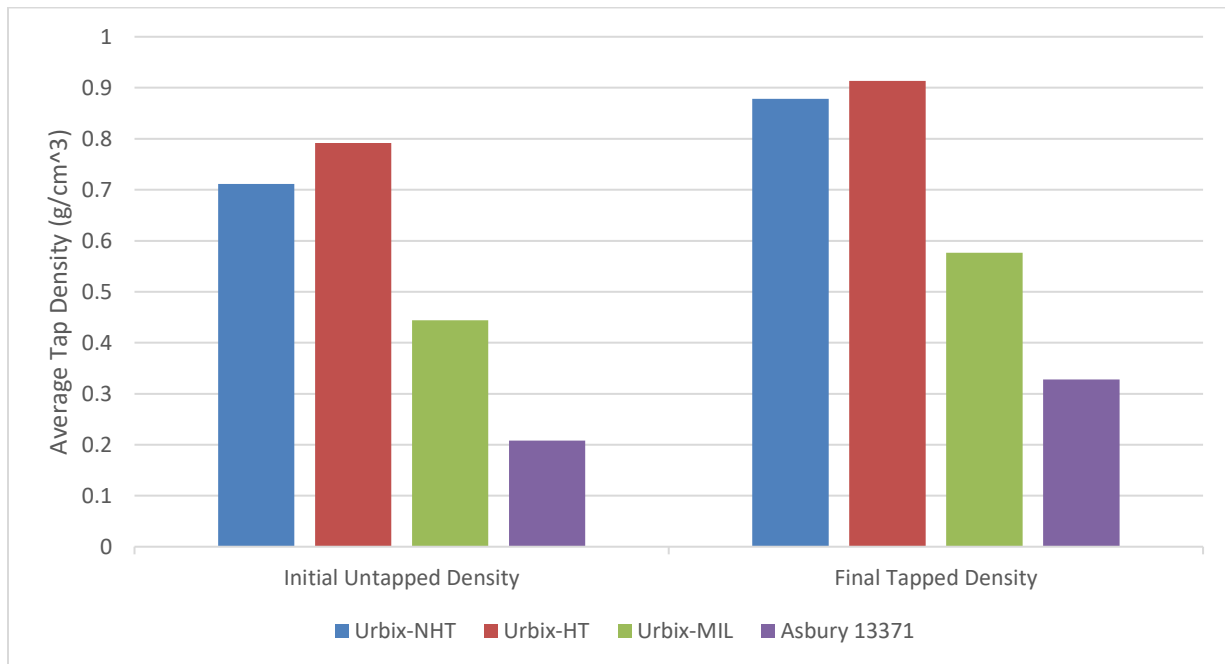


**Figure 2. Shows the initial and final tap density results averaged over three tests for each graphite lot tested.**

## 1.5 COMPRESSIBILITY TESTING

Compressibility testing was performed to determine the relationship between uniaxial compaction pressure and the resulting density of compacts composed of each graphite. Cylindrical specimens were produced in accordance with ASTM standard B331-16 [7] with one exception. Method 3 of ASTM standard B331-16 was chosen for testing, which includes pressing compacts of the material at multiple pressures. This allows for the formulation of a compressibility curve, relating compacting pressure to specimen density over a range of values. For the purposes of this test, compacting pressures of 12,500, 25,000, 37,500, and 50,000 psi were chosen. Three compacts were created for each graphite powder/pressure combination. Compacts were pressed in a D2 tool steel die with an inner diameter measuring 1.524 cm, and they were pressed to a height of  $1.000 \pm 0.010$  cm. The 25.4 mm diameter and 7.11 mm thick specimen called for in the ASTM standard could not be produced since there was not a die available with that diameter that could withstand such pressures. Pressing was performed on an automated press in accordance with ASTM standard B331-16 at constant strain rate of 0.005 up to the target load, resulting in the desired pressure. Unloading began immediately when the target load was reached and was performed at the same strain rate that was used during loading. Samples were then ejected from the die and measured to ensure that each sample met the required height tolerance. The end surface of each compact was then sanded flat to remove any surface irregularities. Final height, diameter, and mass measurements were taken to obtain the density evaluation for each compact.

A graph of the compressibility testing results can be found in Figure 3. Each point shows the density for one of three tests at each compression pressure using each powder. A polynomial line was then fit to the results to give an approximation of the trend in density as a function of compression pressure. The as-received Urbix powder was shown to compress to the highest density on average across all pressures, with the milled powder displaying similar albeit lower densities. The compression testing of the heat-treated powder resulted in the least dense compacts composed of Urbix powder. This may have been the result of graphite oxidization that occurred during heat treatment, weakening the bond between flakes due to Van der Waals forces. In fact, only one of the three compacts pressed at 12,500 psi was strong enough to hold together during the sanding process for the heat-treated powder. The Asbury compacts showed a much lower density in all tests relative to that of the Urbix compacts. An expanded table showing the results for all compressibility tests can be found in Table 7 and Table 8 of APPENDIX A.

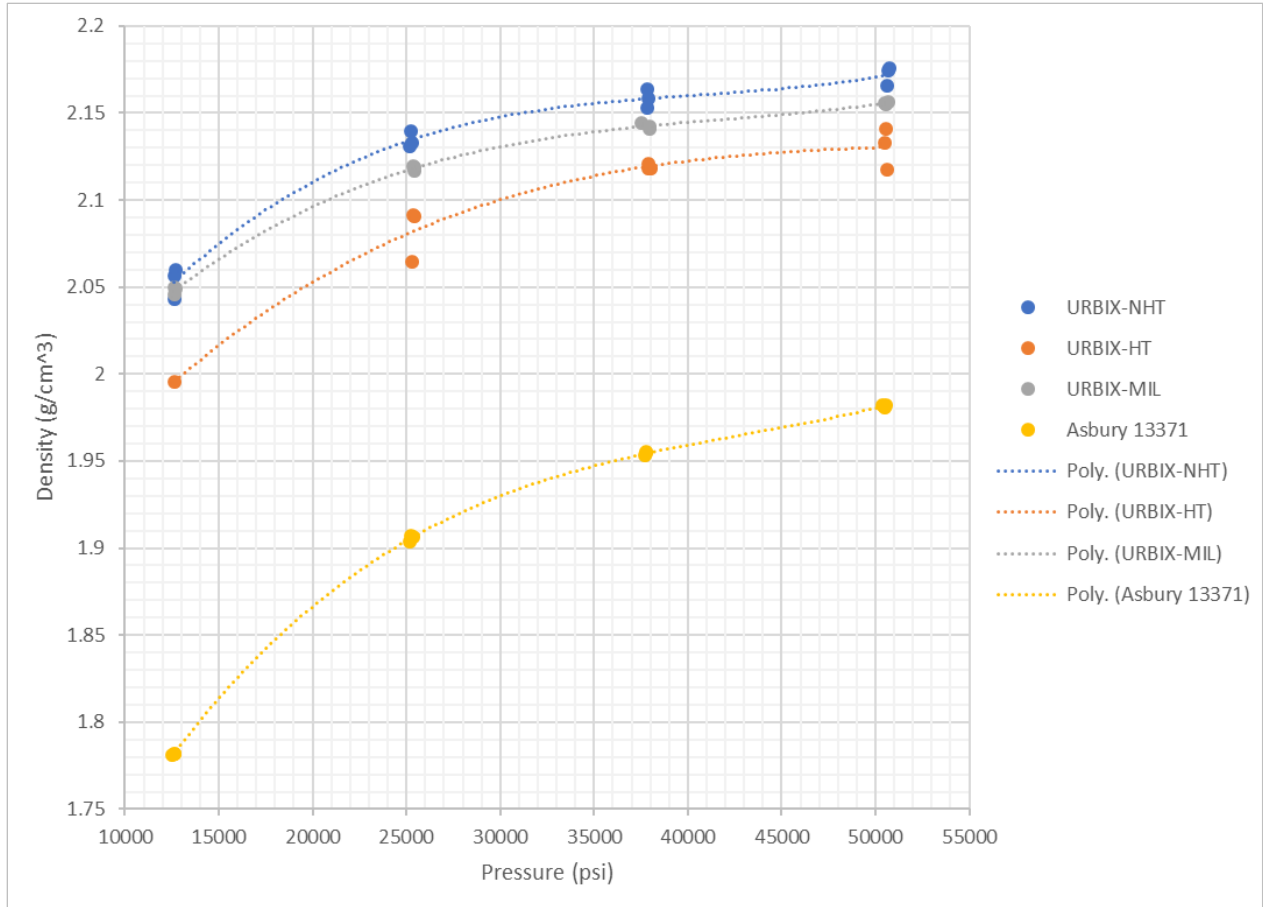


**Figure 3. Relationship between uniaxial compression pressure and density for Urbix and Asbury graphite powders (note that the y-axis starts at 1.75 g/cm<sup>3</sup>).**

## 1.6 STRENGTH AFTER COMPACTION

Compacts that were created during compressibility testing were also used to test the compressive strength of each powder at the given compression pressures. The specimens were measured and the height to diameter ratio for all specimens averaged approximately 0.63 as opposed to the 1.9 to 2.1 called for in ASTM standard C695-15 [8]. This was due to the loose packing of the graphite powders that would not allow enough powder to be loaded into the compaction die to form a compact of that geometry. The diameter for each compact was also measured to allow for stress calculations during testing. The system used for testing was a 10,000 lb electromechanical Instru-Met test frame with 4 in. outer diameter Inconel 718 platens attached to a 10 kip load cell. Testing was displacement controlled at a constant rate of 0.0003 in./s once contact was made with the specimen. Loading continued until failing occurred in the specimen. The maximum stress recorded during testing was considered the ultimate strength of the specimen. Since three compressibility specimens were produced for each given compression pressure and powder, three specimens for each condition were available for strength testing.

A graph summarizing the strength testing results can be found in Figure 4. Out of the three forms of Urbix powders tested, the milled powder was shown to have formed the strongest compacts with the lowest deviation in its results. At a compression pressure of 50 ksi, the milled Urbix compacts had an average strength of 1.798 ksi, a 23% increase in strength when compared to the average strength of compacts made using its as-received counterpart. This shows that decreasing the particle size of the

powder has a notable effect on compact strength. The compacts formed using heat-treated powder showed the lowest strength in all cases, with an average of 0.606 ksi at a compaction pressure of 50 ksi. This substantial decrease in strength could be the result of the possible oxidization effects discussed in Section 1.5. Compacts composed of Asbury powder, however, showed the overall highest compression strength, with an average ultimate strength of 2.821 ksi at the same 50 ksi compaction pressure. With the milled powder showing a marked increase in strength due to smaller flake sizes, it stands to reason that the much smaller flake size of the Asbury powder could be a significant factor in this substantial difference in strength between powders. Further testing is required to determine whether further milling of the Urbix powder would result in compacts with strengths closer to that of the Asbury composed compacts. A table of all strength testing results can be found in Table 9 through Table 12 of APPENDIX A.

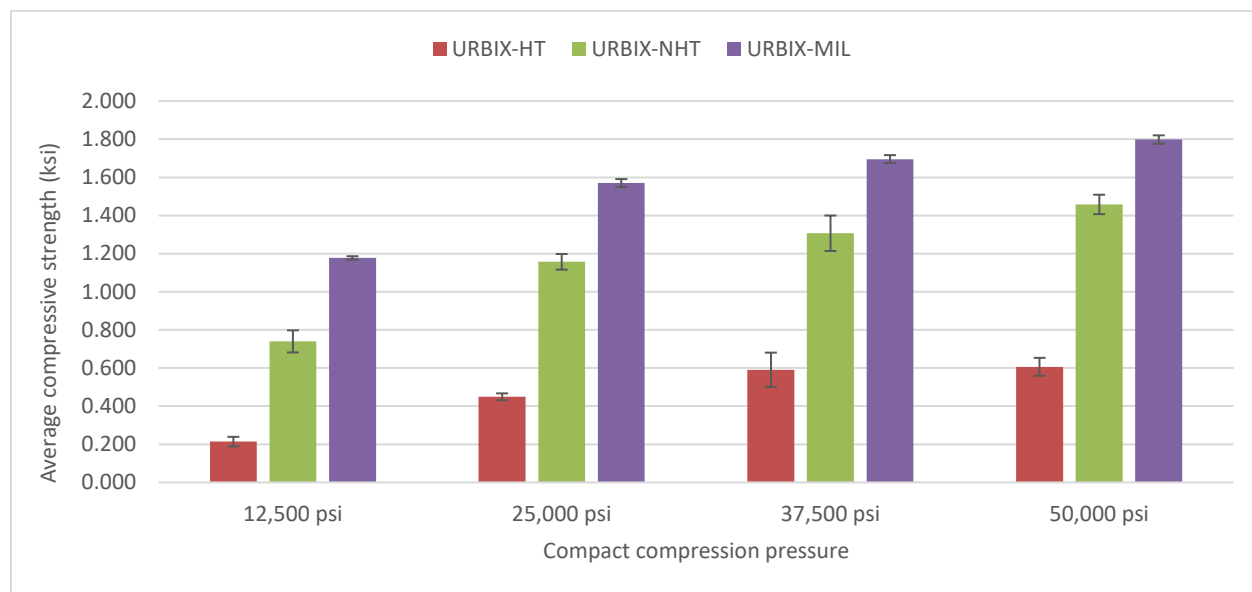


**Figure 4. Average compressive strength of each graphite compact formed at four different uniaxial compression pressures.**

## 1.7 X-RAY DIFFRACTION

XRD analysis was conducted on URBIX-HT, URBIX-NHT, and Asbury 13371. Due to the strong tendency of graphite to preferentially orient, simple powder XRD methods provided only limited data. To obtain a more random and informational XRD pattern, the three graphite powders were mixed with 5 wt% Carbowax resin as a binder and pressed into pucks  $\sim 25 \times 10$  mm (d  $\times$  t). The pucks were then cut in half and gently polished (see Figure 5). The cross section face provided a more random arrangement of the flaky graphite powders [9]. Continuous  $\Theta-2\Theta$  scans were performed on the PANalytical X'pert diffractometer from nominally 10 to 90° and 10 to 150° 2 $\Theta$  using CuK $\alpha$  radiation ( $\lambda=1.5405981$  Å), and the X'Celerator detector was used for the graphite and Carbowax samples, as well as the Si powder standard. A search match was conducted for each data set using the Jade software [10] and the International Centre for Diffraction Data (ICDD) database [11].

In general, broad XRD peaks indicate small crystallite size and/or a gradient (chemistry and stress/strain). In this work, a crystallite size analysis was performed based on the full width half maximums (FWHMs) from the profile fitting, assuming that there were no chemistry or stress/strain gradients present. The Scherrer formula [9, 12] was used for this calculation.

The FWHMs of the peaks were corrected for instrumental broadening (inherent broadening due to the chosen optics of the diffractometer, the spectrum coming from the x-ray source, etc.). In the absence of a large crystallite carbon reference sample, the x-ray peak broadening from National Institute of Standards and Technology (NIST) Standard Reference Materials (SRM) 640c [12] silicon peaks, which has a grain size of 4.9 microns, was taken to be the instrumental broadening. These FWHMs (see Figure 28 in APPENDIX A) were plotted as function of  $2\Theta$  and were fit with a third-order polynomial (see Figure 29 in APPENDIX A). The Bragg angle of the graphite reflection was inserted into the equation given in Figure 29 to calculate  $FWHM_{inst}$  at that particular Bragg angle, which was then used to correct the individual FWHMs from the graphite samples, as follows:

$$FWHM_{cor} = (FWHM_{uncor} - FWHM_{inst})/2$$

(division by 2, as the FWHM are expressed in  $^{\circ}2\Theta$ ),

where the subscripts *cor*, *uncor*, and *inst* represent *corrected*, *uncorrected*, and *instrumental*. The Scherrer equation is as follows:

$$t = 0.9\lambda/[FWHM_{cor} \cos(2\Theta_B / 2)],$$

where  $t$  is the crystallite size,  $\lambda$  is the wavelength, and  $2\Theta_B$  is the Bragg angle for a reflection.

Figure 30 shows the XRD pattern of the Carbowax resin alone and is provided for reference. Figure 31, Figure 32, and Figure 33 in APPENDIX A show the XRD patterns from the cross sections of the URBIX-HT #1, URBIX-NHT #1, and Asbury #1 samples, respectively. Similarly, Figure 34, Figure 35, and Figure 36 in APPENDIX A show the XRD patterns from the puck faces of the URBIX-HT #1, URBIX-NHT #1, and Asbury #1 samples, respectively. The natural habit or flaky nature of the graphite powder/flakes resulted in the extreme preferred orientation observed in Figure 34, Figure 35, and Figure 36 (note log scale on Y axes), which necessitated the special sample preparation, also referred to as *briquetting* in ASTM D5187 [9]. A diffraction-side Ni filter was used to remove the Cu  $k\beta$  radiation peaks [12]. An absorption edge is present before all of the reflections but is generally lost in the background. However, given the large crystallite size (more on this below) and the extreme preferred orientation in the puck faces of Figure 34, Figure 35, and Figure 36, the Ni filter absorption edge is very pronounced and clearly seen at  $\sim 26^{\circ} 2\Theta$ . For comparison, note the absence of this absorption edge in Figure 31, Figure 32, and Figure 33 taken from the cross sections. This absorption edge is noticeably larger in the URBIX samples than in the Asbury sample.

Table 13, Table 14, and Table 15 in APPENDIX A list the crystallite sizes for the URBIX-HT #1, URBIX-NHT#1 and Asbury #1 samples. On average, all three samples exhibit a large ( $>100$  nm) crystallite size. It should be noted that when the crystallite size exceeds 100 nm, the XRD peak broadening is essentially indistinguishable from that of a larger crystallite. That is, above 100 nm, crystallite size broadening effectively goes to zero, or XRD peak broadening is negligible above 100 nm in crystallite size. Thus, any crystallite sizes listed in Table 13, Table 14, and Table 15 exceeding 100 nm cannot be quoted except to say that they are  $>100$  nm. Examination of the data in these tables reveals that there are several reflections with crystallite sizes less than 100 nm which seem to be orientation-dependent (viz. cross section vs. puck face).

Future work beyond this study may include Rietveld refinements to discern the relative amounts of hexagonal and rhombohedral graphite, assuming the cross section plane is regarded as random. A better option could be to procure a piezoelectric vibrating powder sample holder to greatly reduce the preferred orientation during XRD data collection [13].

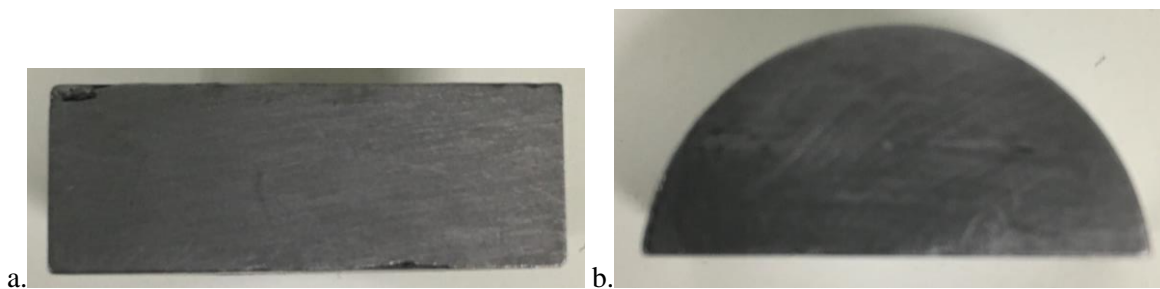


**Figure 5. Cross section of a graphite puck (a), and cross section of a puck face (b).**

## **1.8 PARTICLE SIZE DISTRIBUTION**

Particle size distribution for URBIX-NHT, URBIX-HT, and Asbury 13371 was performed by Particle Testing Authority using laser diffraction particle analysis. Testing was performed in accordance with International Organization for Standardization (ISO) 13320 [14]. Sample preparation involved adding 0.5 g of each graphite to 20 mL of distilled water, along with one drop of Nonidet P40. The samples were then sonicated for 2 minutes each to break apart any agglomerates. The graphite refractive index was taken as 1.800 for the real value and 1.000 for the imaginary, while the water's refractive index was taken as 1.331.

Laser diffraction analysis was also performed on URBIX-MIL; however, this test was performed at ORNL, as the milled powder was produced later in the testing process. Both testing cases were performed under similar conditions in which graphite samples were suspended in water using a dispersant and were sonicated before testing. The same refractive index values that were used to characterize the other powders were also used in testing the URBIX-MIL powder.

A summary of the laser diffraction results can be found in Table 1. As can be expected, the as-received and heat-treated Urbix powder measured nearly identical to one another on average and at each distribution percentage. This particle size of approximately 300  $\mu\text{m}$  is on the high end of most graphite powders available on the market today. The milled Urbix powder was reduced to half the mean particle size of the as-received powder. However, all variants of Urbix graphite powder particle size measured over an order of magnitude larger than the Asbury powder tested. This disparity is likely a factor in the differences in physical properties found in other testing methods, as discussed above. Further details on the particle size distributions of these powders can be found in Figure 37 through Figure 40 in APPENDIX A.

**Table 1. Summary of particle size analysis results from laser diffraction testing four separate graphite powder lots**

<b>Graphite lot</b>	<b>Mean particle size (<math>\mu\text{m}</math>)</b>	<b>D10 (<math>\mu\text{m}</math>)</b>	<b>D50 (<math>\mu\text{m}</math>)</b>	<b>D90 (<math>\mu\text{m}</math>)</b>
URBIX-NHT	306.964	138.831	311.717	455.943
URBIX-HT	303.536	142.078	309.954	449.604
URBIX-MIL	122.531	14.135	94.565	266.710
Asbury 13371	7.309	2.892	6.823	12.345

## 1.9 SURFACE AREA ANALYSIS

Specific surface area calculations for URBIX-NHT, URBIX-HT, and Asbury 13371 were performed by Particle Testing Authority. This method uses the adsorption of a gas (in this case nitrogen) onto the surface of a given sample to determine the surface area of a powder per gram of material. Measurements were performed on a TriStar II Plus according to ISO standard 9277 [15] and calculated using BET theory. The sample was held under vacuum at 350 °C for 300 minutes to bake out any volatiles before testing was performed.

The results from this analysis are in line with the results found during laser diffraction testing, as the specific surface area of a powder is a function of the powder’s particle size, among other properties. A smaller particle size for a powder results in more surface area for a given mass of powder, which is likely why Asbury powder was shown to have the highest specific surface area of 10.3325 m<sup>2</sup>/g. Testing the as-received and heat-treated powders resulted in much lower specific surface areas of 1.0811 m<sup>2</sup>/g and 0.9012 m<sup>2</sup>/g. More data from surface area testing can be found in Figure 41 through Figure 43 in APPENDIX A.

## 2. FUEL BODY FABRICATION AND CHARACTERIZATION

### 2.1 RESINATED GRAPHITE PRODUCTION

Under the AGR program, a graphite matrix recipe was developed in which natural flake graphite, synthetic graphite, and a resin binder are blended in a 64:16:20 ratio, respectively. The materials selected in this effort included Asbury 13371 (natural graphite), SGL KRB 2000 (synthetic graphite), and Hexion Durite SC-1008 (resin binder). For this project, a small reference batch using these materials was fabricated for compaction. Additional batches, referred to as *Urbix matrix*, were fabricated by replacing Asbury 13371 with natural graphite provided by Urbix. The feedstock material used for fabrication of the Urbix matrix was URBIX-MIL. The milled material was selected based on results from the strength-after-compaction study shown in Figure 4. The milled graphite materials exhibited a higher strength after compaction and had a particle size more in line with traditional materials in matrix production.

The initial fabrication step included adding the appropriate quantity of each material to a large container, along with an excess of alcohol to form a slurry. Two separate batches were blended for uniaxial and isostatic pressing studies. The slurries were ball milled to distribute the components and to evenly coat the graphite particles with resin. After ball milling, the slurries were poured into pans and allowed to dry, and then a Holmes Pulverizer was used to break up the material into a fine powder.

## 2.2 RESINATED GRAPHITE COMPACTION

There are two primary methods of compaction used in the fabrication of graphite-based fuel bodies: uniaxial pressing and isotactic pressing. Uniaxial pressing is used to create cylindrical fuel forms for prismatic-style reactors, whereas isostatic pressing is used to form spheres for pebble reactors. It is important to note that, for graphite-based fuel, fuel particles are coated with graphite matrix and then compacted. For this project, fuel bodies are fabricated by compacting matrix only, so the properties reported are for reference and comparison, as the data may be different in an actual fuel form.

Uniaxial pressing was achieved by loading ~5 g of matrix material into a heated (~80 °C) steel die and pressing to a target density of 1.5 g/cm<sup>3</sup> using a 2,000 lb servo electric press. Figure 6 shows the density as a function of peak pressing force. The average force to achieve the target density was ~163 lb for the URBIX-MIL material. As a reference, the target force required to achieve target density with traditional AGR matrix was 370 lb. The lower force required for the URBIX-MIL material is desirable in a fuel fabrication process, as it reduces overall stress on fuel particles during fabrication. This reduction in force may be related to the larger particle size of the flake graphite. Since a graphite flake is near theoretical density, having a larger particle size may yield higher density at the same force. The resulting compacts (see Figure 7) measure nominally 12.7 mm in diameter and 25.4 mm in length.

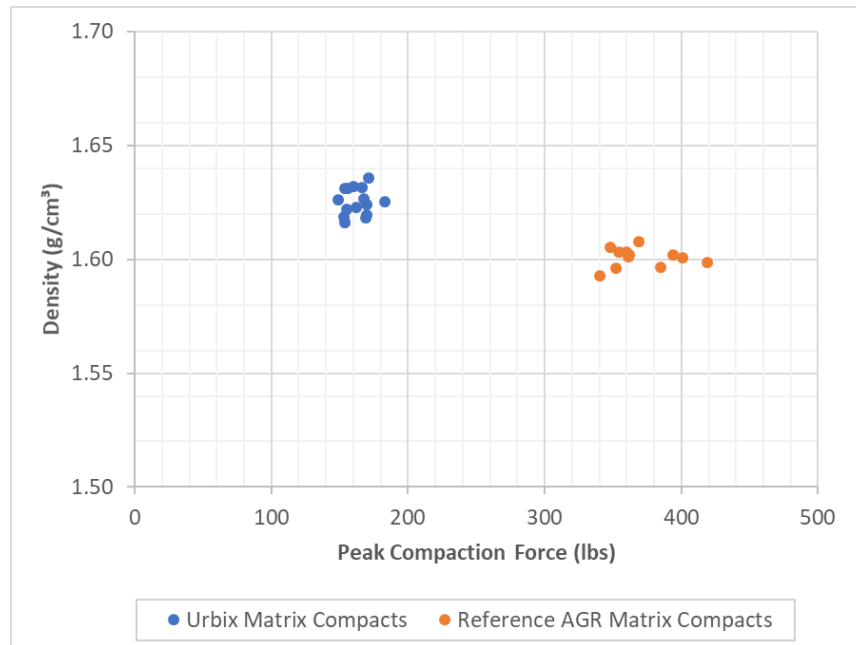
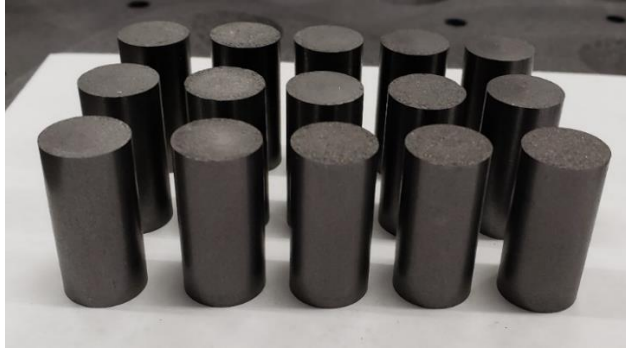


Figure 6. Density for each compact and the peak compaction force used to obtain that density value.



**Figure 7. Uniaxially pressed graphite matrix compacts created using milled Urbix powder.**

Isostatic pressing of matrix material was achieved by loading nominally 50 g of matrix material into a cylindrical dry mold (see Figure 8). The molds were evacuated of air, vacuum sealed, and pressed to 1,000 psi in a cold isostatic press. The resulting rods (see Figure 9) had a slightly flared end caused by the mold, and they measured approximately 100 mm long. Their diameters ranged from approximately 17 to 20 mm, depending on the amount of material that could be loaded into the mold.



**Figure 8. A polymer mold used to densify graphite matrix specimens in an isostatic press.**



**Figure 9. Graphite matrix rods formed by isostatic pressing. Testing specimens were machined from these rods for use in characterizing isostatically pressed Urbix matrix.**

## 2.3 HEAT TREATMENT OF FUEL BODIES

The final fabrication step for both uniaxially and isostatically pressed materials was a two-stage furnace operation that included carbonization and final heat treatment. In the first stage, the compacts were heated at 2 °C/min to a temperature of 900 °C under flowing argon. During this stage, the resin binder was cured and then carbonized into an interconnected network of glassy carbon that bound the natural and synthetic graphite particles together. Once carbonization was complete, the heating rate was increased to 10 °C/min, and the compacts were heated in vacuum to 1,800 °C. During carbonization, a significant fraction of the resin binder volatilized and caused typical shrinkage of the solid bodies in all directions. Shrinkage values for compacts made with URBIX-MIL graphite and traditionally fabricated AGR compacts are compared in Figure 10. Isostatically pressed compacts were not measured due to their irregular shapes.

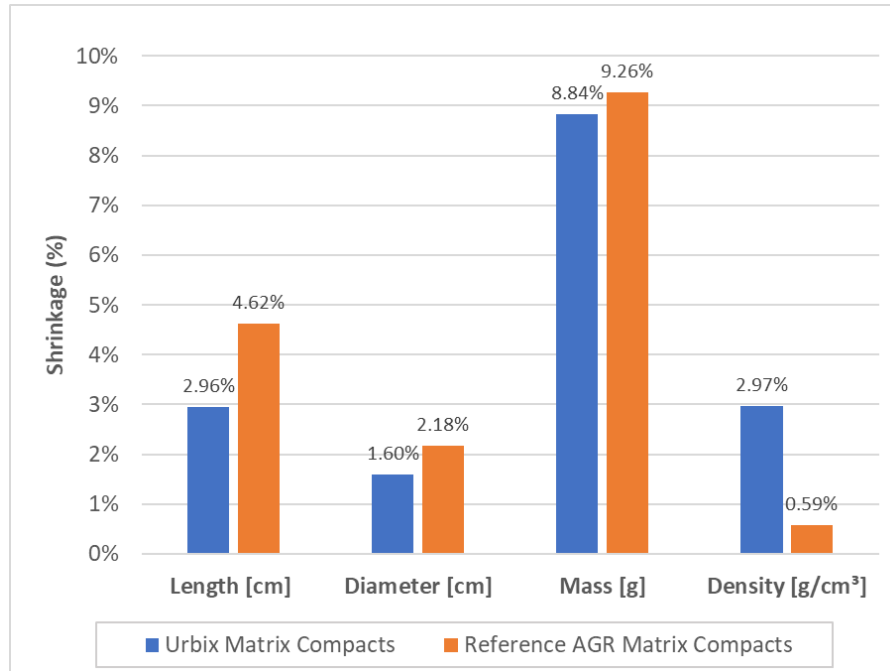


**Figure 10. Percent of dimensional change for Urbix and AGR compacts resulting from heat treatment.**

## 2.4 ULTIMATE COMPRESSIVE STRENGTH

The ultimate compressive strength of each graphite matrix was tested using the same equipment and parameters used to test the monolithic graphite specimens discussed in Section 1.6. These specimens were also measured to accurately calculate the stresses they experienced. The height-to-diameter ratio of these specimens was approximately 2, as the powder for the graphite matrices was much denser than the graphite powders on their own. Tests were performed on 8 AGR compacts, 11 uniaxially pressed Urbix compacts, and 5 isostatically pressed Urbix compacts.

A graph displaying the differences in compressive strength between each graphite matrix can be found below in Figure 11. The results show that while both types of Urbix powder compacts had similar compressive strengths, the uniaxially pressed compacts were consistently stronger than the isostatically pressed compacts, ~16% stronger on average. As might be expected from the monolithic graphite strength results, the compacts composed of Asbury powder (or AGR compacts) showed a much higher strength.

This could be the result of the smaller particle size, as discussed in Section 1.6. Strength test results are available in APPENDIX A, Table 16.

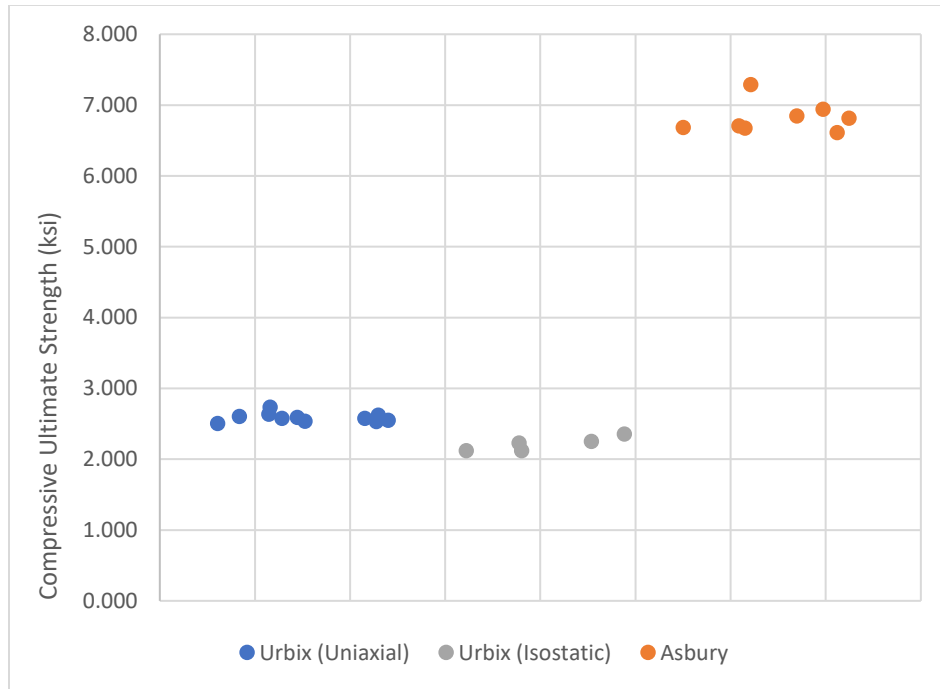


**Figure 11. Ultimate compressive strength of several graphite matrix compacts created using two types of natural graphite powders and two compaction methods (Urbix and Asbury 13371).**

## 2.5 DENSITY AND POROSITY MEASUREMENTS

Density and porosity measurements of the graphite matrix compacts were performed at ORNL using helium pycnometry. Cylindrical specimens were machined out of uniaxially pressed Urbix compacts, isostatically pressed Urbix compacts, and AGR compacts. Two specimens were created for each type of compact. Each specimen was weighed and measured to find its measured density and helium pycnometry data to determine information on compact porosity.

The results from the helium pycnometry tests are tabulated below in Table 2. The pycnometry results for the uniaxially pressed Urbix compacts, the isostatically pressed Urbix compacts, and the AGR compacts are quite similar in terms of measured density, pycnometry density, total porosity, and closed porosity values. All samples measure approximately 70% dense, with 9–10% of the void space measured as closed porosity, only varying from each other by a few percent. Helium pycnometry test results are shown in Figure 44, Figure 45, and Figure 46 of APPENDIX A.

**Table 2. A table of the results found by way of performing helium pycnometry tests on two different graphite matrix compacts**

	<b>AGR</b>	<b>Urbix (uniaxial)</b>	<b>Urbix (isostatic)</b>
Theoretical density (g/cm <sup>3</sup> )	2.267	2.267	2.267
Measured density (g/cm <sup>3</sup> )	1.594	1.584	1.539
Pycnometry density (g/cm <sup>3</sup> )	2.0556	2.0444	2.0597
Total porosity %	29.69	30.13	32.12
Closed porosity %	9.33	9.82	9.14

## 2.6 COEFFICIENT OF THERMAL EXPANSION

The coefficient of thermal expansion (CTE) was measured for each type of compact produced. Square cross sectioned specimens measuring  $4 \times 4 \times 25$  mm were machined from the graphite compacts for the purposes of these tests. All tests were performed on a Netzsch dilatometer (DIL) 402 CD and were performed from 21 °C up to approximately 1,000 °C, with a heating rate of 3 °C/min. Measurements were taken 15 times per minute. All values were taken during the heat ramp as opposed to during the cooling period. A tungsten standard was used to ensure that the equipment returned accurate results. Figure 47 in APPENDIX A shows the results of these tungsten verification runs. The changes in length and temperature allow for the calculation of CTE ( $\alpha$ ) for each type of graphite compact. Two measurements of CTE are available from this data: the instantaneous CTE ( $\alpha$ ), and the mean CTE (technical  $\alpha$  or T.  $\alpha$ ). The mean CTE measurements are the focus of these results.

The T.  $\alpha$  values calculated for each test as a function of temperature can be found in Figure 12. Tables listing the measurements at 50 °C intervals can be found in Table 17 and Table 18 of APPENDIX A for mean and instantaneous results, respectively. One AGR and one uniaxially pressed Urbix compact (URBIX-UNI) were tested because the extra specimens for each type of matrix were damaged due to oxidation during early testing. However, two isostatically pressed Urbix specimens (URBIX-ISO) were tested. The CTE for the three types of matrix compacts vary significantly from one another. This discrepancy in measurements is most clear when analyzing the results of the URBIX-ISO tests, which measured approximately 30–40% of the AGR and URBIX-UNI values at 500 °C. The only difference between the URBIX-UNI and URBIX-ISO compact processes was the pressing method; therefore, the pressing method is deemed the key factor in the URBIX-ISO compacts having lower CTE values.

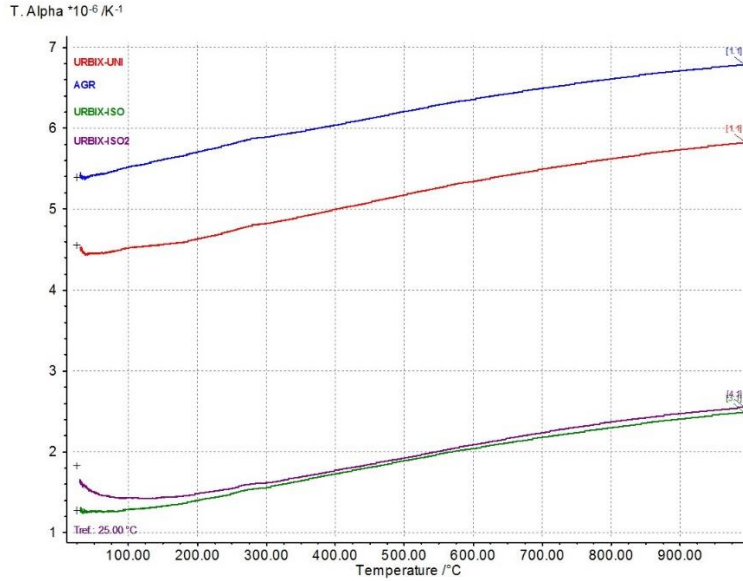


**Figure 12. T.  $\alpha$  values for each type of graphite compact calculated as a function of temperature.**

## 2.7 THERMAL CONDUCTIVITY

A material's thermal conductivity is a function of its specific heat capacity, thermal diffusivity, and density. Each of these properties varies with temperature, so experiments must be conducted to determine how these properties are affected over a range of temperatures relevant to the material in question. Then the values can be plugged into the following equation relating thermal conductivity ( $k$ ) to specific heat capacity ( $c_p$ ), thermal diffusivity ( $\alpha$ ), and density ( $\rho$ ):

$$k = \alpha \rho c_p$$

These properties must be calculated as a function of temperature for each matrix available to determine thermal conductivity as a function of temperature. To perform these measurements, a laser flash diffusivity system was used to determine each specimen's thermal diffusivity, a high-temperature differential scanning calorimeter was used to determine specific heat capacity, and the coefficient of thermal expansion results provided in Section 2.6 were used to determine density as a function of temperature: the changing volume of a material over a range of temperatures dictates its density. Each test was performed to approximately 1,000 °C.

Specific heat capacity was measured according to ASTM E1269 [16] in a temperature range of 30–1,000 °C at 10 °C/min, with measurements taken 100 times per min using a Netzsch differential scanning calorimeter (DSC) 404C. Platinum pans and lids were used during the DSC runs; an empty Pt pan with a lid served as a reference. Sapphire was used as a standard material. Prior to the experiments, the DSC cell was purged with argon. The heating and cooling were conducted with flowing titanium-gettered argon, and the oxygen level was kept below 10-8 ppm. After each heating cycle, samples were held at the maximum temperature for 30 minutes before the cooling cycle was initiated.

The results of the specific heat capacity tests are presented in Figure 13, and a table of specific heat capacity measurements taken at 50 °C increments is provided in Table 19 of APPENDIX A. Plots of each test can be found in APPENDIX A, Figure 48 through Figure 52. Two uniaxially pressed Urbix compact specimens designated URBIX-UNI 1 and URBIX-UNI 2 were each tested twice; hence the -1 and -2

naming scheme found in Figure 13. Two AGR compacts were also tested twice and used the same naming scheme. Two isostatically pressed Urbix compact specimens labelled URBIX-ISO 1 and URBIX-ISO 2 were also tested once each. As shown in Figure 13, the heat capacities measured relatively similar values for each test until reaching approximately 400 °C, at which point the isostatically pressed Urbix compacts began to lag behind the specific heat capacity values measured for the uniaxially pressed Urbix compacts and the AGR compacts.

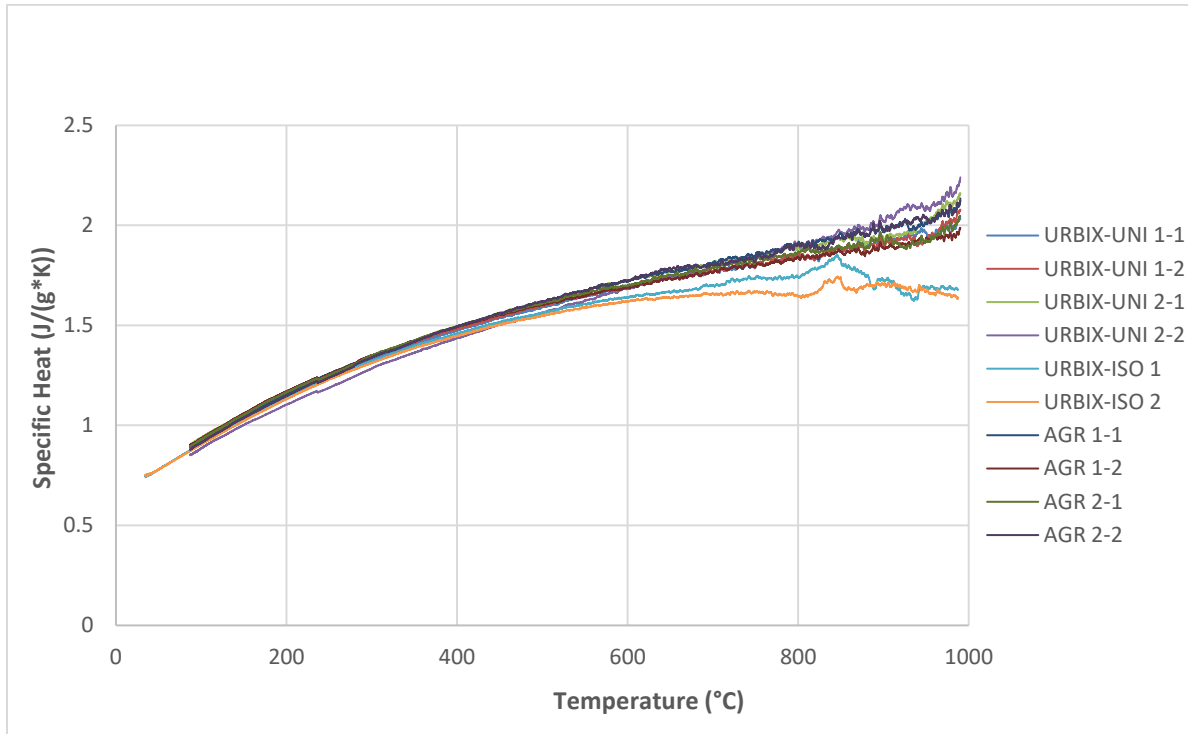


**Figure 13. Specific heat capacities of AGR and Urbix matrix compacts as a function of temperature.**

Diffusivity measurements were performed according to ASTM E1461 [17] in the temperature range from 25–950 °C using a Netzsch laser flash apparatus (LFA) 457 system. Samples were approximately 3 mm thick and 12.7 mm in diameter. No coating was applied to the samples. The testing was performed under flowing argon purge. Three measurements were performed at each temperature set point for every sample. The diffusivity values were calculated based on the sample thickness and temperature rise curve after each laser pulse as described in ASTM E1461.

A plot displaying the results from the thermal diffusivity testing can be found in Figure 14. Tables of the exact values measured during these tests can also be found in APPENDIX A, Table 20 through Table 22. Three diffusivity tests were performed for both AGR and uniaxially pressed Urbix (URBIX-UNI) compacts, and two were performed on isostatically pressed Urbix (URBIX-ISO) compacts. The graph shows that URBIX-UNI compacts have a noticeably higher diffusivity at lower temperature compared to that of AGR compacts, but they converge to similar values at higher temperatures (around 800–950 °C). However, both have relatively lower diffusivity values than those of URBIX-ISO compacts at all temperatures tested. The reason for this discrepancy is most likely a result of the pressing method, as both the AGR and URBIX-UNI compacts were uniaxially pressed. This method of pressing may influence the orientation of the graphite flakes during pressing, possibly resulting in a variation in thermal properties.

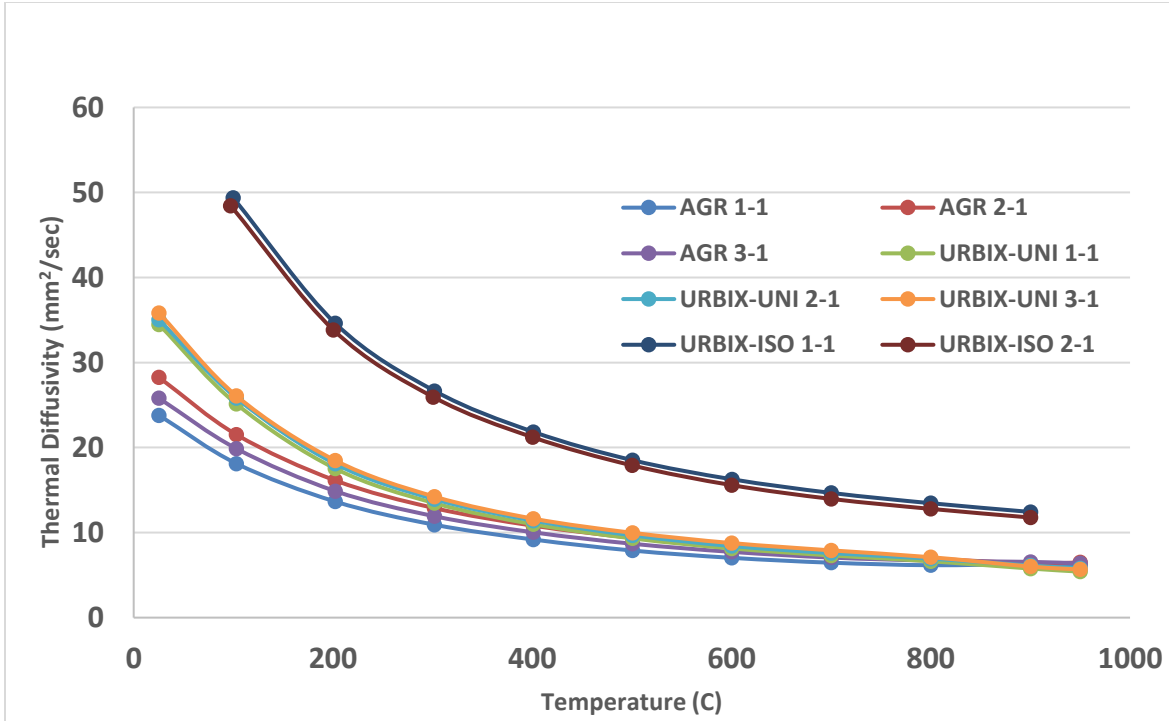


**Figure 14. Relationship between thermal diffusivity and temperature for Urbix (uniaxially and isostatically pressed) and AGR compacts.**

Thermal expansion results in a change in a material's volume over a range of temperatures, and therefore, it also results in a change in the material's density. To calculate how this expansion will affect a material's density, an equation is needed to relate the coefficient of thermal expansion (mean CTE or  $T.\alpha$  will be used in these calculations) to a change in volume. The following equations that have been used in past characterization studies [18] demonstrate this relationship.

$$\varepsilon = \frac{dL}{L_0} = T.\alpha * dT$$

$$V = V_0(1 + \varepsilon)^3$$

$$\rho = \frac{m}{V_0(1+\varepsilon)^3}$$

In these equations,  $\varepsilon$  (strain) is equal to the change in length of a material relative to its initial length,  $T.\alpha$  is the mean coefficient of thermal expansion,  $dT$  is the difference between the recorded temperature and the reference temperature (25 °C),  $V$  and  $V_0$  are final and initial volume of the material given some epsilon, respectively, and  $\rho$  and  $m$  are density and mass, respectively. Therefore, plugging in the recorded  $T.\alpha$  and temperature allow for the calculation of density at a given temperature. A graph displaying the change in thermal conductivity calculated as a function of temperature can be found below in Figure 15. Table 23 presents the measured variables used in calculating the thermal conductivity. Values in these tables were calculated by taking the average temperature and diffusivity values from thermal diffusivity tests and finding the nearest match in temperature for the specific heat capacity and CTE tests. This approach was used because the diffusivity tests took data points at discrete temperatures with relatively large intervals between temperatures compared to the specific heat and CTE tests. If multiple specific heat or CTE tests were performed for one type of graphite matrix sample, then the values were averaged. The values listed for the specific heat and CTE were typically taken within 0.2 °C of the listed temperature. At

all given temperatures, URBIX-ISO samples were calculated to have the highest thermal conductivity of the samples tested, with over twice the value of that calculated for AGR samples at 100 °C. This difference is primarily due to the high thermal diffusivity measured for URBIX-ISO compacts. Samples created using URBIX-UNI and AGR matrix showed closer thermal conductivity measurements, with URBIX-UNI displaying a higher conductivity relative to AGR samples at lower temperatures and a lower conductivity at higher temperatures. The change in thermal conductivity as a result of change in density is minimal at only 1–2%.

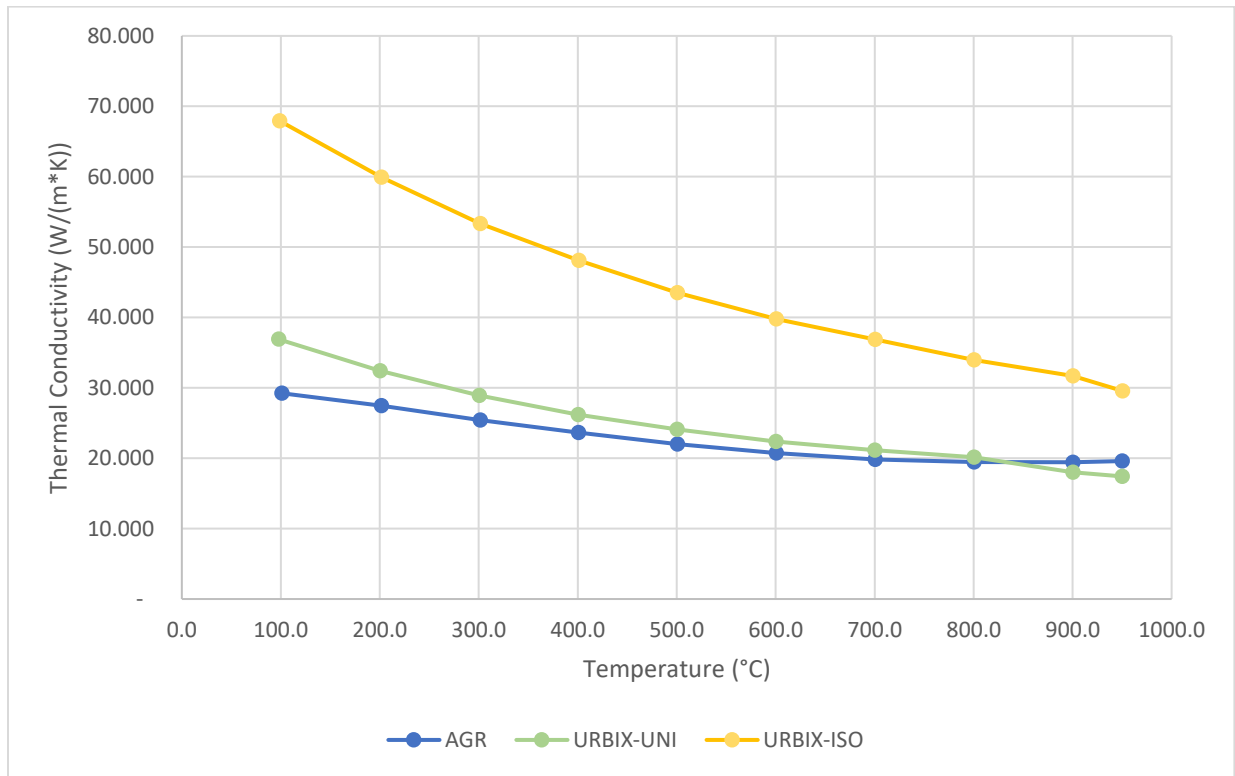


**Figure 15. Variation in thermal conductivity over a range of temperatures for three graphite matrix recipes.**

### 3. CONCLUSIONS

Powder was received by Urbix, LLC and divided into multiple lots for characterization. One lot was tested in its as-received condition, one was heat treated up to 2,800 °C, and one was milled in a pulverizer to reduce the aggregate particle size. These powders were also tested alongside a nuclear-grade graphite used in past fuel experiments as a reference point. These characterization experiments showed that the purity of the as-received powder is high relative to that of the Asbury powder (except for a sharp peak in silicon content), and the purity improves further with the use of heat treatment. While this heat treatment did reduce the powder's impurities, it also seemed to produce specimens with lower compressive strength than the as-received powder. It has been theorized that this discrepancy in strength is due to oxidation that may have occurred during heat treatment. The flake size for the Urbix powder is also orders of magnitude larger on average than that of the Asbury powder. This variation in flake size likely has a notable effect on the physical properties of the compacted powder, as shown when comparing the results of the milled and as-received powder testing. Further testing of these particle size effects would require new equipment such as a jet mill to reduce the average flake size of the Urbix powder to near that of the Asbury powder. Graphite matrix was also created by blending the milled Urbix powder with a synthetic graphite and resin binder used in the AGR program. The AGR matrix recipe was also used as a reference point for characterization purposes, which used the Asbury powder in place of the Urbix powder. Different compaction methods were also used for the Urbix powder to determine how the properties of uniaxially pressed compacts compared to that of isostatically pressed compacts. With each type of compact showing similar densities, the AGR matrix showed a notably higher compressive strength than either of the Urbix compacts. This again could be the result of varying flake sizes between the two graphite powders, as discussed in Section 1.6. The compaction method for the compacts also appeared to be an important factor in the thermal properties of the Urbix matrix. The isostatically pressed matrix displayed relatively high thermal conductivity measurements when compared with the uniaxially pressed matrix as a result of its high thermal diffusivity measurements. Future work with these powders could clarify these results and could provide valuable insights into the effects of graphite flake size and compaction method on the physical properties of graphite and graphite matrix specimens.

## REFERENCES

1. Demkowicz, P. A., B. Liu, and J. D. Hunn, "Coated Particle Fuel: Historical Perspectives and Current Progress." *Journal of Nuclear Materials*, 2019. **515**: pp. 434–450.
2. Petti, D. et al., "The DOE Advanced Gas Reactor Fuel Development and Qualification Program." *JOM*, 2010. **62**(9): pp. 62–66.
3. Pappano, P. J. et al., "A Novel Approach to Fabricating Fuel Compacts for the Next Generation Nuclear Plant (NGNP)." *Journal of Nuclear Materials*, 2008. **381**(1): pp. 25–38.
4. Hunn, J. D., *AGR-2 Fuel Compacts Information Summary: Prepared for the NRC MELCOR Project*. 2010, Oak Ridge National Laboratory: Oak Ridge, Tennessee, USA.
5. *ASTM C1233-15, Standard Practice for Determining Equivalent Boron Contents of Nuclear Materials*. 2015, ASTM International: West Conshohocken, PA.
6. *ASTM D7481-18, Standard Test Methods for Determining Loose and Tapped Bulk Densities of Powders using a Graduated Cylinder*. 2018, ASTM International: West Conshohocken, PA.
7. *ASTM B331-16, Standard Test Method for Compressibility of Metal Powders in Uniaxial Compaction*. 2016, ASTM International: West Conshohocken, PA.
8. *ASTM C695-15, Standard Test Method for Compressive Strength of Carbon and Graphite*. ASTM International: West Conshohocken, PA, 2015.
9. *ASTM D5187-10(2015)e1, Standard Test Method for Determination of Crystallite Size (Lc) of Calcined Petroleum Coke by X-Ray Diffraction*. 2015, ASTM International: West Conshohocken, PA.
10. *Jade 2010 version 7.6.0 (computer software)*. 2019, Materials Data Inc.: Livermore, CA 94550, USA.
11. ICDD, *PDF-4+ 2019, International Centre for Diffraction Data*. Newtown Square, PA.
12. Cullity, B. D., *Elements of X-ray Diffraction*. 1978, Reading, MA: Addison-Wesley Publishing Company, Inc.
13. *BTX III Benchtop XRD Analyzer*. Available from: [https://www.olympus-ims.com/en/xrf-xrd/mobile-benchtop-xrd/btx/?gclid=EAJaIQobChMI2Le58reB5gIVA6SzCh3KrQHAEAAAYASAAEgK-ePD\\_BwE](https://www.olympus-ims.com/en/xrf-xrd/mobile-benchtop-xrd/btx/?gclid=EAJaIQobChMI2Le58reB5gIVA6SzCh3KrQHAEAAAYASAAEgK-ePD_BwE).
14. *ISO 13320:2009, Particle Size Analysis — Laser Diffraction Methods*. 2009, International Organization for Standardization.
15. *ISO 9277:2010, Determination of the Specific Surface Area of Solids by Gas Adsorption — BET Method*. 2010, International Organization for Standardization.
16. *ASTM E1269-11(2018), Standard Test Method for Determining Specific Heat Capacity by Differential Scanning Calorimetry*. 2018, ASTM International: West Conshohocken, PA.
17. *ASTM E1461-13, Standard Test Method for Thermal Diffusivity by the Flash Method*. 2013, ASTM International: West Conshohocken, PA.
18. McEligot, D. et al., *Thermal Properties of G-348 Graphite*. 2016: United States.

APPENDIX A.

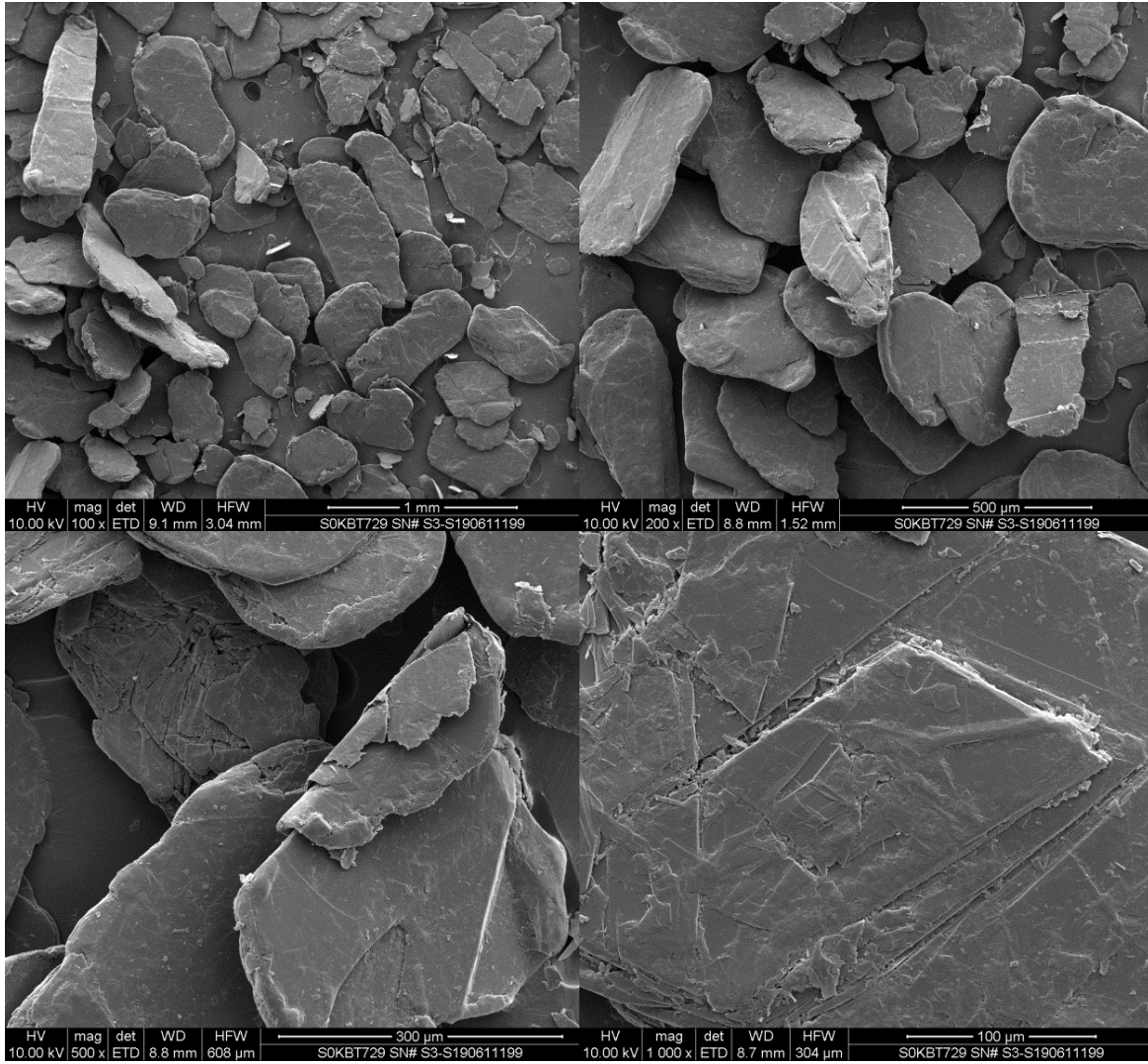
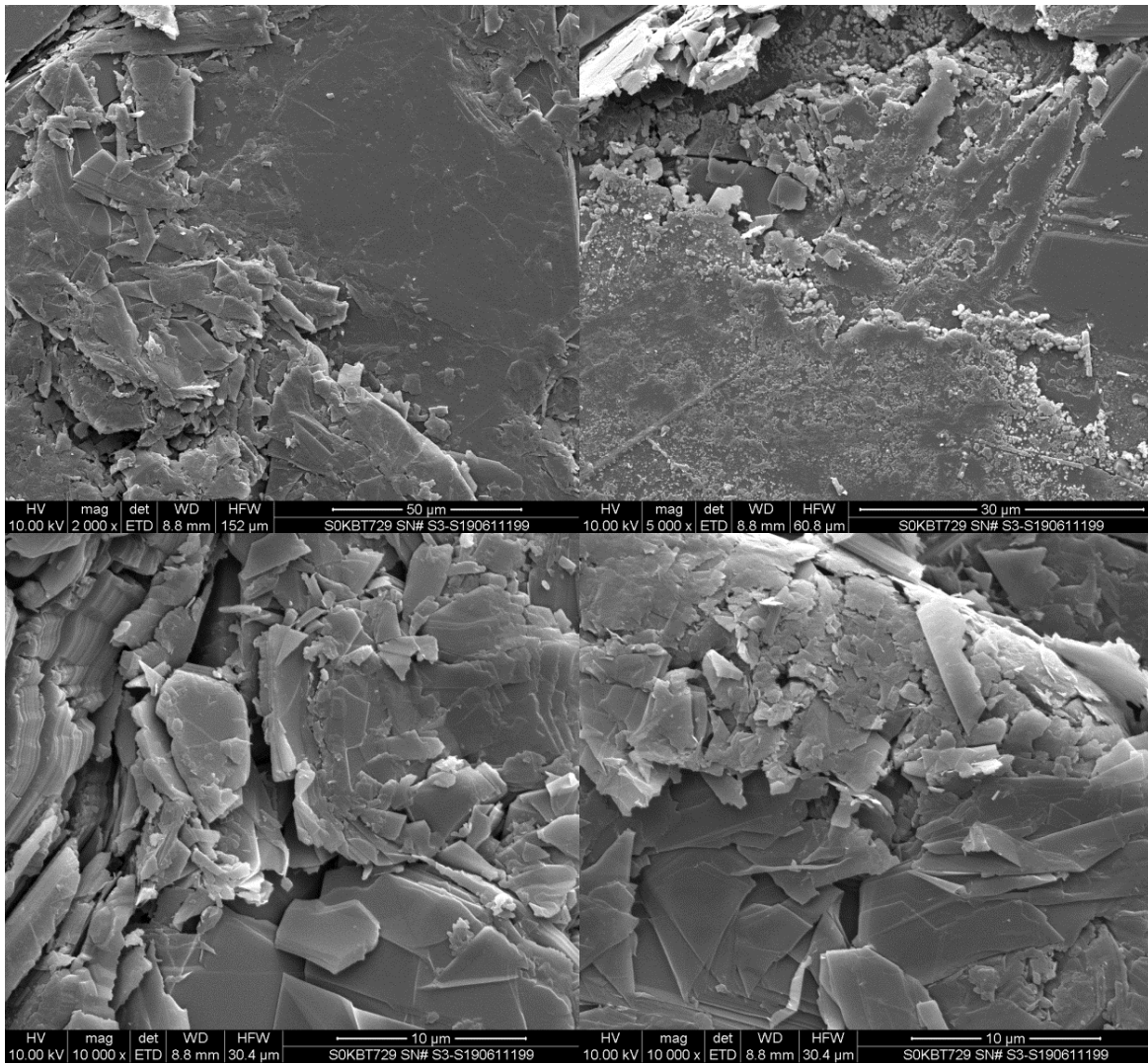
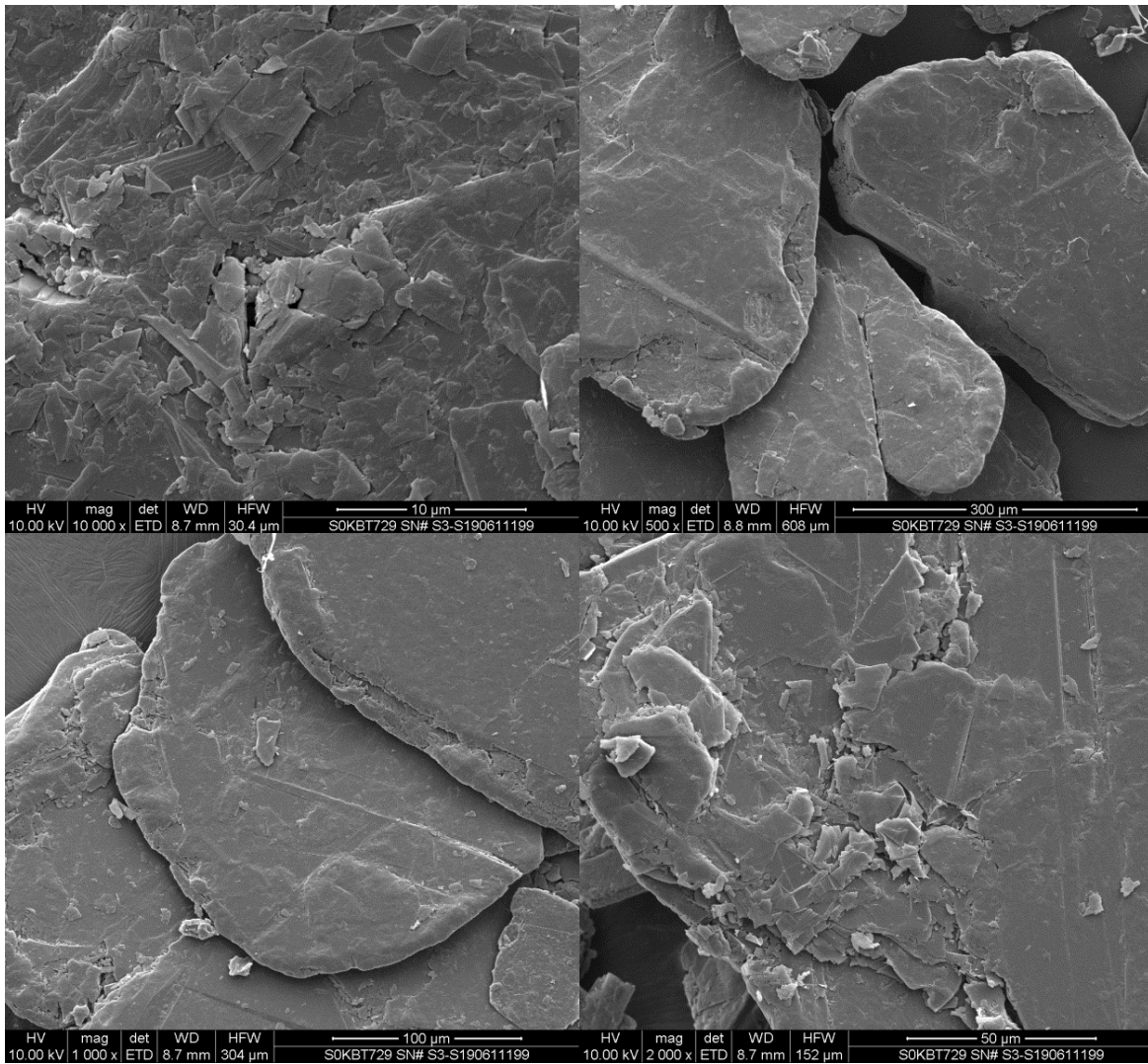


Figure 16. SEM images of the as-received Urbix graphite powder.



**Figure 17. SEM images of the as-received Urbix graphite powder.**



**Figure 18. SEM images of the as-received Urbix graphite powder.**

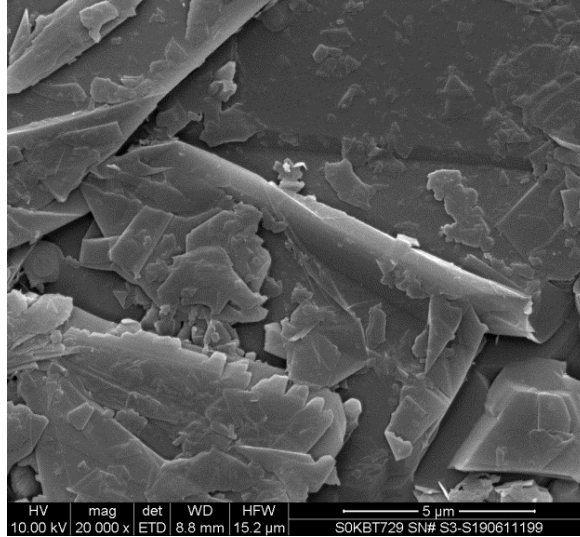
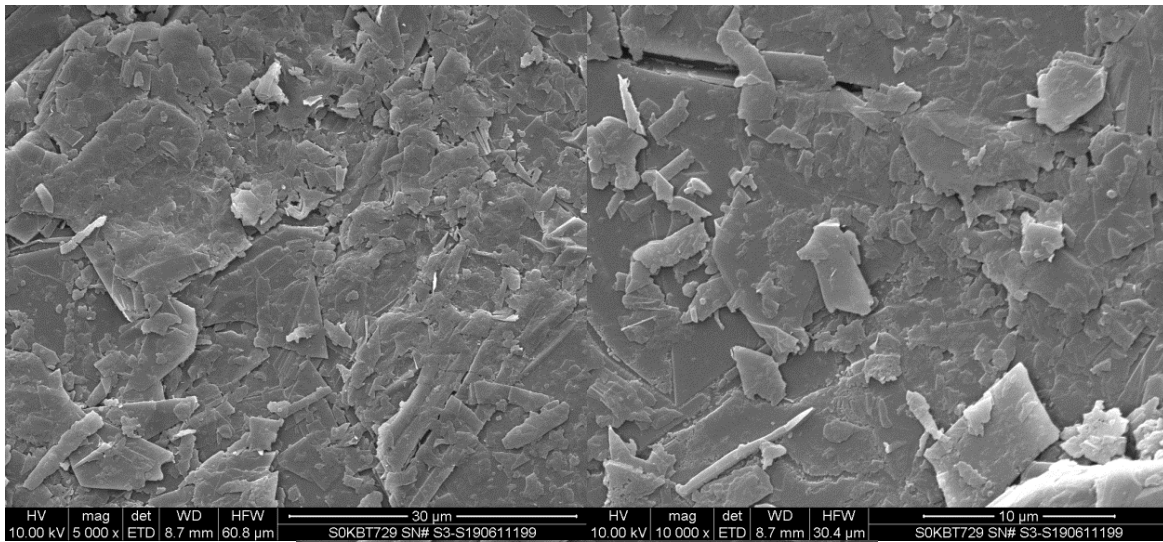


**Figure 19. SEM images of the as-received Urbix graphite powder.**

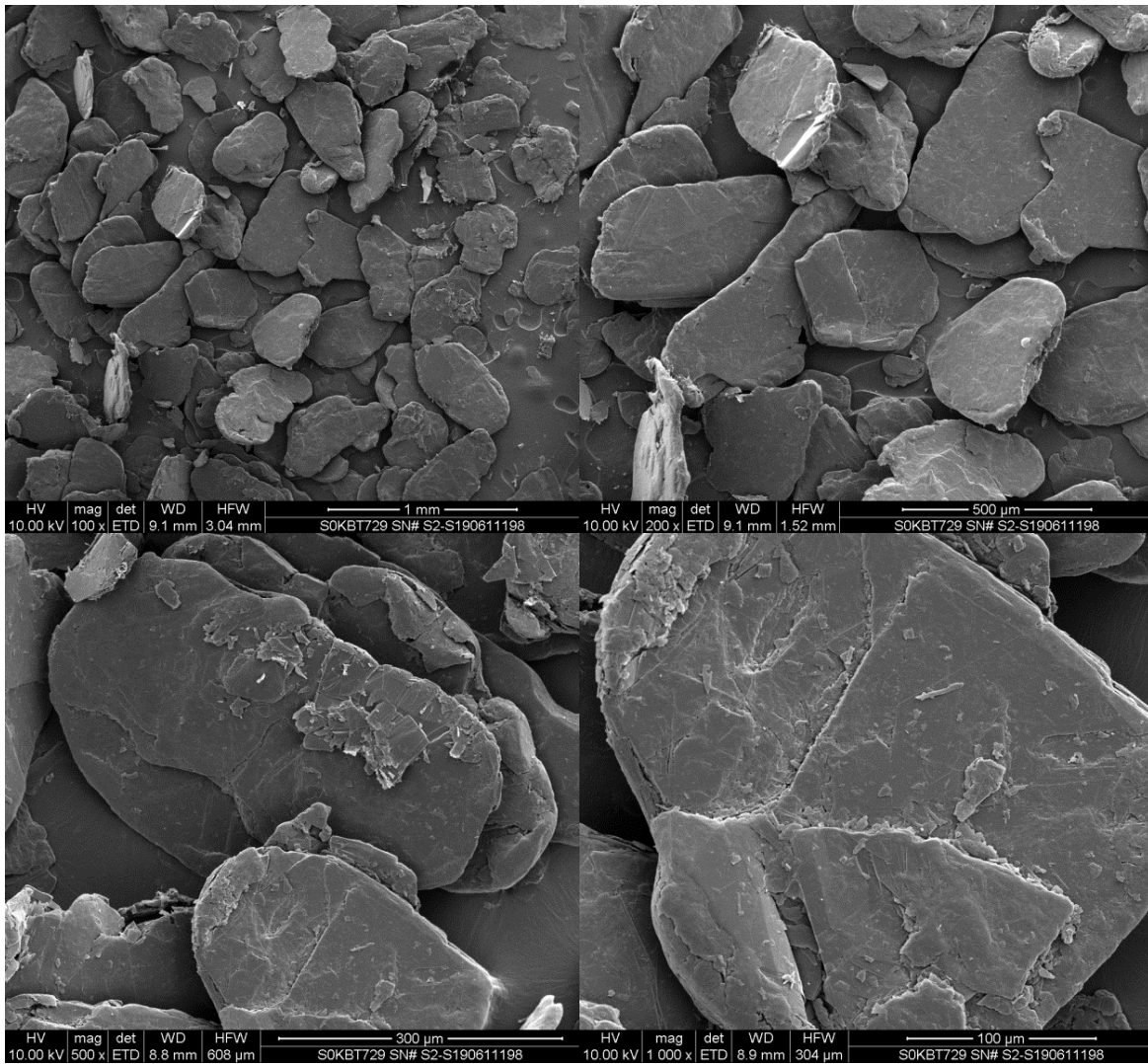


**Figure 20. SEM images of heat-treated Urbix graphite powder.**

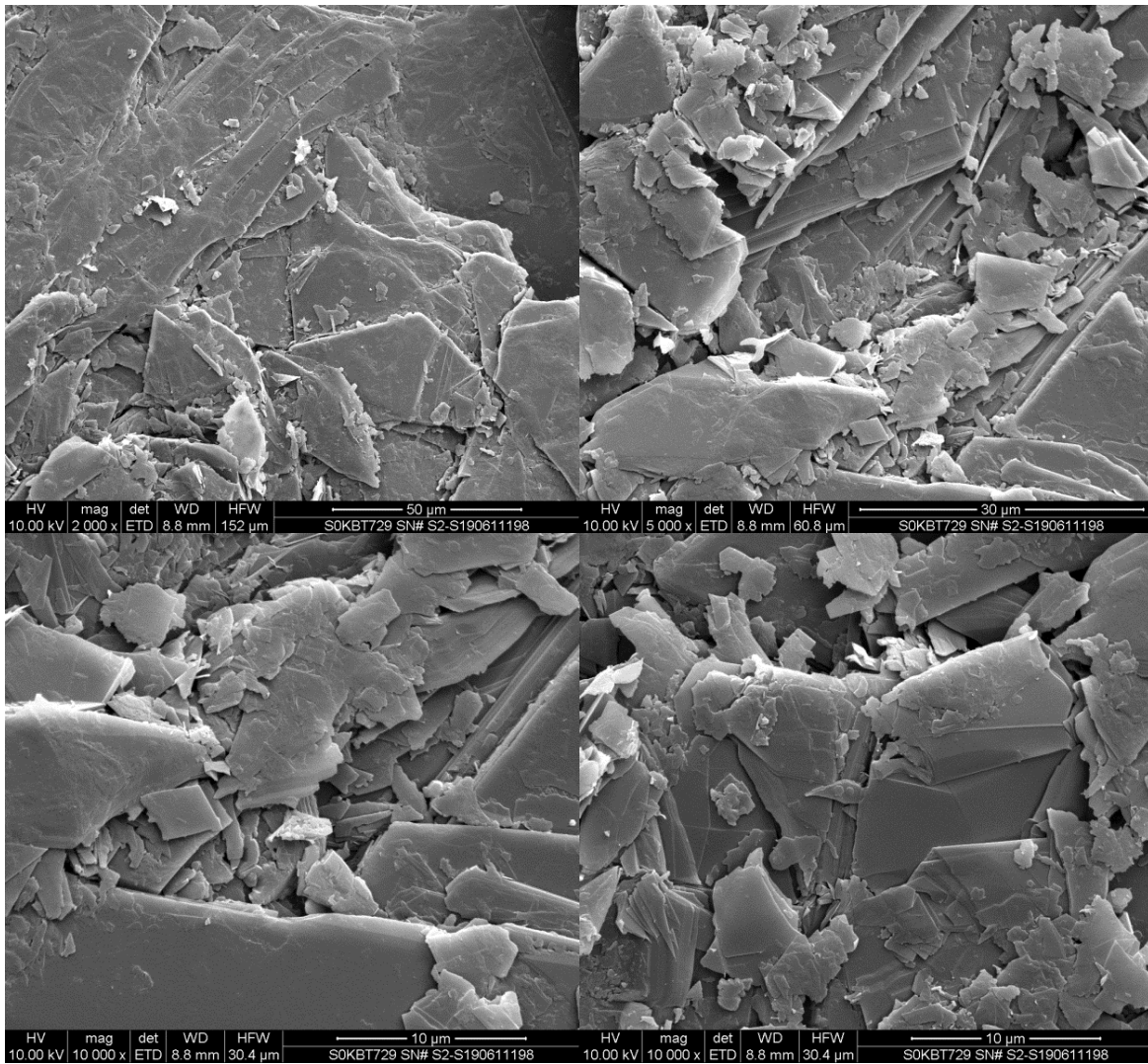


**Figure 21. SEM images of heat-treated Urbix graphite powder.**

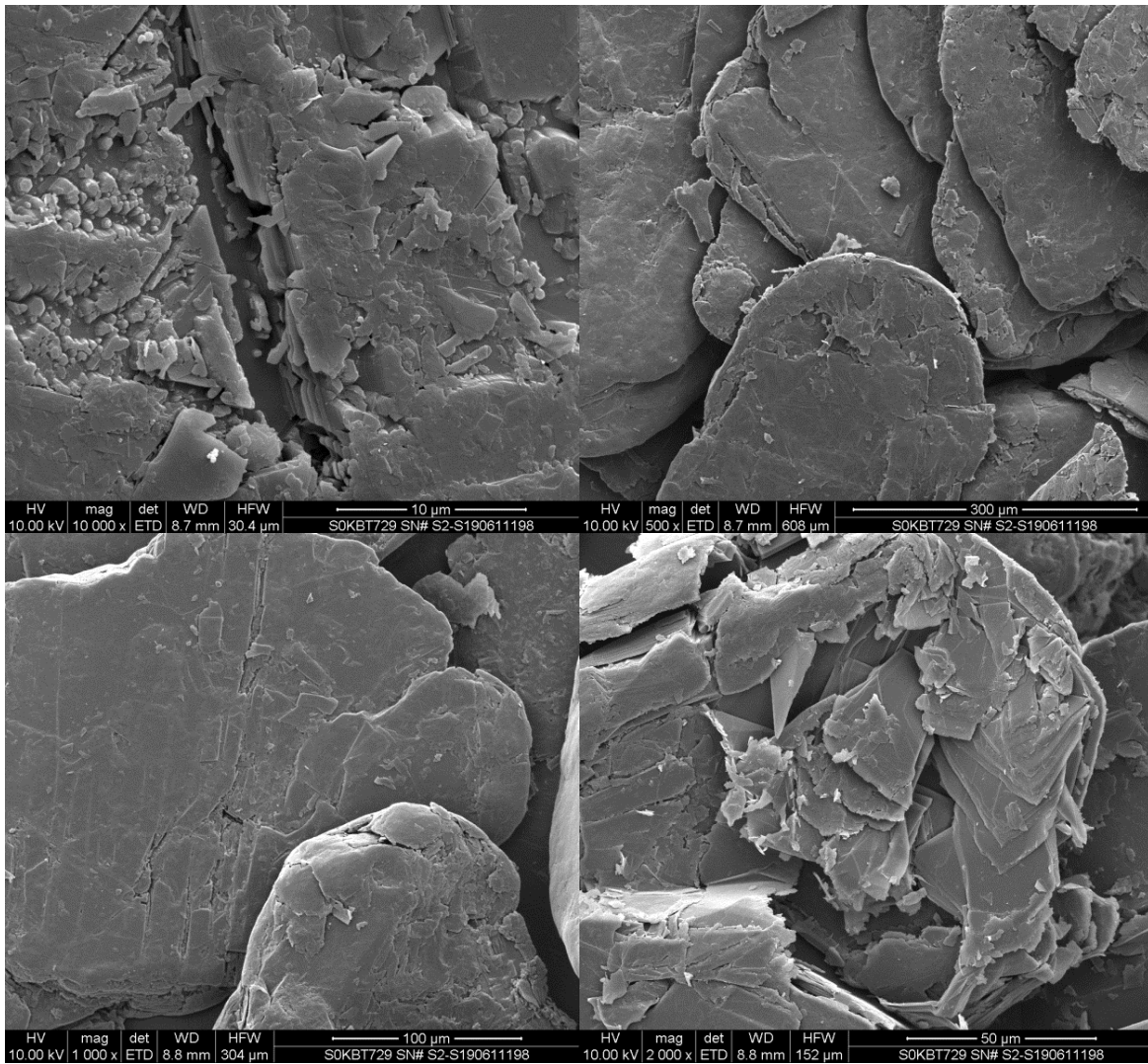


**Figure 22. SEM images of heat-treated Urbix graphite powder.**

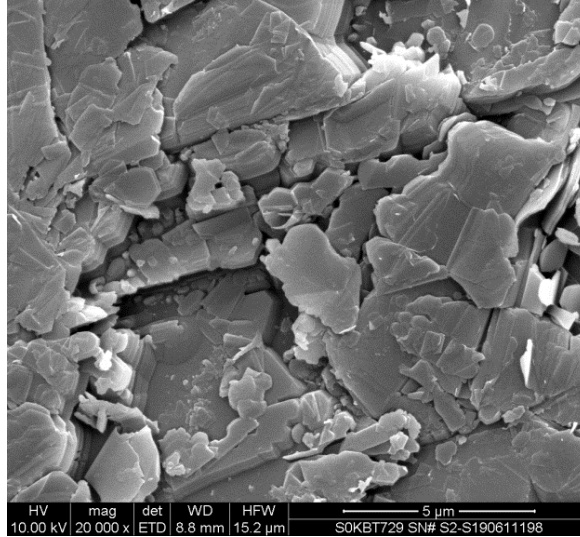
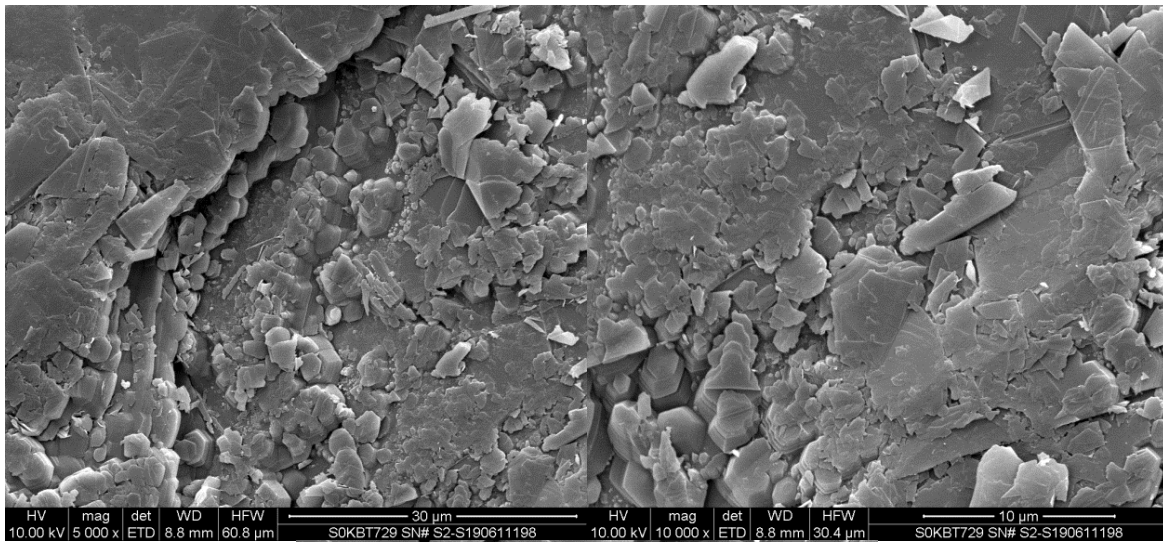


**Figure 23. SEM images of heat-treated Urbix graphite powder.**

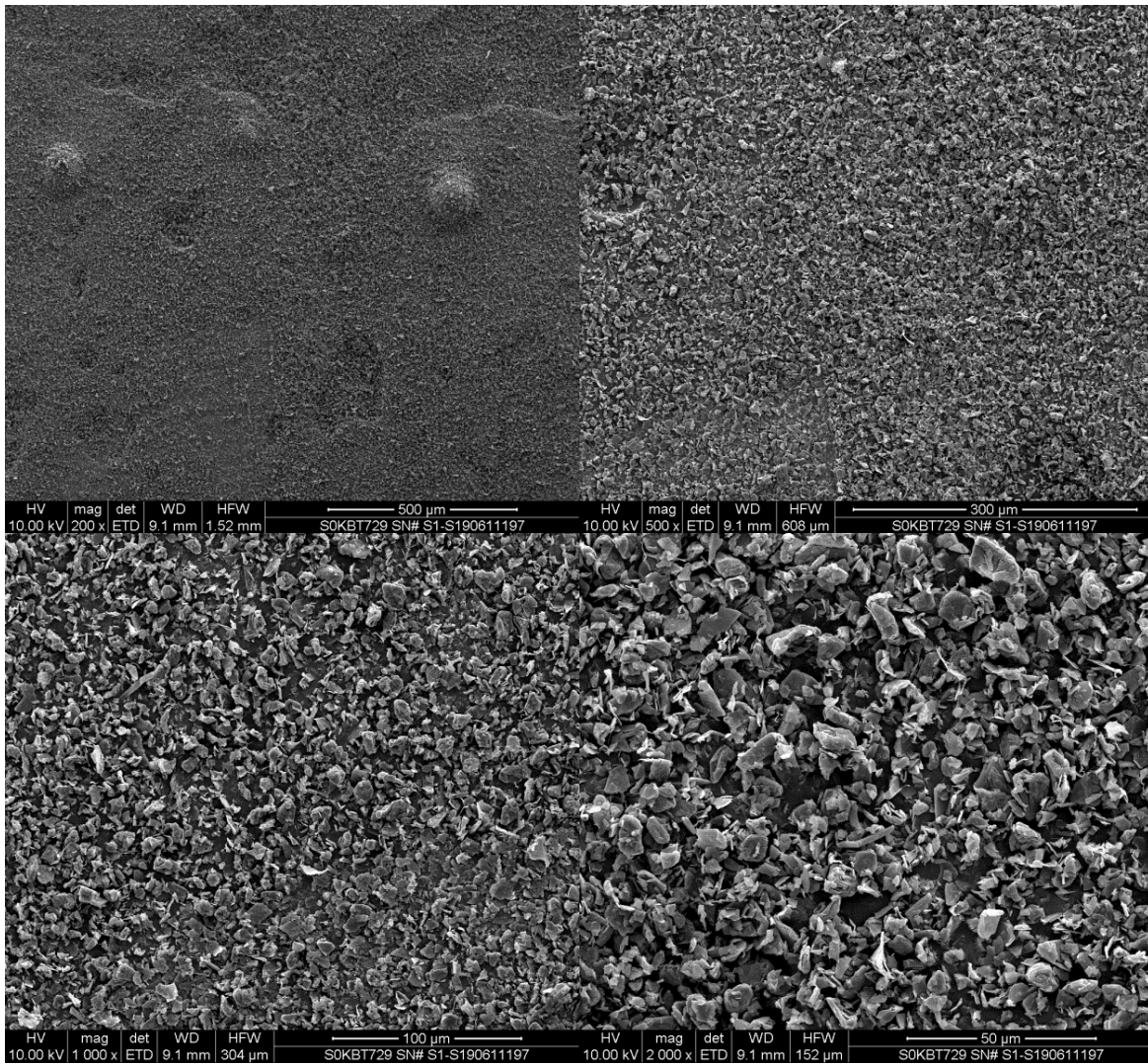


**Figure 24. SEM images of Asbury 13371 natural graphite powder.**

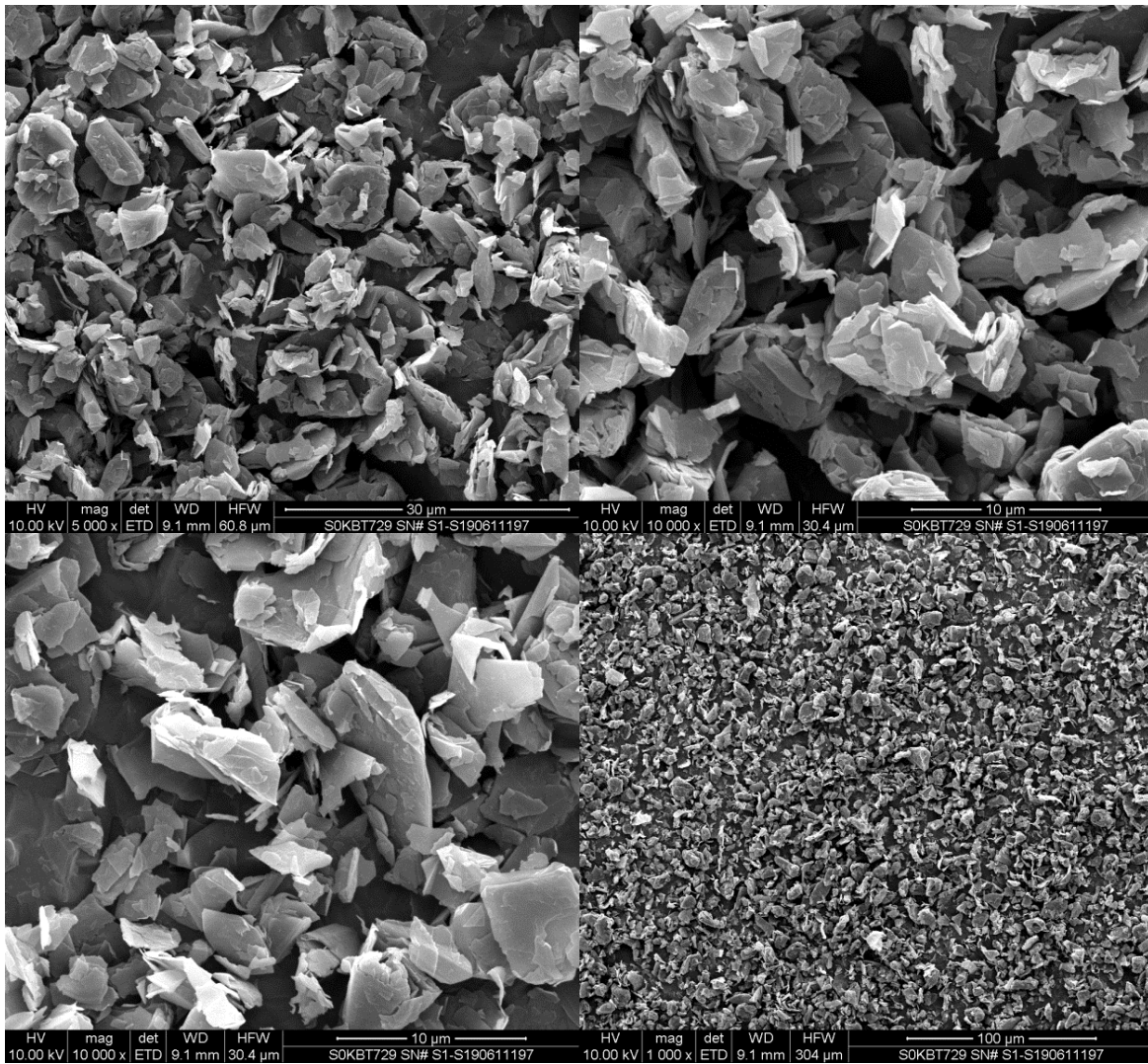


**Figure 25. SEM images of Asbury 13371 natural graphite powder.**

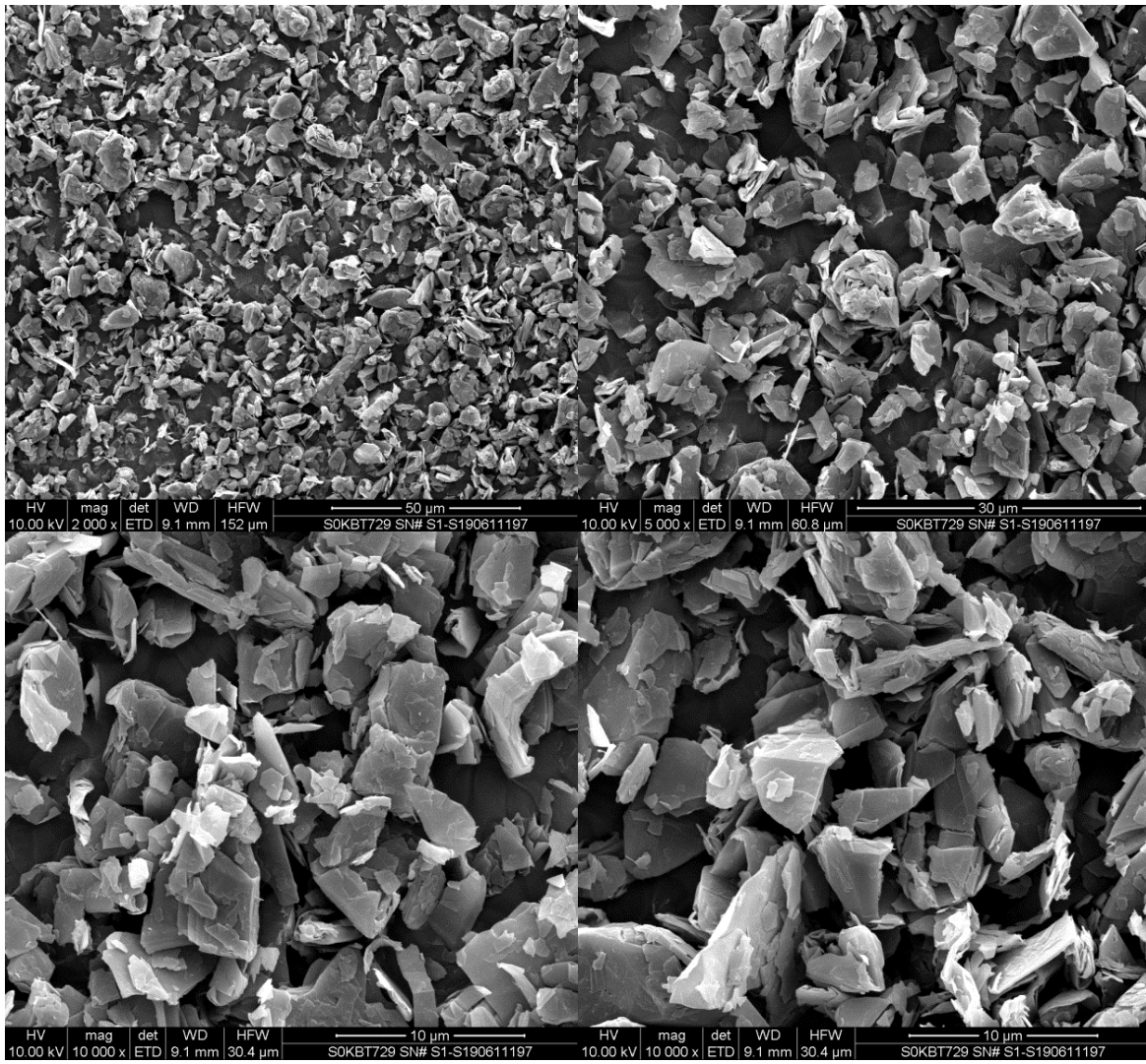


**Figure 26. SEM images of Asbury 13371 natural graphite powder.**

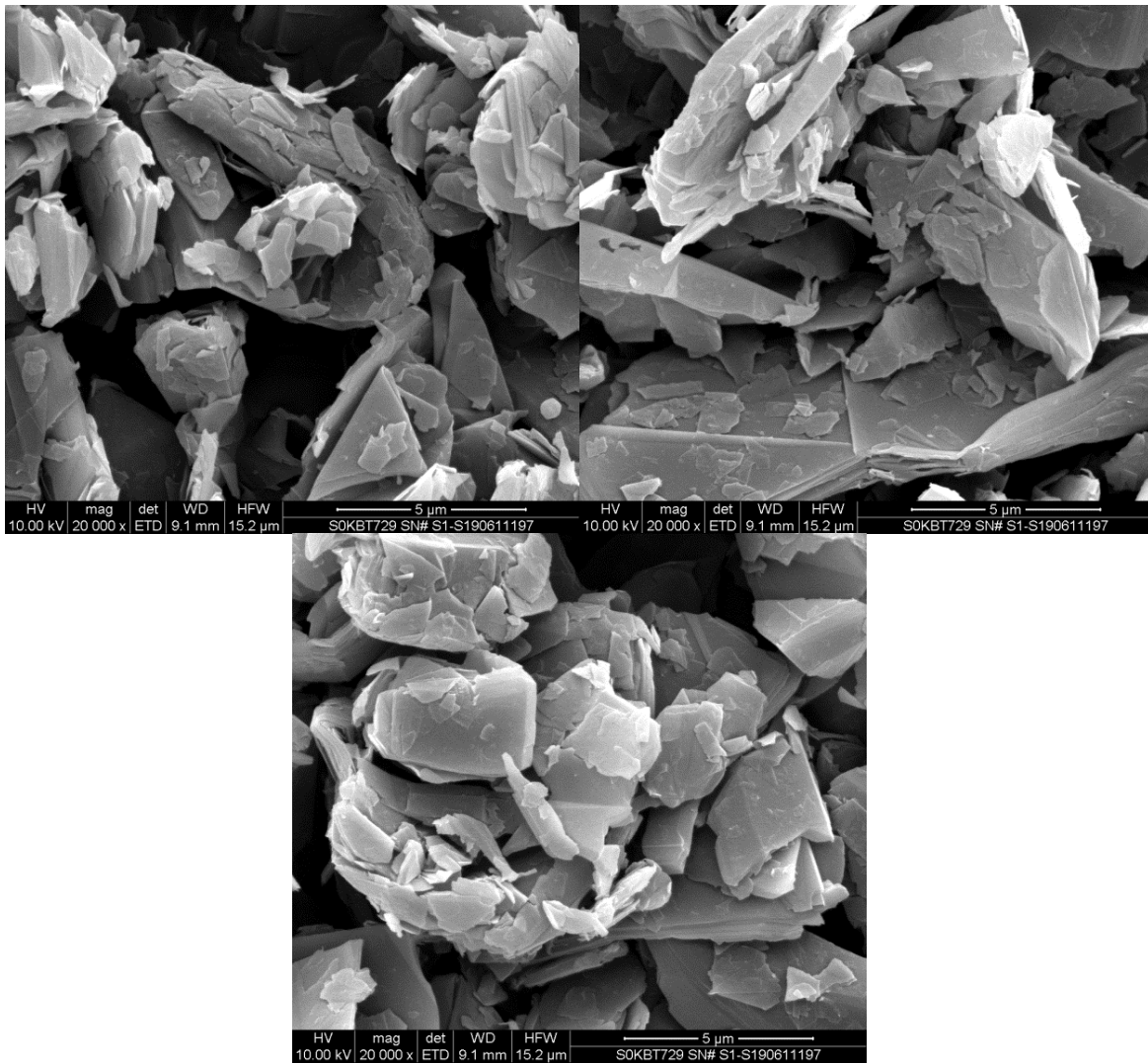


**Figure 27. SEM images of Asbury 13371 natural graphite powder.**

Table 3. Glow discharge mass spectroscopy results for the as-received Urbix graphite powder



**Eurofins  
Materials Science**

**GDMS  
Analytical Report**

100 Commerce Blvd. Liverpool, NY 13086  
T (315) 431-8900 F (315) 431-8900  
info.ny@eag.com www.eag.com

**Customer:** UT-Battelle Oak Ridge  
1 Bethel Valley Rd, Oak Ridge, TN 37823-8063 USA  
**Date:** 25-Nov-19  
**Customer ID:** Graphite Powder  
URBIX-NHT

**P.O.#** 4000175858  
**Job #** S0KDS082  
**Sample ID:** S191122019

[Rev: 2019-11-25 12:50:16]

Element	Concentration [ ppm wt ]	Element	Concentration [ ppm wt ]
Li	< 0.05	Pd	< 0.5
Be	< 0.05	Ag	< 0.5
B	< 0.05	Cd	< 1
C	Matrix	In	< 1
N	-	Sn	< 1
O	-	Sb	< 1
F	30 *	Te	< 0.5
Na	< 0.1	I	< 1
Mg	< 0.5	Cs	< 1
Al	14	Ba	< 0.1
Si	0.13 wt%	La	< 1
P	0.31	Ce	< 0.5
S	23	Pr	< 0.5
Cl	0.59	Nd	< 0.1
K	< 0.5	Sm	< 0.1
Ca	1.4	Eu	< 0.5
Sc	< 0.05	Gd	< 0.1
Ti	0.45	Tb	< 0.1
V	0.38	Dy	< 0.1
Cr	1	Ho	< 0.1
Mn	0.08	Er	< 0.1
Fe	23	Tm	< 0.1
Co	< 0.05	Yb	< 0.1
Ni	0.9	Lu	< 0.1
Cu	< 0.1	Hf	< 0.1
Zn	0.6	Ta	< 100
Ga	< 0.5	W	0.19
Ge	< 1	Re	< 0.05
As	< 0.5	Os	< 0.05
Se	< 1	Ir	< 0.05
Br	< 1	Pt	< 0.1
Rb	< 0.1	Au	< 5
Sr	< 0.1	Hg	< 0.5
Y	0.09	Tl	< 0.1
Zr	< 0.05	Pb	< 0.5
Nb	< 0.5	Bi	< 0.1
Mo	0.48	Th	< 0.05
Ru	< 0.5	U	< 0.05
Rh	< 0.5		

F for information only.



Page 1 of 1 - GDMS  
Analyzed according to WI F rev. 11/10/17

Reviewed by   
B. CIARLEI (Analyst)

Precision and bias typical of GDMS measurements are discussed under ASTM F1863.  
This shall not be reproduced except in full without written approval of the laboratory.

Table 4. Glow discharge mass spectroscopy results for the heat-treated Urbix graphite powder



**Eurofins  
Materials Science**

**GDMS  
Analytical Report**

100 Commerce Blvd. Liverpool, NY 13086  
T (315) 431-8900 F (315) 431-8900  
info.ny@eag.com www.eag.com

**Customer:** UT-Battelle Oak Ridge

**P.O.#** 4000171595

**Date:** 21-Jun-19

**Job #** S0KBT729

**Customer ID:** Graphite Powder  
URBIX-HT

**Sample ID:** S190611198

[Rev: 2019-06-21 12:35:52]

Element	Concentration [ ppm wt ]	Element	Concentration [ ppm wt ]
Li	< 0.05	Pd	< 0.5
Be	< 0.05	Ag	< 0.5
B	0.07	Cd	< 1
C	Matrix	In	< 1
N	-	Sn	< 1
O	-	Sb	< 1
F	24 *	Te	< 0.5
Na	< 0.1	I	< 1
Mg	< 0.5	Cs	< 1
Al	< 0.1	Ba	< 0.1
Si	0.57	La	< 1
P	< 0.1	Ce	< 0.5
S	7.6	Pr	< 0.5
Cl	0.15	Nd	< 0.1
K	< 0.5	Sm	< 0.1
Ca	< 1	Eu	< 0.5
Sc	< 0.05	Gd	< 0.1
Ti	0.59	Tb	< 0.1
V	0.22	Dy	< 0.1
Cr	< 1	Ho	< 0.1
Mn	< 0.05	Er	< 0.1
Fe	< 0.05	Tm	< 0.1
Co	< 0.05	Yb	< 0.1
Ni	< 0.05	Lu	< 0.1
Cu	< 0.1	Hf	< 0.1
Zn	< 0.5	Ta	< 100
Ga	< 0.5	W	0.72
Ge	< 1	Re	< 0.05
As	< 0.5	Os	< 0.05
Se	< 1	Ir	< 0.05
Br	< 1	Pt	< 0.1
Rb	< 0.1	Au	< 5
Sr	< 0.1	Hg	< 0.5
Y	0.15	Tl	< 0.1
Zr	0.1	Pb	< 0.5
Nb	< 0.5	Bi	< 0.1
Mo	1.6	Th	< 0.05
Ru	< 0.5	U	< 0.05
Rh	< 0.5		

F for information only.



Page 1 of 1 - GDMS  
Analyzed according to W1 F rev. 11/10/17  
Reviewed by \_\_\_\_\_

B. CIARLEI (Analyst)

*Precision and bias typical of GDMS measurements are discussed under ASTM F1883.  
This shall not be reproduced except in full without written approval of the laboratory.*

Table 5. Glow discharge mass spectroscopy results for Asbury 13371 graphite powder



**Eurofins  
Materials Science**

**GDMS  
Analytical Report**

100 Commerce Blvd. Liverpool, NY 13086  
T (315) 431-8900 F (315) 431-8900  
info.ny@eag.com www.eag.com

**Customer:** UT-Battelle Oak Ridge

**P.O.#** 4000171595

**Date:** 21-Jun-19

**Job #** S0KBT729

**Customer ID:** Graphite Powder  
ASBURY 13371

**Sample ID:** S190611197

[Rev: 2019-06-21 12:35:16]

Element	Concentration [ ppm wt ]	Element	Concentration [ ppm wt ]
Li	< 0.05	Pd	< 0.5
Be	< 0.05	Ag	< 0.5
B	< 0.05	Cd	< 1
C	Matrix	In	< 1
N	-	Sn	< 1
O	-	Sb	< 1
F	35 *	Te	< 0.5
Na	0.39	I	< 1
Mg	1.4	Cs	< 1
Al	4	Ba	0.15
Si	59	La	< 1
P	0.64	Ce	< 0.5
S	230	Pr	< 0.5
Cl	1.2	Nd	< 0.1
K	< 0.5	Sm	< 0.1
Ca	1	Eu	< 0.5
Sc	< 0.05	Gd	< 0.1
Ti	0.11	Tb	< 0.1
V	< 0.05	Dy	< 0.1
Cr	< 1	Ho	< 0.1
Mn	0.09	Er	< 0.1
Fe	5.2	Tm	< 0.1
Co	< 0.05	Yb	< 0.1
Ni	< 0.05	Lu	< 0.1
Cu	0.47	Hf	< 0.1
Zn	0.62	Ta	< 100
Ga	< 0.5	W	< 0.05
Ge	< 1	Re	< 0.05
As	< 0.5	Os	< 0.05
Se	< 1	Ir	< 0.05
Br	< 1	Pt	< 0.1
Rb	< 0.1	Au	< 5
Sr	< 0.1	Hg	< 0.5
Y	< 0.05	Tl	< 0.1
Zr	< 0.05	Pb	< 0.5
Nb	< 0.5	Bi	< 0.1
Mo	< 0.1	Th	< 0.05
Ru	< 0.5	U	< 0.05
Rh	< 0.5		

F for information only.



Page 1 of 1 - GDMS  
Analyzed according to W1 F rev. 11/10/17  
Reviewed by \_\_\_\_\_

B. CIARLEI (Analyst)

*Precision and bias typical of GDMS measurements are discussed under ASTM F1883.  
This shall not be reproduced except in full without written approval of the laboratory.*

**Table 6. Tap density results for Urbix and Asbury 13371 graphite powders are shown. The initial unpacked density and the final tapped density are recorded. Each set of testing conditions was performed three times.**

<b>Powder</b>	<b>Mass (g)</b>	<b>Initial volume (mL)</b>	<b>Initial density (g/cm<sup>3</sup>)</b>	<b>Average density (g/cm<sup>3</sup>)</b>	<b>Final volume (mL)</b>	<b>Final density (g/cm<sup>3</sup>)</b>	<b>Average density (g/cm<sup>3</sup>)</b>
Urbix (As-Received)-1	71.0	100	0.710	0.712	81	0.877	0.879
Urbix (As-Received)-2	70.9	100	0.709		81	0.875	
Urbix (As-Received)-3	71.6	100	0.716		81	0.884	
Urbix (Heat-Treated)-1	79.1	100	0.791	0.792	87	0.909	0.913
Urbix (Heat-Treated)-2	80.3	100	0.803		87	0.923	
Urbix (Heat-Treated)-3	78.1	100	0.781		86	0.908	
Urbix (Milled)-1	43.6	100	0.436	0.444	76	0.574	0.577
Urbix (Milled)-2	43.8	100	0.438		76	0.576	
Urbix (Milled)-3	45.8	100	0.458		79	0.580	
Asbury 13371-1	19.8	100	0.198	0.208	62	0.319	0.328
Asbury 13371-2	20.7	100	0.207		63	0.329	
Asbury 13371-3	21.9	100	0.219		65	0.337	

**Table 7. The density of graphite powders compacted at 12,500 and 25,000 psi**

Powder	12,500 psi					
	Height (cm)	Width (cm)	Mass (g)	Maximum load (lb)	Pressure (psi)	Density (g/cm <sup>3</sup> )
Urbix (As-Received)-1	0.9772	1.5264	3.6534	3578.5	12656.4	2.043
Urbix (As-Received)-2	0.9162	1.5268	3.4556	3585.0	12679.2	2.060
Urbix (As-Received)-3	0.9091	1.5272	3.4251	3567.2	12616.6	2.057
Urbix (Heat-Treated)-1	Specimen did not hold together					
Urbix (Heat-Treated)-2	0.9720	1.5276	3.5551	3568.1	12619.4	1.996
Urbix (Heat-Treated)-3	Specimen did not hold together					
Urbix (Milled)-1	0.9741	1.5259	3.6500	3596.2	12719.1	2.049
Urbix (Milled)-2	0.8278	1.5260	3.1031	3572.9	12636.5	2.050
Urbix (Milled)-3	0.9620	1.5259	3.5992	3574.5	12642.2	2.046
Asbury 13371-1	0.9904	1.5316	3.2512	3571.3	12630.8	1.782
Asbury 13371-2	0.9912	1.5315	3.2524	3535.8	12505.5	1.781
Asbury 13371-3	0.9511	1.5316	3.1225	3568.1	12619.4	1.782

Powder	25,000 psi					
	Height (cm)	Width (cm)	Mass (g)	Maximum load (lb)	Pressure (psi)	Density (g/cm <sup>3</sup> )
Urbix (As-Received)-1	0.9840	1.5257	3.8496	7128.5	25211.8	2.140
Urbix (As-Received)-2	0.9500	1.5263	3.7038	7114.0	25160.6	2.131
Urbix (As-Received)-3	0.9763	1.5262	3.8091	7159.1	25320.1	2.133
Urbix (Heat-Treated)-1	0.9632	1.5282	3.6948	7175.2	25377.0	2.091
Urbix (Heat-Treated)-2	0.9479	1.5277	3.5870	7151.0	25291.6	2.064
Urbix (Heat-Treated)-3	0.9842	1.5273	3.7698	7192.9	25439.7	2.091
Urbix (Milled)-1	0.9832	1.5258	3.8099	7168.7	25354.2	2.119
Urbix (Milled)-2	0.9937	1.5260	3.8472	7182.4	25402.7	2.117
Urbix (Milled)-3	0.9807	1.5259	3.7995	7196.1	25451.1	2.119
Asbury 13371-1	0.9830	1.5319	3.4556	7132.5	25226.1	1.907
Asbury 13371-2	0.9805	1.5322	3.4461	7164.7	25340.0	1.906
Asbury 13371-3	0.9747	1.5322	3.4209	7113.2	25157.7	1.903

**Table 8. Density of graphite powders compacted at 37,500 and 50,000 psi**

Powder	37,500 psi					
	Height (cm)	Width (cm)	Mass (g)	Maximum load (lb)	Pressure (psi)	Density (g/cm <sup>3</sup> )
Urbix (As-Received)-1	0.9752	1.5262	3.8509	10709.0	37875.5	2.159
Urbix (As-Received)-2	0.9723	1.5269	3.8325	10693.7	37821.4	2.153
Urbix (As-Received)-3	0.9924	1.5260	3.9275	10690.5	37810.0	2.164
Urbix (Heat-Treated)-1	0.9783	1.5295	3.8072	10742.9	37995.1	2.118
Urbix (Heat-Treated)-2	0.9820	1.5281	3.8199	10707.4	37869.8	2.121
Urbix (Heat-Treated)-3	0.9777	1.5285	3.8004	10720.3	37915.4	2.118
Urbix (Milled)-1	0.9835	1.5261	3.8575	10603.0	37500.4	2.144
Urbix (Milled)-2	0.9864	1.5262	3.8660	10734.0	37963.8	2.142
Urbix (Milled)-3	0.9803	1.5262	3.8394	10737.2	37975.2	2.141
Asbury 13371-1	0.9686	1.5331	3.4945	10684.1	37787.2	1.954
Asbury 13371-2	0.9662	1.5332	3.4838	10664.7	37718.8	1.953
Asbury 13371-3	0.9777	1.5326	3.5271	10685.7	37792.9	1.956

Powder	50,000 psi					
	Height (cm)	Width (cm)	Mass (g)	Maximum load (lb)	Pressure (psi)	Density (g/cm <sup>3</sup> )
Urbix (As-Received)-1	0.9765	1.5265	3.8701	14308.9	50607.5	2.166
Urbix (As-Received)-2	0.9874	1.5259	3.9283	14347.6	50744.3	2.176
Urbix (As-Received)-3	0.9641	1.5264	3.8356	14333.9	50695.8	2.174
Urbix (Heat-Treated)-1	0.9786	1.5273	3.7958	14321.0	50650.3	2.117
Urbix (Heat-Treated)-2	0.9851	1.5279	3.8528	14279.1	50502.2	2.133
Urbix (Heat-Treated)-3	0.9686	1.5278	3.8017	14286.4	50527.8	2.141
Urbix (Milled)-1	0.9141	1.5263	3.6038	14293.6	50553.4	2.155
Urbix (Milled)-2	0.9810	1.5263	3.8709	14334.7	50698.7	2.157
Urbix (Milled)-3	0.9910	1.5262	3.9080	14280.0	50505.0	2.156
Asbury 13371-1	0.9630	1.5339	3.5275	14234.9	50345.5	1.982
Asbury 13371-2	0.9572	1.5338	3.5033	14271.1	50473.7	1.981
Asbury 13371-3	0.9838	1.5335	3.6015	14296.9	50564.8	1.982

**Table 9. Ultimate compressive strength of as-received Urbix powder pressed at four different pressures and tested three times for each pressure**

<b>Sample name</b>	<b>Compression pressure (psi)</b>	<b>Compressive strength (ksi)</b>	<b>Average</b>	<b>Standard deviation</b>
URBIX-NHT-12500-1	12,500	0.782	0.740	0.058
URBIX-NHT-12500-2	12,500	0.780		
URBIX-NHT-12500-3	12,500	0.657		
URBIX-NHT-25000-1	25,000	1.214	1.157	0.041
URBIX-NHT-25000-2	25,000	1.119		
URBIX-NHT-25000-3	25,000	1.138		
URBIX-NHT-37500-1	37,500	1.279	1.307	0.093
URBIX-NHT-37500-2	37,500	1.209		
URBIX-NHT-37500-3	37,500	1.432		
URBIX-NHT-50000-1	50,000	1.390	1.458	0.051
URBIX-NHT-50000-2	50,000	1.472		
URBIX-NHT-50000-3	50,000	1.512		

**Table 10. Ultimate compressive strength of heat-treated Urbix powder pressed at four different pressures and tested three times for each pressure**

<b>Sample name</b>	<b>Compression pressure (psi)</b>	<b>Compressive strength (ksi)</b>	<b>Average</b>	<b>Standard deviation</b>
URBIX-HT-12500-1	12,500	NA	0.214	0.025
URBIX-HT-12500-2	12,500	0.239		
URBIX-HT-12500-3	12,500	0.189		
URBIX-HT-25000-1	25,000	0.448	0.449	0.018
URBIX-HT-25000-2	25,000	0.472		
URBIX-HT-25000-3	25,000	0.427		
URBIX-HT-37500-1	37,500	0.494	0.591	0.090
URBIX-HT-37500-2	37,500	0.710		
URBIX-HT-37500-3	37,500	0.568		
URBIX-HT-50000-1	50,000	0.670	0.606	0.047
URBIX-HT-50000-2	50,000	0.591		
URBIX-HT-50000-3	50,000	0.558		

**Table 11. Ultimate compressive strength of milled Urbix powder pressed at four different pressures and tested three times for each pressure**

<b>Sample name</b>	<b>Compression pressure (psi)</b>	<b>Compressive strength (ksi)</b>	<b>Average</b>	<b>Standard deviation</b>
URBIX-MIL-12500-1	12,500	1.182	1.177	0.009
URBIX-MIL-12500-2	12,500	1.165		
URBIX-MIL-12500-3	12,500	1.185		
URBIX-MIL-25000-1	25,000	1.574	1.570	0.021
URBIX-MIL-25000-2	25,000	1.594		
URBIX-MIL-25000-3	25,000	1.542		
URBIX-MIL-37500-1	37,500	1.666	1.696	0.021
URBIX-MIL-37500-2	37,500	1.716		
URBIX-MIL-37500-3	37,500	1.705		
URBIX-MIL-50000-1	50,000	1.767	1.798	0.022
URBIX-MIL-50000-2	50,000	1.811		
URBIX-MIL-50000-3	50,000	1.817		

**Table 12. Ultimate compressive strength of Asbury 13371 powder pressed at four different pressures and tested three times for each pressure**

<b>Sample name</b>	<b>Compression pressure (psi)</b>	<b>Compressive strength (ksi)</b>	<b>Average</b>	<b>Standard deviation</b>
Asbury-12500-1	12500	1.615	1.615	0.004
Asbury-12500-2	12500	1.620		
Asbury-12500-3	12500	1.609		
Asbury-25000-1	25000	2.330	2.341	0.021
Asbury-25000-2	25000	2.371		
Asbury-25000-3	25000	2.322		
Asbury-37500-1	37500	2.561	2.632	0.079
Asbury-37500-2	37500	2.593		
Asbury-37500-3	37500	2.742		
Asbury-50000-1	50000	2.774	2.821	0.047
Asbury-50000-2	50000	2.804		
Asbury-50000-3	50000	2.886		

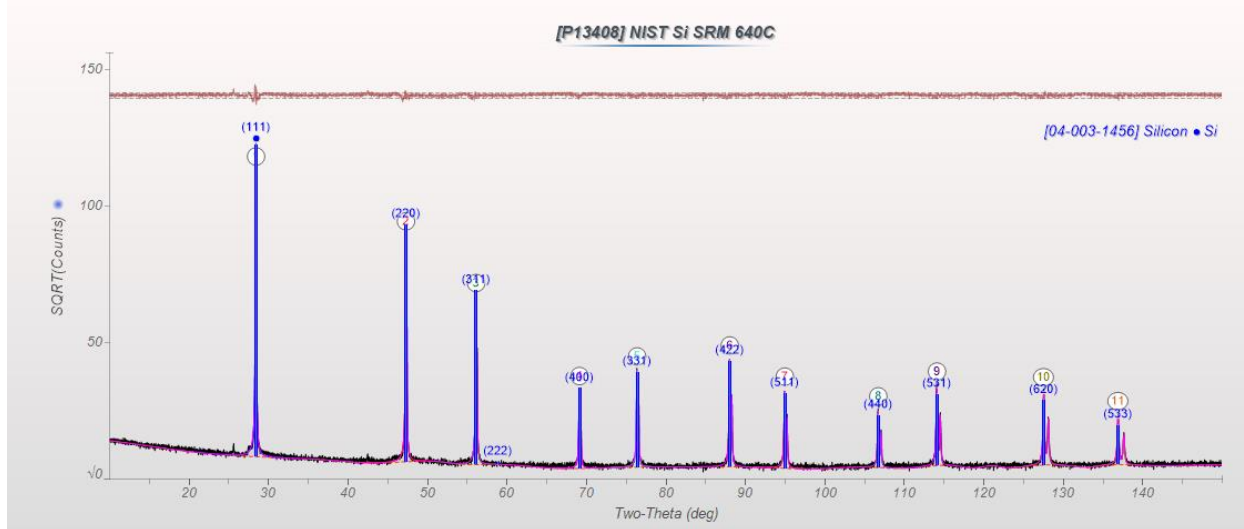


**Figure 28. X-ray diffraction patterns of the NIST SRM 640c silicon powder. The small peak at ~26° 2θ is the (111) Si Cu kβ reflection.**

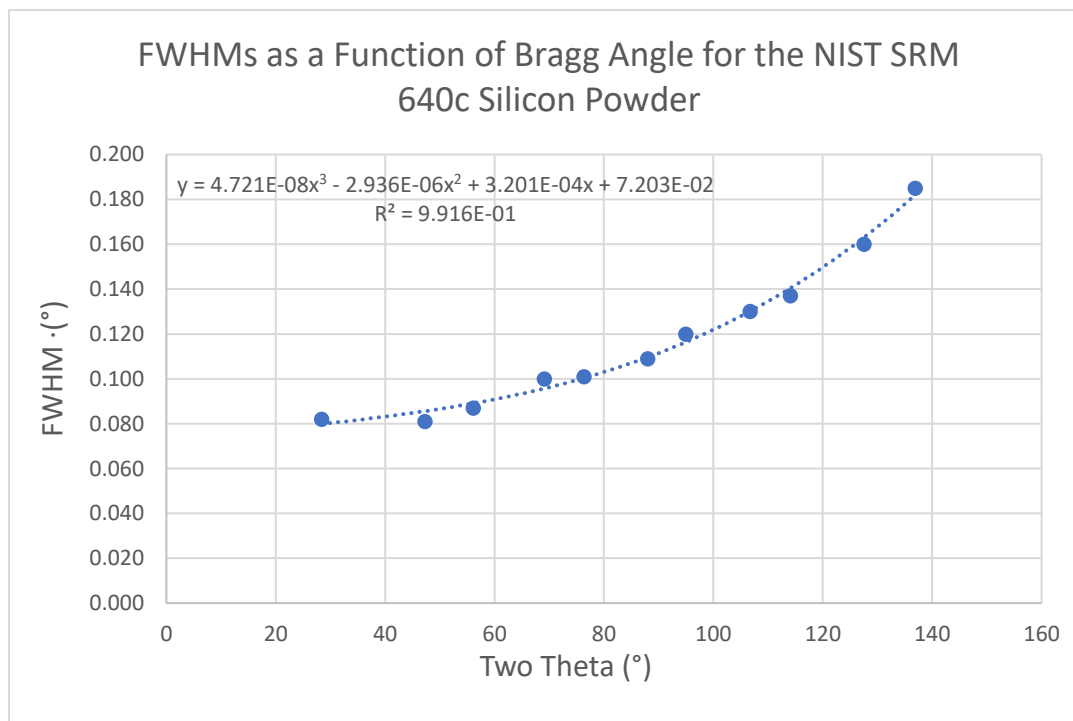


**Figure 29. The FWHMs from Figure 28 as a function of Bragg Angle for the NIST SRM 640c silicon powder. The fitted curve used for instrumental broadening correction is shown.**

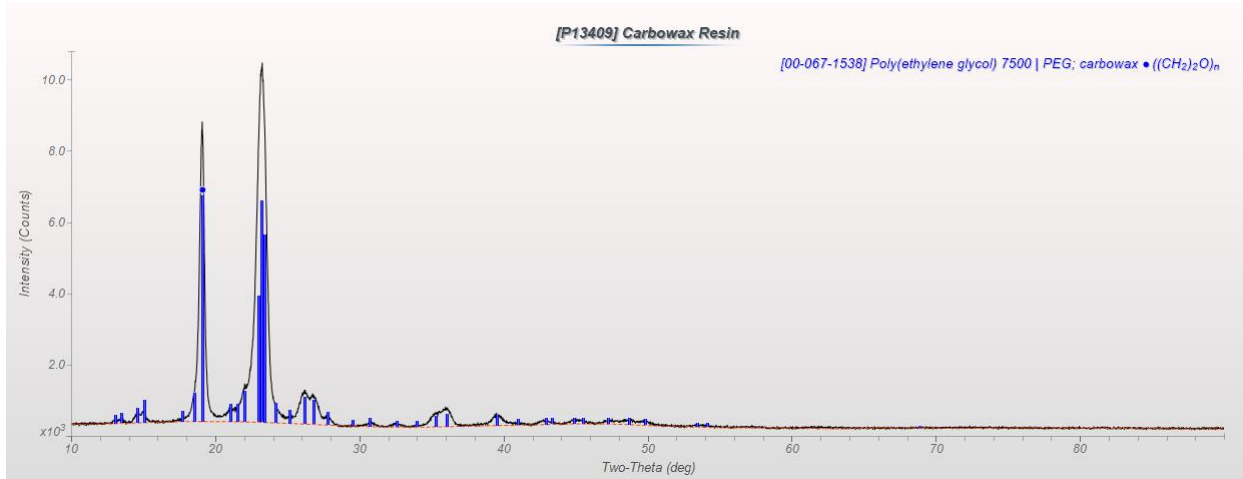


Figure 30. X-ray diffraction pattern of Carbowax resin.

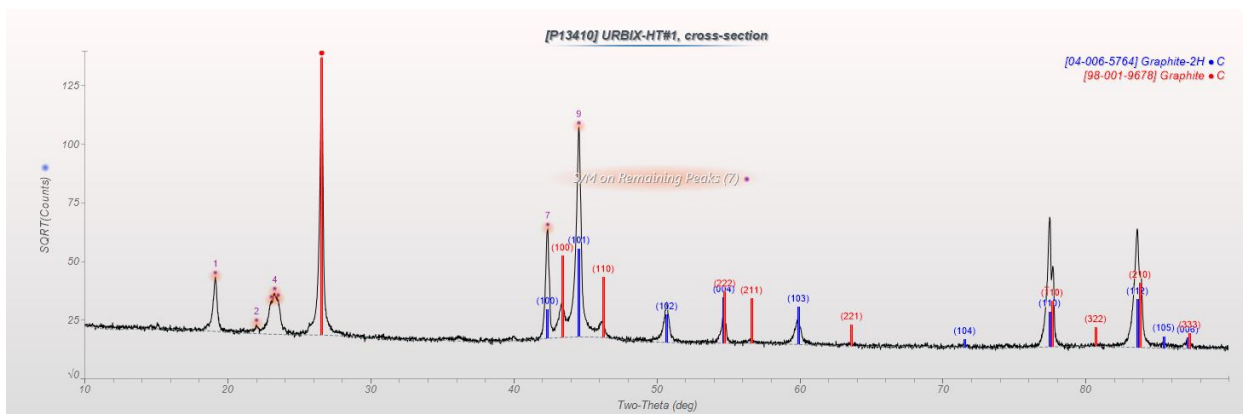


Figure 31. X-ray diffraction pattern of the cross section of the URBIX-HT#1 puck showing the presence of both hexagonal and rhombohedral graphite. Peaks 1–5 originate from the 5 wt% Carbowax resin.

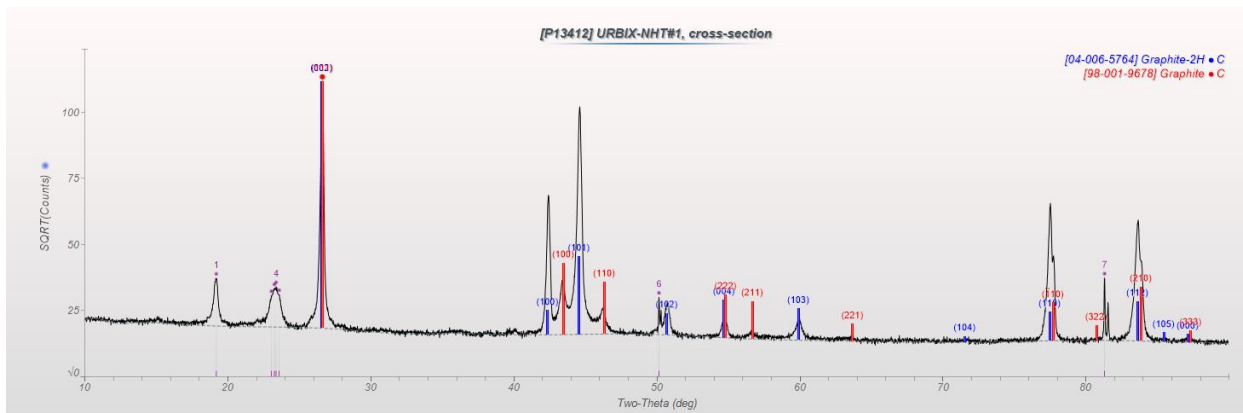
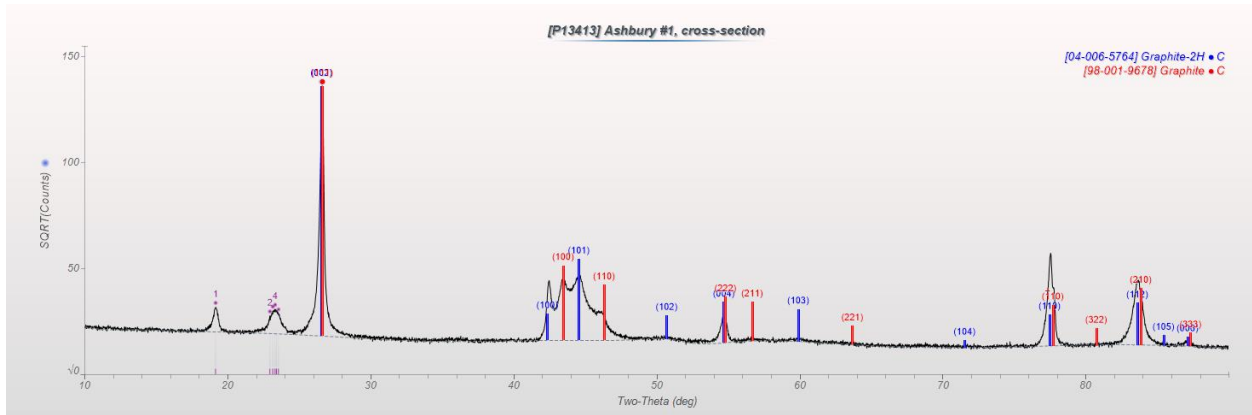
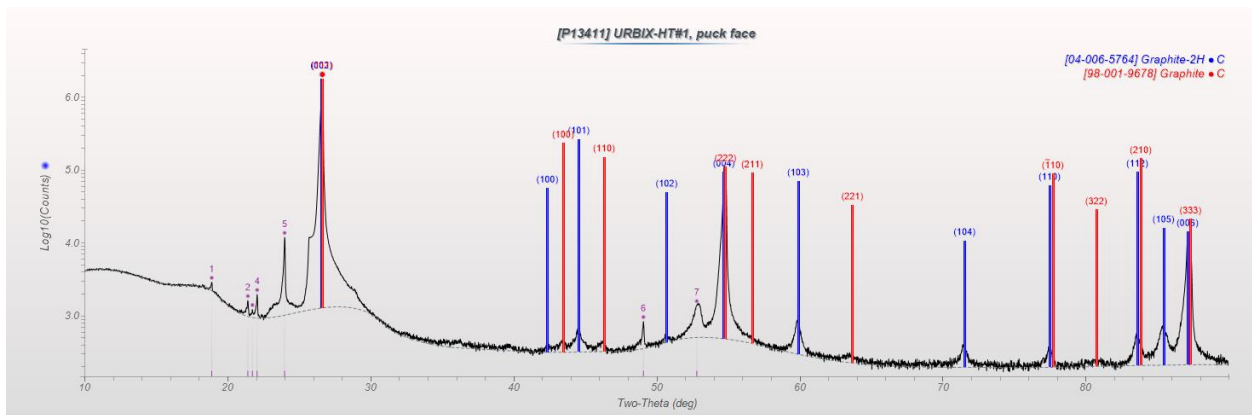


Figure 32. X-ray diffraction pattern of the cross section of the URBIX-NHT#1 puck showing the presence of both hexagonal and rhombohedral graphite. Peaks 1–5 originate from the 5 wt% Carbowax resin. Sharp peaks 6 and 7 likely originate from a contaminant phase from either the cross sectioning process or picked up in the XRD lab.



**Figure 33. X-ray diffraction pattern of the cross section of the Asbury 1 puck showing the presence of both hexagonal and rhombohedral graphite. Peaks 1–5 originate from the 5 wt% Carbowax resin.**



**Figure 34. X-ray diffraction pattern of the puck face of the URBIX-HT#1 puck showing the presence of both hexagonal and rhombohedral graphite. Peaks —5 are the graphite H(002)/R(111) reflection from  $WL\gamma_1$ ,  $WL\beta_2$ ,  $WL\beta_1$ ,  $CuK\beta$ , and  $WL\alpha_2$  radiation, respectively. Peak 6 is the graphite H(004)/R(222) reflection from  $CuK\beta$  radiation. Peak 7 is presumed to originate from the 5 wt% Carbowax resin.**

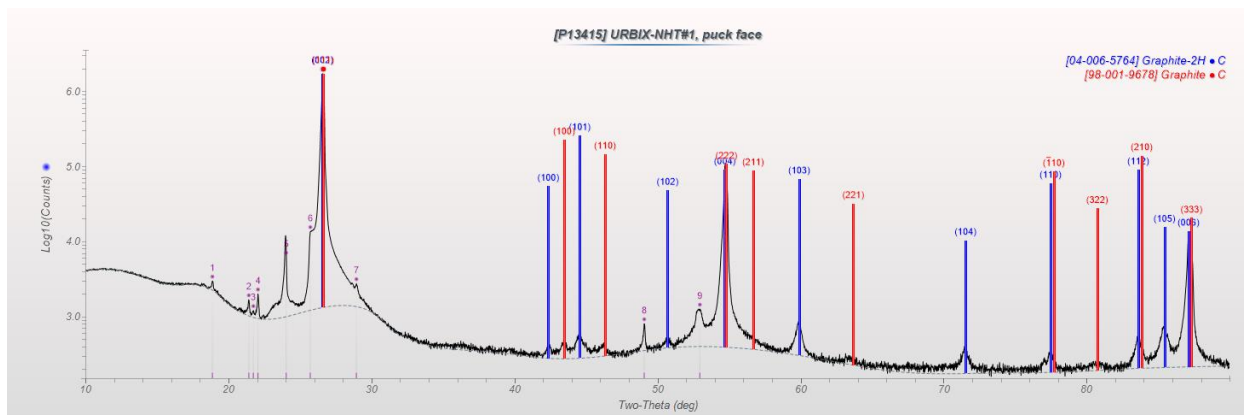


**Figure 35. X-ray diffraction pattern of the puck face of the URBIX-NHT#1 puck showing the presence of both hexagonal and rhombohedral graphite. Peaks 1–5 are the graphite H(002)/R(111) reflection from  $W\text{L}\gamma_1$ ,  $W\text{L}\beta_2$ ,  $W\text{L}\beta_1$ ,  $\text{CuK}\beta$ , and  $W\text{L}\alpha_2$  radiation, respectively. The feature at 6 is due to the absorption edge of the Ni filter. Peak 7 is unidentified. Peak 8 is the graphite H(004)/R(222) reflection from  $\text{CuK}\beta$  radiation. Peak 9 is presumed to originate from the 5 wt% Carbowax resin.**

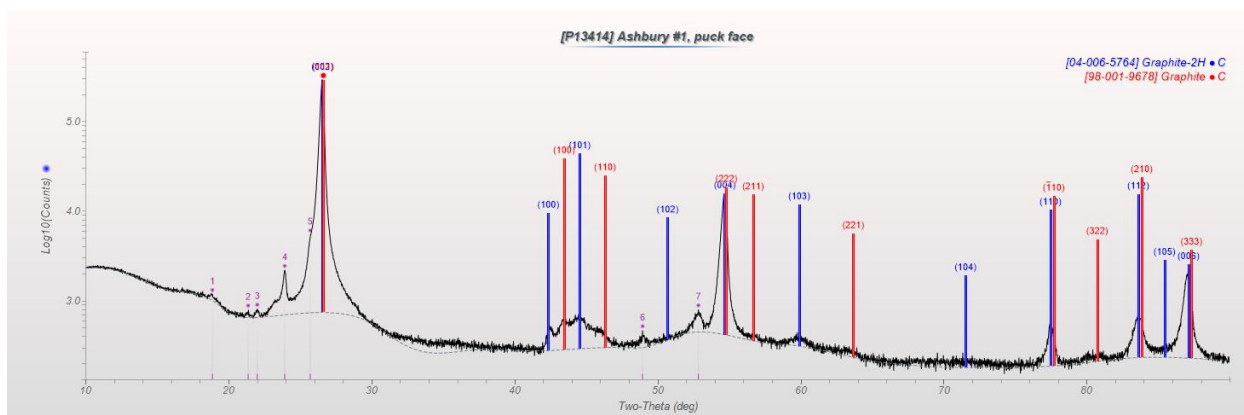


**Figure 36. X-ray diffraction pattern of the puck face of the Asbury 1 puck showing the presence of both hexagonal and rhombohedral graphite. Peaks 1–5 are the graphite H(002)/R(111) reflection from  $W\text{L}\gamma_1$ ,  $W\text{L}\beta_2$ ,  $W\text{L}\beta_1$ ,  $\text{CuK}\beta$ , and  $W\text{L}\alpha_2$  radiation, respectively. Peak 6 is the graphite H(004)/R(222) reflection from  $\text{CuK}\beta$  radiation. Peak 7 is presumed to originate from the 5 wt% Carbowax resin.**

**Table 13. Crystallite sizes for various reflections present in the URBIX-HT#1 sample**

[P13410] URBIX-HT#1, cross-section					[P13411] URBIX-HT#1, puck face				
				Crystallite Size					Crystallite Size
H-Graphite	(h k l)	Rhom-Graphite	(h k l)	nm	H-Graphite	(h k l)	Rhom-Graphite	(h k l)	nm
H-Graph	(002)	R-Graph	(111)	216 (Lc)	H-Graph	(002)	R-Graph	(111)	1114 (Lc)
H-Graph	(100)			230 (La)	H-Graph	(100)			606 (La)
		R-Graph	(100)	65			R-Graph	(100)	24
H-Graph	(101)			114	H-Graph	(101)			45
		R-Graph	(110)	32			R-Graph	(110)	15
H-Graph	(102)			73	H-Graph	(102)			274
H-Graph	(004)	R-Graph	(222)	124	H-Graph	(004)	R-Graph	(222)	1700
H-Graph	(103)			59	H-Graph	(103)			74
							R-Graph	(221)	5
H-Graph	(110)	R-Graph	(-110)	208	H-Graph	(104)			41
H-Graph	(112)	R-Graph	(210)	136	H-Graph	(110)	R-Graph	(-110)	73
					H-Graph	(112)	R-Graph	(210)	88
					H-Graph	(105)			45
					H-Graph	(006)	R-Graph	(333)	508
H-Graph			AVE	145	H-Graph			AVE	415
		R-Graph	AVE	130			R-Graph	AVE	441

##### = >100 nm

**Table 14. Crystallite sizes for various reflections present in the URBIX-NHT#1 sample**

[P13412] URBIX-NHT#1, cross-section					[P13415] URBIX-NHT#1, puck face				
				Crystallite Size					Crystallite Size
H-Graphite	(h k l)	Rhom-Graphite	(h k l)	nm	H-Graphite	(h k l)	Rhom-Graphite	(h k l)	nm
H-Graph	(002)	R-Graph	(111)	146 (Lc)	H-Graph	(002)	R-Graph	(111)	293 (Lc)
H-Graph	(100)			203 (La)	H-Graph	(100)			67 (La)
		R-Graph	(100)	51			R-Graph	(100)	26
H-Graph	(101)			98	H-Graph	(101)			32
		R-Graph	(110)	18			R-Graph	(110)	13
H-Graph	(102)			71	H-Graph	(102)			45
H-Graph	(004)	R-Graph	(222)	99	H-Graph	(004)	R-Graph	(222)	376
H-Graph	(103)			37	H-Graph	(103)			48
							R-Graph	(221)	9
H-Graph	(110)	R-Graph	(-110)	163	H-Graph	(104)			29
					H-Graph	(110)	R-Graph	(-110)	42
							R-Graph	(322)	6
H-Graph	(112)	R-Graph	(210)	120	H-Graph	(112)	R-Graph	(210)	61
					H-Graph	(105)			35
					H-Graph	(006)	R-Graph	(333)	312
H-Graph			AVE	117	H-Graph			AVE	122
		R-Graph	AVE	99.5			R-Graph	AVE	127

##### = >100 nm

**Table 15. Crystallite sizes for various reflections present in the Asbury 1 sample**

[P13413] Asbury #1, cross-section					[P13414] Asbury #1, puck face				
				Crystallite Size					Crystallite Size
H-Graphite	(h k l)	Rhom-Graphite	(h k l)	nm	H-Graphite	(h k l)	Rhom-Graphite	(h k l)	nm
H-Graph	(002)	R-Graph	(111)	104 (Lc)	H-Graph	(002)	R-Graph	(111)	138 (Lc)
H-Graph	(100)			122 L(a)	H-Graph	(100)			85 (La)
		R-Graph	(100)	28			R-Graph	(100)	27
H-Graph	(101)			18	H-Graph	(101)			26
		R-Graph	(110)	12			R-Graph	(110)	6
H-Graph	(004)	R-Graph	(222)	58	H-Graph	(004)	R-Graph	(222)	81
H-Graph	(110)	R-Graph	(-110)	117	H-Graph	(110)	R-Graph	(-110)	71
H-Graph	(112)	R-Graph	(210)	49	H-Graph	(112)	R-Graph	(210)	38
					H-Graph	(006)	R-Graph	(333)	62
H-Graph			AVE	78	H-Graph			AVE	72
		R-Graph	AVE	61			R-Graph	AVE	61

#### =>100 nm





4356 Communications Dr Norcross GA 30093

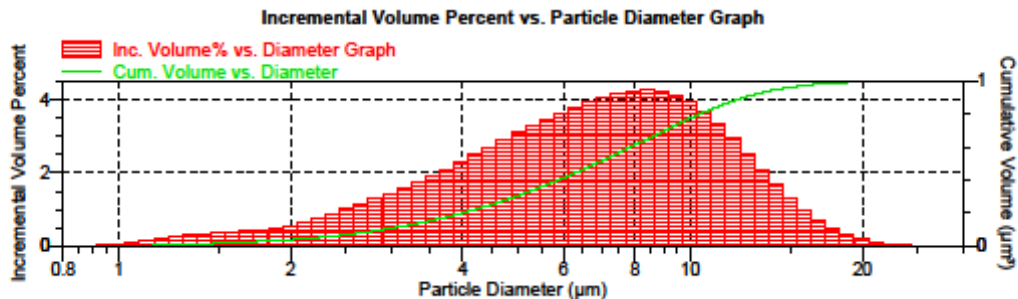
Saturn DigiSizer II 5205 V1.04    Saturn DigiSizer II 5205 V1.04    5200 LSHU V3.00 S/N 208    Page 1

Sample: Ashbury 13371  
 Operator: JG  
 Submitter: MATERIALS CHARACTERIZATION SERVICES  
 File: C:\...\06JUN1903556.SMP

Test Number: 2	Model: (1.800, 1.0000000), 1.331
Analyzed: 6/21/2019 11:41:30AM	Material: Graphite / Water
Reported: 6/21/2019 2:45:21PM	Background: Water RI 1.331
Background: 6/21/2019 11:05:24AM	Smoothing: Medium

Comments: Sample prep: Add 0.5 g of sample to 20 mL of DI water. Add one drop of Nonidet P40. Sonicate for 2 minutes. Samples are run in accordance with ISO 13320. Reference material(s) used for instrument performance verification available upon request. The results on this report reflect only the sample(s) received by Particle Testing Authority. Total pages: 6

### Combined Report



### Summary Report

#### Analysis Conditions

FlowRate: 12.0 l/m	Ultrasonic intensity: Not Used
Circulation time: Not Used	Ultrasonic time: Not Used

#### Sample

Sample Concentration: 0.00633 %  
 Obscuration: 18.1 %

#### Weighted Statistics (Volume Distribution)

Mean	7.309	Std Dev of 2	0.004	Mode	8.408	Std Dev of 2	0.000
Median	6.823		0.001				

#### Selected Percentiles by Volume

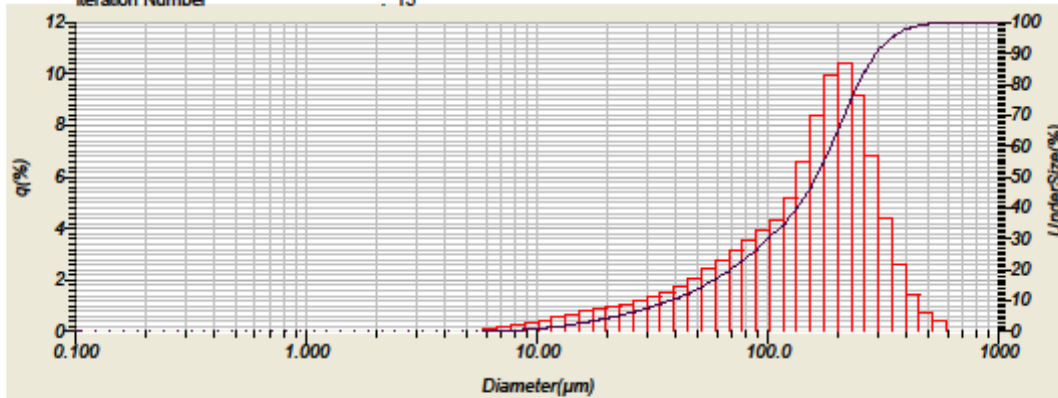
Percent Finer	Diameter (µm)
90.0	12.345
50.0	6.823
10.0	2.892

Figure 39. Particle size distribution results for Ashbury 13371 graphite powder.

**HORIBA** Laser Scattering Particle Distribution Analyzer LA-950

Horiba LA950 for Windows [Wet] Ver6.00

Sample Name	: URBIX-MIL	Median Size	: 162.79437(μm)
ID#	: 201911141108416	Mean Size	: 167.54369(μm)
Material	: URBIX-MIL	Mode Size	: 212.9403(μm)
Circulation Speed	: 15	Diameter on Cumulative %	: (1)10.00 (%) - 38.1938(μm)
Ultra Sonic	: OFF		: (2)50.00 (%) - 162.7944(μm)
Agitation Speed	: OFF		: (3)90.00 (%) - 297.5537(μm)
Transmittance(R)	: 85.4(%)		
Transmittance(B)	: 89.5(%)		
Sample Data Acquisition Times (LD)	: 5000		
Sample Data Acquisition Times (LED)	: 5000		
Refractive Index (R)	: Urbix Graphite - Water[Urbix Graphite( 1.800 - 1.000i),Water( 1.331)]		
Refractive Index (B) <input type="checkbox"/>	: Urbix Graphite - Water[Urbix Graphite( 1.800 - 1.000i),Water( 1.331)]		
Distribution Base	: Volume		
Iteration Number	: 15		



No.	Diameter(μm)	q(%)	UnderSize(%)	No.	Diameter(μm)	q(%)	UnderSize(%)	No.	Diameter(μm)	q(%)	UnderSize(%)	No.	Diameter(μm)	q(%)	UnderSize(%)
1	0.115	0.000	0.000	23	2.269	0.000	0.000	45	44.936	1.777	12.063	67	690.116	0.000	100.000
2	0.131	0.000	0.000	24	2.599	0.000	0.000	46	51.471	2.062	14.144	68	1000.000	0.000	100.000
3	0.150	0.000	0.000	25	2.976	0.000	0.000	47	58.953	2.400	16.544				
4	0.172	0.000	0.000	26	3.409	0.000	0.000	48	67.523	2.787	19.331				
5	0.197	0.000	0.000	27	3.905	0.000	0.000	49	77.339	3.167	22.498				
6	0.226	0.000	0.000	28	4.472	0.000	0.000	50	88.583	3.551	26.048				
7	0.259	0.000	0.000	29	5.122	0.000	0.000	51	101.460	3.919	29.966				
8	0.296	0.000	0.000	30	5.867	0.000	0.000	52	116.210	4.280	34.248				
9	0.339	0.000	0.000	31	6.720	0.126	0.126	53	133.103	5.135	39.383				
10	0.389	0.000	0.000	32	7.697	0.175	0.300	54	152.453	6.580	45.962				
11	0.445	0.000	0.000	33	8.816	0.243	0.543	55	174.616	8.350	54.312				
12	0.510	0.000	0.000	34	10.097	0.330	0.873	56	200.000	9.917	64.230				
13	0.584	0.000	0.000	35	11.565	0.437	1.310	57	229.075	10.355	74.585				
14	0.669	0.000	0.000	36	13.246	0.556	1.866	58	262.376	9.120	83.713				
15	0.766	0.000	0.000	37	15.172	0.679	2.546	59	300.518	6.782	90.495				
16	0.877	0.000	0.000	38	17.377	0.782	3.329	60	344.206	4.400	94.895				
17	1.005	0.000	0.000	39	19.904	0.863	4.192	61	394.244	2.590	97.485				
18	1.151	0.000	0.000	40	22.797	0.946	5.138	62	451.556	1.405	98.890				
19	1.318	0.000	0.000	41	26.111	1.058	6.196	63	517.200	0.714	99.604				
20	1.510	0.000	0.000	42	29.907	1.203	7.399	64	592.367	0.396	100.000				
21	1.729	0.000	0.000	43	34.255	1.363	8.763	65	678.504	0.000	100.000				
22	1.981	0.000	0.000	44	39.234	1.543	10.306	66	777.141	0.000	100.000				

Figure 40. Particle size distribution results for the milled Urbix graphite powder.

Sample: URBIX-NHT TG1/W  
Operator: SX  
Submitter: Materials Characterization Services  
File: C:\win3020\data\2019\06Jun\1903558.SMP

Started: 6/27/2019 9:04:58 AM	Analysis adsorptive: N2
Completed: 6/27/2019 10:41:30 AM	Analysis bath temp.: 77.300 K
Report time: 7/2/2019 3:31:27 PM	Thermal correction: No
Sample mass: 0.6498 g	Ambient free space: 15.3525 cm <sup>3</sup> Measured
Analysis free space: 47.3886 cm <sup>3</sup>	Equilibration interval: 10 s
Low pressure dose: None	Sample density: 1.000 g/cm <sup>3</sup>
Automatic degas: No	

Comments: Sample was under vacuum at 350C for 300 minutes. Total pages: 9  
Analyzed per ISO 9277  
Reference material(s) used for instrument performance verification available upon request

#### Summary Report

##### Surface Area

Single point surface area at  $p/p^0 = 0.100407836$ : 0.8540 m<sup>2</sup>/g

BET Surface Area: 1.0811 m<sup>2</sup>/g

Figure 41. Surface area analysis results for the as-received Urbix graphite powder.

Sample: URBIX-HT BM2/10  
Operator: SX  
Submitter: Materials Characterization Services  
File: C:\TriStar II Plus\data\2019\07\Jul\1903557.SMP

Started: 7/1/2019 4:40:45 PM	Analysis adsorptive: N2
Completed: 7/1/2019 6:17:37 PM	Analysis bath temp.: 77.300 K
Report time: 7/2/2019 3:34:27 PM	Thermal correction: No
Sample mass: 1.0652 g	Ambient free space: 14.5646 cm <sup>3</sup> Measured
Analysis free space: 45.0190 cm <sup>3</sup>	Equilibration interval: 10 s
Low pressure dose: None	Sample density: 1.000 g/cm <sup>3</sup>
Automatic degas: No	

Comments: Sample was under vacuum at 350C for 300 minutes. Total pages: 9  
Analyzed per ISO 9277  
Reference material(s) used for instrument performance verification available upon request

#### Summary Report

##### Surface Area

Single point surface area at  $p/p^0 = 0.100352025$ : 0.8121 m<sup>2</sup>/g

BET Surface Area: 0.9012 m<sup>2</sup>/g

Figure 42. Surface area analysis results for the heat-treated Urbix graphite powder.

Sample: Ashbury 13371 BM1/A  
Operator: SX  
Submitter: Materials Characterization Services  
File: C:\win3020\data\2019\06Jun\1903556.SMP

Started: 6/27/2019 9:04:58 AM	Analysis adsorptive: N2
Completed: 6/27/2019 10:41:30 AM	Analysis bath temp.: 77.300 K
Report time: 7/2/2019 8:22:45 AM	Thermal correction: No
Sample mass: 0.3644 g	Ambient free space: 15.8518 cm <sup>3</sup> Measured
Analysis free space: 48.3328 cm <sup>3</sup>	Equilibration interval: 10 s
Low pressure dose: None	Sample density: 1.000 g/cm <sup>3</sup>
Automatic degas: No	

Comments: Sample was under vacuum at 350C for 300 minutes. Total pages: 9  
Analyzed per ISO 9277  
Reference material(s) used for instrument performance verification available upon request

#### Summary Report

##### Surface Area

Single point surface area at  $p/p^* = 0.200046402$ : 9.9638 m<sup>2</sup>/g

BET Surface Area: 10.3325 m<sup>2</sup>/g

Figure 43. Surface area analysis results for Ashbury 13371 graphite powder.

**Table 16. Results from ultimate compressive strength testing of all graphite matrix compacts**

Sample name	Compressive strength (ksi)	Sample name	Compressive strength (ksi)	Sample name	Compressive strength (ksi)
AGR-COMP-1	6.611	URBIX-COMP-1	2.531	URBIX-COMP-1	2.118
AGR-COMP-2	6.843	URBIX-COMP-2	2.550	URBIX-COMP-2	2.119
AGR-COMP-3	7.288	URBIX-COMP-3	2.731	URBIX-COMP-3	2.251
AGR-COMP-4	6.680	URBIX-COMP-4	2.603	URBIX-COMP-4	2.229
AGR-COMP-5	6.706	URBIX-COMP-5	2.574	URBIX-COMP-5	2.355
AGR-COMP-6	6.674	URBIX-COMP-6	2.587	Average	2.214
AGR-COMP-11	6.940	URBIX-COMP-7	2.536	Standard deviation	0.089
AGR-COMP (Arch)	6.813	URBIX-COMP-8	2.622		
Average	6.819	URBIX-COMP-9	2.503		
Standard deviation	0.204	URBIX-COMP-10	2.577		
		URBIX-COMP (Arch)	2.634		
		Average	2.586		
		Standard deviation	0.059		

Date: 11/14/2019

Quantachrome Instruments  
Quantachrome Ultracycrometer Data Report  
Windows Version 1.12

File Name : UP9b1338.pyc Date : 11/13/2019

Sample Description :  
Comments :  
Operator : A Clark  
Sample ID : URBIX

Cell Size : Large Weight : 2.4859 g  
V added : 8.0378 cc V cell : 9.7574 cc  
Pulse Purge : 20 Target Pressure : 18.0 psi  
Maximum Runs : 25 Analysis Temperature: 25.0 °C  
Equilibration Time : 0 sec. No. Runs Averaged : 3  
Deviation Requested : 0.0000 % Deviation Achieved : ±0.0439 %  
Average Volume : 1.2160 cc Std. Dev. : 0.0012 cc  
Average Density : 2.0444 g/cc Std. Dev. : 0.0020 g/cc  
Coeff. of Variation : 0.0955 %

TABULAR DATA

Run	VOLUME (cc)	DENSITY (g/cc)
1	1.2001	2.0714
2	1.2004	2.0708
3	1.2052	2.0627
4	1.2094	2.0554
5	1.2109	2.0530
6	1.2124	2.0503
7	1.2140	2.0477
8	1.2125	2.0503
9	1.2145	2.0469
10	1.2143	2.0471
11	1.2135	2.0486
12	1.2148	2.0463
13	1.2130	2.0494
14	1.2159	2.0446
15	1.2142	2.0473
16	1.2156	2.0449
17	1.2148	2.0463
18	1.2155	2.0453
19	1.2160	2.0443
20	1.2147	2.0466
21	1.2163	2.0439
22	1.2153	2.0455
23	1.2144	2.0471
24	1.2165	2.0435
25	1.2171	2.0425

Figure 44. Helium pycnometry test results for uniaxially pressed graphite matrix created using Urbix powder.

QUANTACHROME CORPORATION  
Ultrapycnometer 1000 Version 2.2  
Analysis Report

Sample & User Parameters

Sample ID: *AGR*  
Weight: 2.5138 grams  
Analysis Temperature: 25.4 degC

Date: 11-13-19  
Time: 17:34:50  
User ID: 4363

Analysis Parameters

Cell Size: Large  
V added - Large: 8.0378 cc  
V cell: 9.7574 cc  
Target Pressure: 18.0 psi  
Equilibrium Time: Auto  
Vacuum Purge: 15:00 min.  
Maximum Runs: 25  
Number of Runs Averaged: 3

Results

Deviation Requested: 0.000 %  
Average Volume: 1.2229 cc  
Average Density: 2.0556 g/cc  
Coefficient of Variation: 0.1625 %

Deviation Achieved: +/- 0.0764 %  
Std. Dev. : 0.0020 cc  
Std. Dev. : 0.0033 g/cc

Tabular Data

RUN	VOLUME (cc)	DENSITY (g/cc)
1	1.2035	2.0886
2	1.2136	2.0713
3	1.2137	2.0712
4	1.2135	2.0714
5	1.2150	2.0689
6	1.2158	2.0676
7	1.2100	2.0775
8	1.2201	2.0604
9	1.2179	2.0640
10	1.2173	2.0651
11	1.2218	2.0574
12	1.2203	2.0599
13	1.2176	2.0644
14	1.2159	2.0674
15	1.2195	2.0613
16	1.2207	2.0593
17	1.2181	2.0637
18	1.2156	2.0680
19	1.2224	2.0564
20	1.2212	2.0584
21	1.2184	2.0631
22	1.2181	2.0636
23	1.2217	2.0576
24	1.2213	2.0582
25	1.2257	2.0509

Figure 45. Helium pycnometry test results for graphite matrix created using the AGR blend of materials (using Asbury powder).

QUANTACHROME CORPORATION  
Ultrapycnometer 1000 Version 2.2  
Analysis Report

Sample & User Parameters

Sample ID: **URBIX -ISO**  
Weight: 2.5060 grams  
Analysis Temperature: 24.8 degC

Date: 01-16-20  
Time: 14:42:36  
User ID: 4363

Analysis Parameters

Cell Size: Large  
V added - Large: 8.0378 cc  
V cell: 9.7486 cc  
Target Pressure: 18.0 psi  
Equilibrium Time: Auto  
Vacuum Purge: 15:00 min.  
Maximum Runs: 25  
Number of Runs Averaged: 3

Results

Deviation Requested: 0.000 %  
Average Volume: 1.2167 cc  
Average Density: 2.0597 g/cc  
Coefficient of Variation: 0.0567 %

Deviation Achieved: +/- 0.0234 %  
Std. Dev. : 0.0007 cc  
Std. Dev. : 0.0012 g/cc

Tabular Data

RUN	VOLUME (cc)	DENSITY (g/cc)
1	1.2052	2.0793
2	1.2055	2.0788
3	1.2092	2.0725
4	1.2137	2.0647
5	1.2137	2.0647
6	1.2154	2.0618
7	1.2111	2.0692
8	1.2164	2.0601
9	1.2146	2.0632
10	1.2170	2.0592
11	1.2159	2.0610
12	1.2131	2.0657
13	1.2145	2.0634
14	1.2178	2.0577
15	1.2173	2.0586
16	1.2169	2.0593
17	1.2147	2.0630
18	1.2180	2.0575
19	1.2147	2.0631
20	1.2154	2.0619
21	1.2156	2.0614
22	1.2168	2.0595
23	1.2166	2.0597
24	1.2175	2.0583
25	1.2158	2.0611

Figure 46. Helium pycnometry test results for isostatically pressed graphite matrix created using Urbix powder.

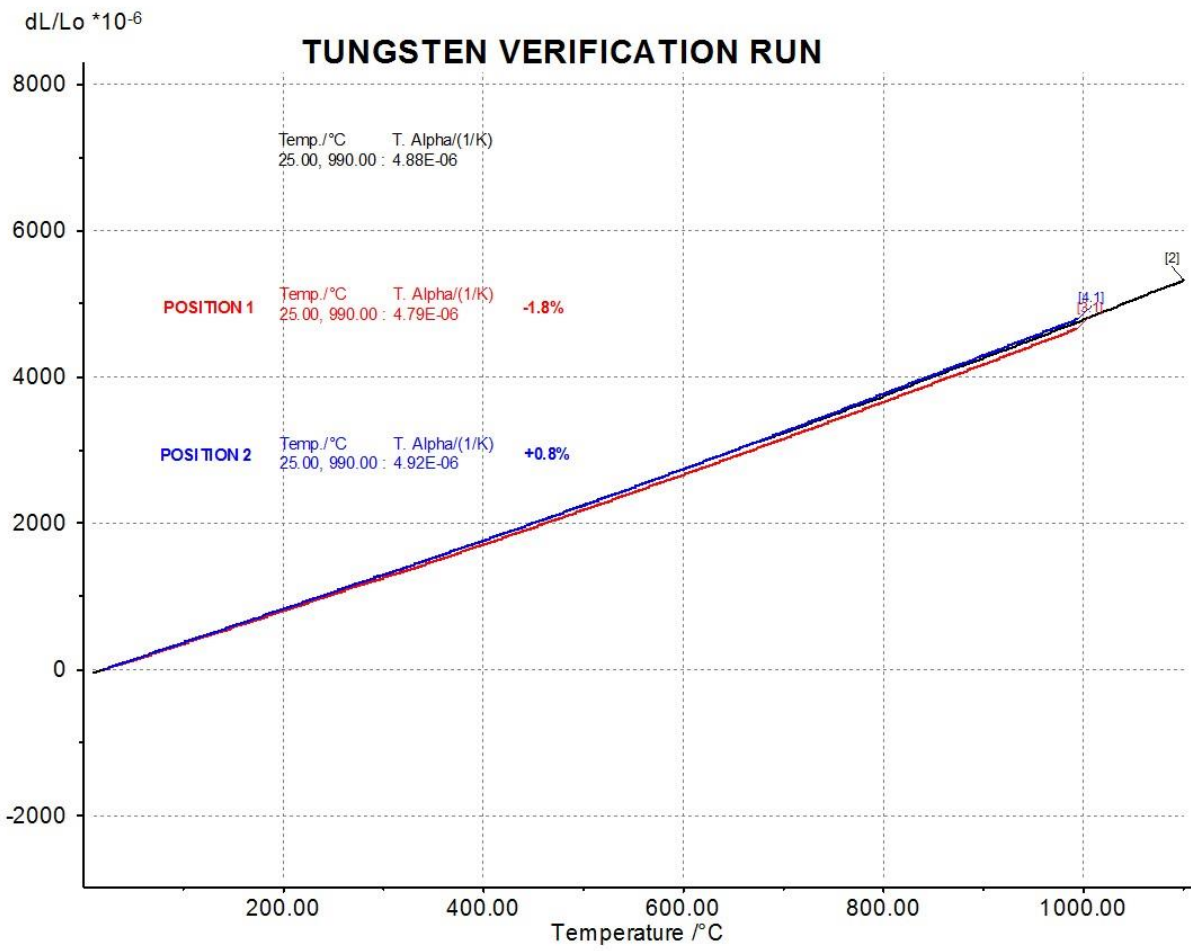


Figure 47. Results from tungsten verification run for coefficient of thermal expansion testing.

**Table 17. Relationship between temperature and mean coefficient of thermal expansion ( $T.\alpha$ ) for the three types of graphite matrix compacts measured at 50 °C increments**

Temperature	Coefficient of thermal expansion ( $1/^\circ\text{C}$ )			
	URBIX-UNI	AGR	URBIX-ISO 1	URBIX-ISO 2
50	4.46E-06	5.43E-06	1.27E-06	1.51E-06
100	4.52E-06	5.52E-06	1.29E-06	1.43E-06
150	4.56E-06	5.61E-06	1.33E-06	1.44E-06
200	4.63E-06	5.70E-06	1.40E-06	1.48E-06
250	4.73E-06	5.81E-06	1.48E-06	1.55E-06
300	4.82E-06	5.89E-06	1.56E-06	1.62E-06
350	4.90E-06	5.96E-06	1.64E-06	1.69E-06
400	5.00E-06	6.04E-06	1.73E-06	1.77E-06
450	5.09E-06	6.12E-06	1.81E-06	1.85E-06
500	5.18E-06	6.21E-06	1.89E-06	1.93E-06
550	5.27E-06	6.29E-06	1.97E-06	2.01E-06
600	5.34E-06	6.36E-06	2.04E-06	2.09E-06
650	5.42E-06	6.43E-06	2.11E-06	2.16E-06
700	5.49E-06	6.49E-06	2.18E-06	2.24E-06
750	5.56E-06	6.55E-06	2.24E-06	2.31E-06
800	5.62E-06	6.61E-06	2.30E-06	2.37E-06
850	5.68E-06	6.66E-06	2.35E-06	2.42E-06
900	5.74E-06	6.71E-06	2.41E-06	2.47E-06
950	5.78E-06	6.75E-06	2.45E-06	2.52E-06

**Table 18. Relationship between temperature and instantaneous coefficient of thermal expansion ( $\alpha$ ) for the three types of graphite matrix compacts measured at 50 °C increments**

Temperature	Coefficient of thermal expansion (1/°C)			
	URBIX-UNI	AGR	URBIX-ISO 1	URBIX-ISO 2
50	4.40E-06	5.45E-06	1.45E-06	1.38E-06
100	4.78E-06	5.80E-06	1.40E-06	1.38E-06
150	4.72E-06	5.96E-06	1.49E-06	1.48E-06
200	5.07E-06	6.06E-06	1.70E-06	1.79E-06
250	5.18E-06	6.42E-06	2.05E-06	2.01E-06
300	5.11E-06	6.04E-06	2.06E-06	1.86E-06
350	5.52E-06	6.23E-06	2.37E-06	2.16E-06
400	5.56E-06	6.46E-06	2.16E-06	2.34E-06
450	5.76E-06	6.87E-06	2.43E-06	2.44E-06
500	6.08E-06	6.91E-06	2.46E-06	2.55E-06
550	6.14E-06	6.98E-06	2.79E-06	2.91E-06
600	6.26E-06	7.06E-06	2.73E-06	3.06E-06
650	6.15E-06	7.26E-06	3.03E-06	3.13E-06
700	6.36E-06	7.22E-06	2.81E-06	3.28E-06
750	6.30E-06	7.31E-06	2.97E-06	3.24E-06
800	6.83E-06	7.53E-06	3.18E-06	3.30E-06
850	6.57E-06	7.39E-06	3.56E-06	3.36E-06
900	6.68E-06	7.68E-06	3.24E-06	3.27E-06
950	6.70E-06	7.50E-06	3.28E-06	3.27E-06

**Table 19. Specific heat capacity for all of the graphite compact samples at 50 °C increments up to 950 °C; measurements taken within 0.1 °C of the stated temperature**

	URBIX-UNI 1-1	URBIX-UNI 1-2	URBIX-UNI 2-1	URBIX-UNI 2-2	URBIX-ISO 1	URBIX-ISO 2	AGR 1-1	AGR 1-2	AGR 2-1	AGR 2-2
Temp	Heat Capacity (J/(g*K))									
50	#N/A	#N/A	#N/A	#N/A	0.779	0.77739	#N/A	#N/A	#N/A	#N/A
100	0.92219	0.92480	0.93781	0.88543	0.90901	0.90398	0.92688	0.93455	0.92873	0.91336
150	1.04376	1.05200	1.05956	1.00250	1.02927	1.02240	1.04960	1.06082	1.05407	1.03796
200	1.14612	1.15686	1.16254	1.10381	1.13969	1.13054	1.15595	1.17025	1.16515	1.14661
250	1.23301	1.24337	1.25179	1.18840	1.23832	1.22908	1.25908	1.25522	1.25149	1.23907
300	1.32902	1.34218	1.34947	1.28406	1.32081	1.31226	1.34714	1.35056	1.34992	1.33921
350	1.40456	1.41481	1.42562	1.36442	1.39813	1.38764	1.42214	1.42481	1.42540	1.41953
400	1.47487	1.48159	1.49529	1.43657	1.45837	1.44603	1.49363	1.49158	1.49441	1.49470
450	1.53750	1.54246	1.56278	1.50499	1.51276	1.50227	1.55896	1.55439	1.55832	1.56197
500	1.59158	1.59761	1.61970	1.56197	1.56396	1.54848	1.61735	1.60408	1.61031	1.61836
550	1.64378	1.65059	1.67473	1.62444	1.60590	1.58801	1.67265	1.64853	1.66107	1.67375
600	1.69125	1.69354	1.72262	1.68303	1.63869	1.61997	1.72218	1.68688	1.69770	1.72036
650	1.74262	1.75092	1.76737	1.74148	1.66395	1.63549	1.77092	1.73390	1.75278	1.78546
700	1.76672	1.76946	1.81443	1.79246	1.70132	1.66014	1.81344	1.76197	1.78919	1.80209
750	1.78834	1.79469	1.84376	1.83774	1.73534	1.66692	1.85027	1.79808	1.81839	1.81934
800	1.85573	1.85593	1.89147	1.91029	1.73970	1.64592	1.91171	1.84048	1.86748	1.90473
850	1.87969	1.87627	1.93115	1.96598	1.83009	1.74024	1.95673	1.86709	1.88720	1.93581
900	1.91718	1.90351	1.93528	2.01861	1.72673	1.70598	1.96680	1.88722	1.91907	1.98150
950	1.96424	1.91874	2.02347	2.08866	1.69204	1.67104	2.00916	1.93434	1.92413	2.03820

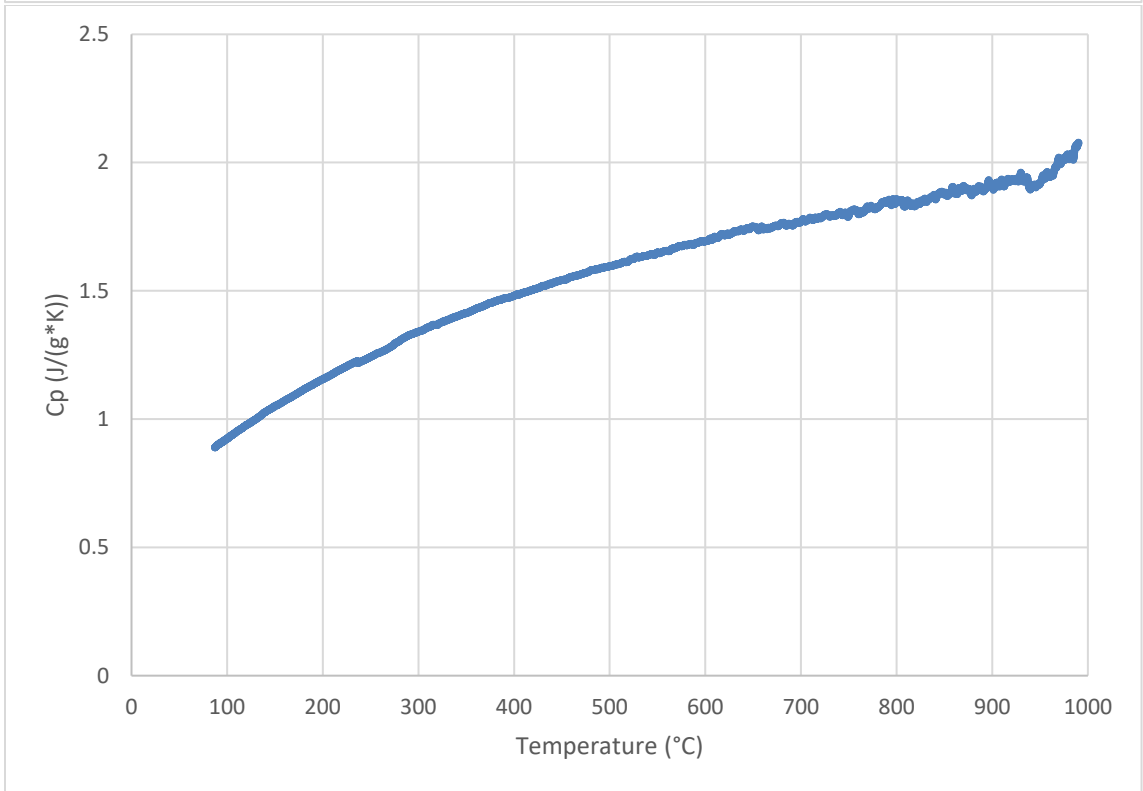
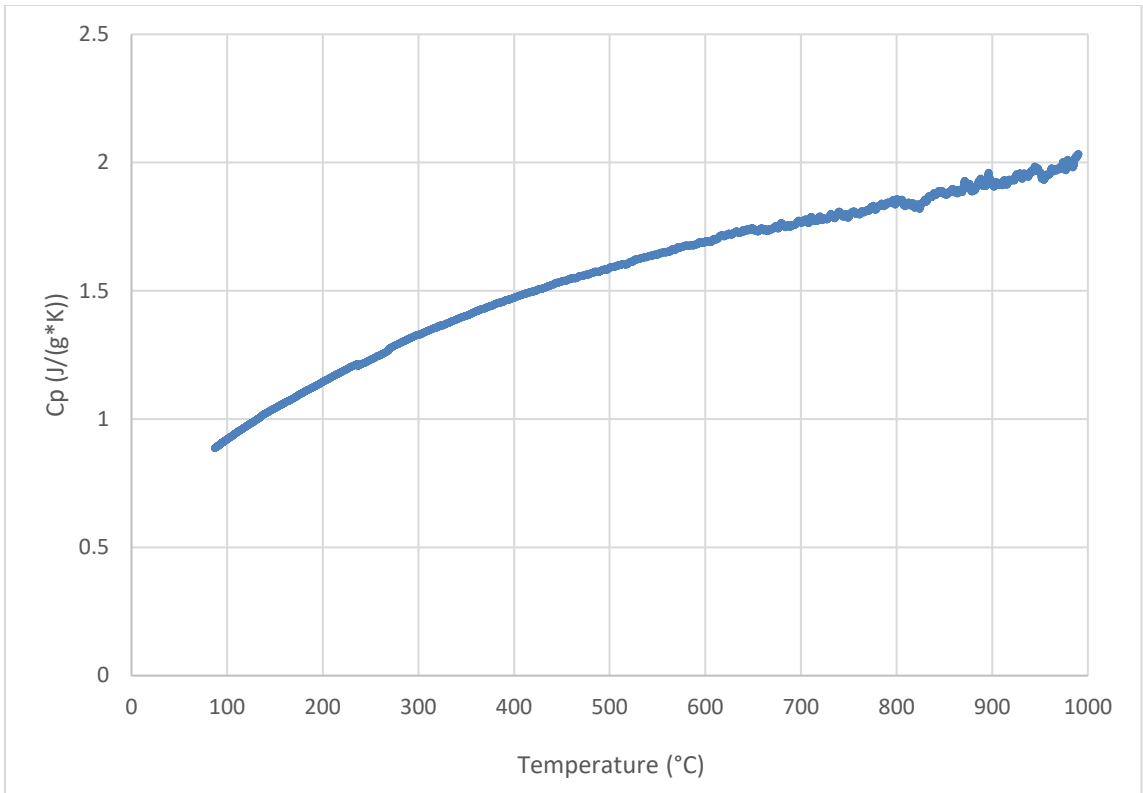


**Figure 48. Plots from Runs 1 (top) and 2 (bottom) of Sample 1, a uniaxially pressed Urbix matrix compact, showing the relationship between temperature and specific heat capacity.**

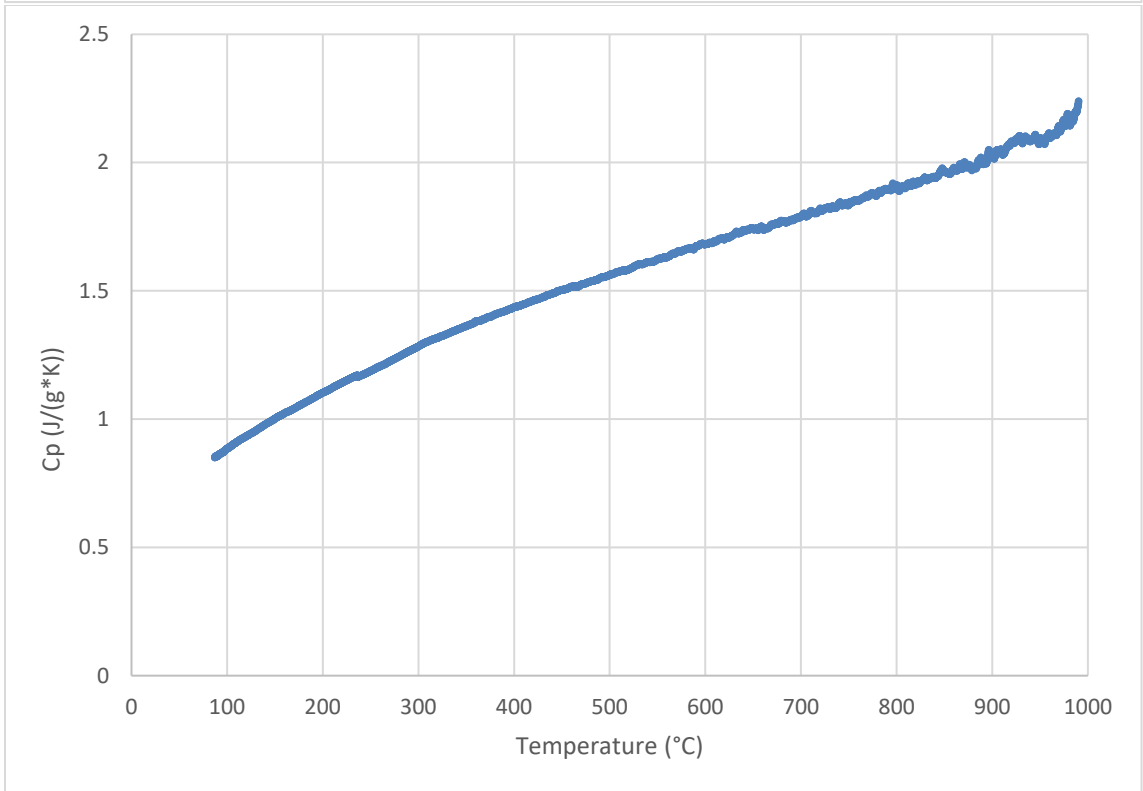
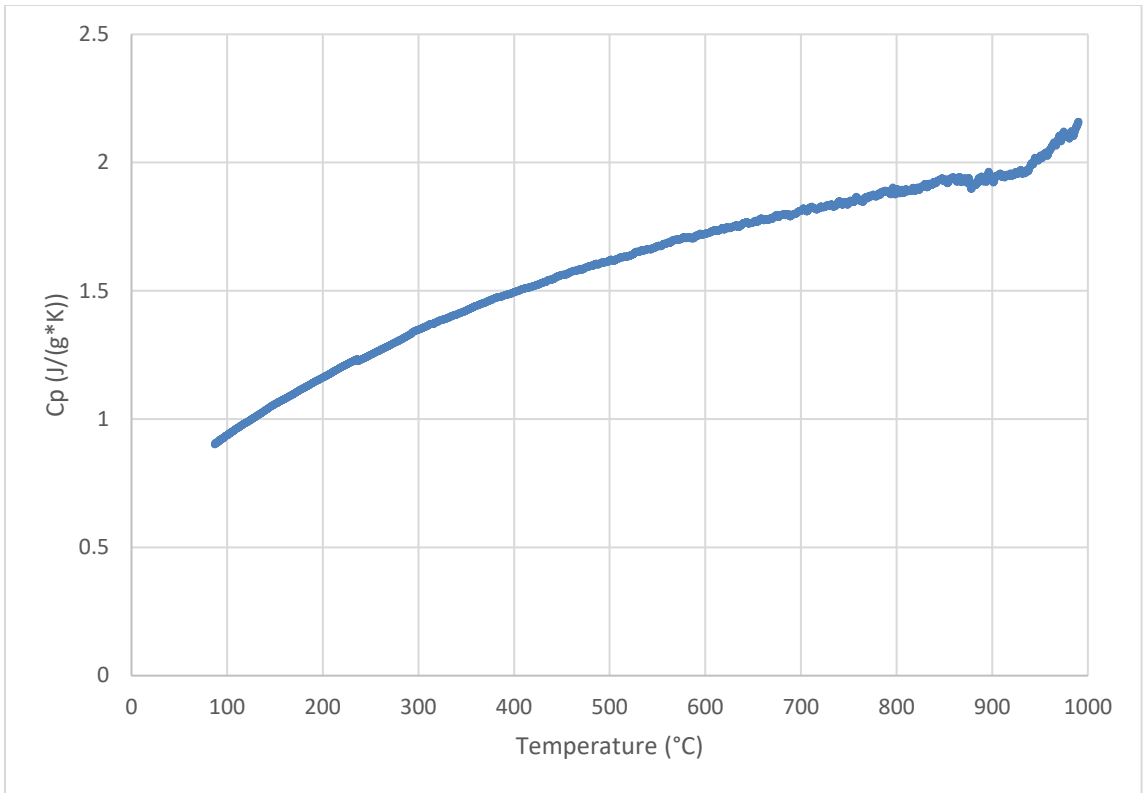


**Figure 49. Plots from Runs 1 (top) and 2 (bottom) of Sample 2, a uniaxially pressed Urbix matrix compact, showing the relationship between temperature and specific heat capacity.**

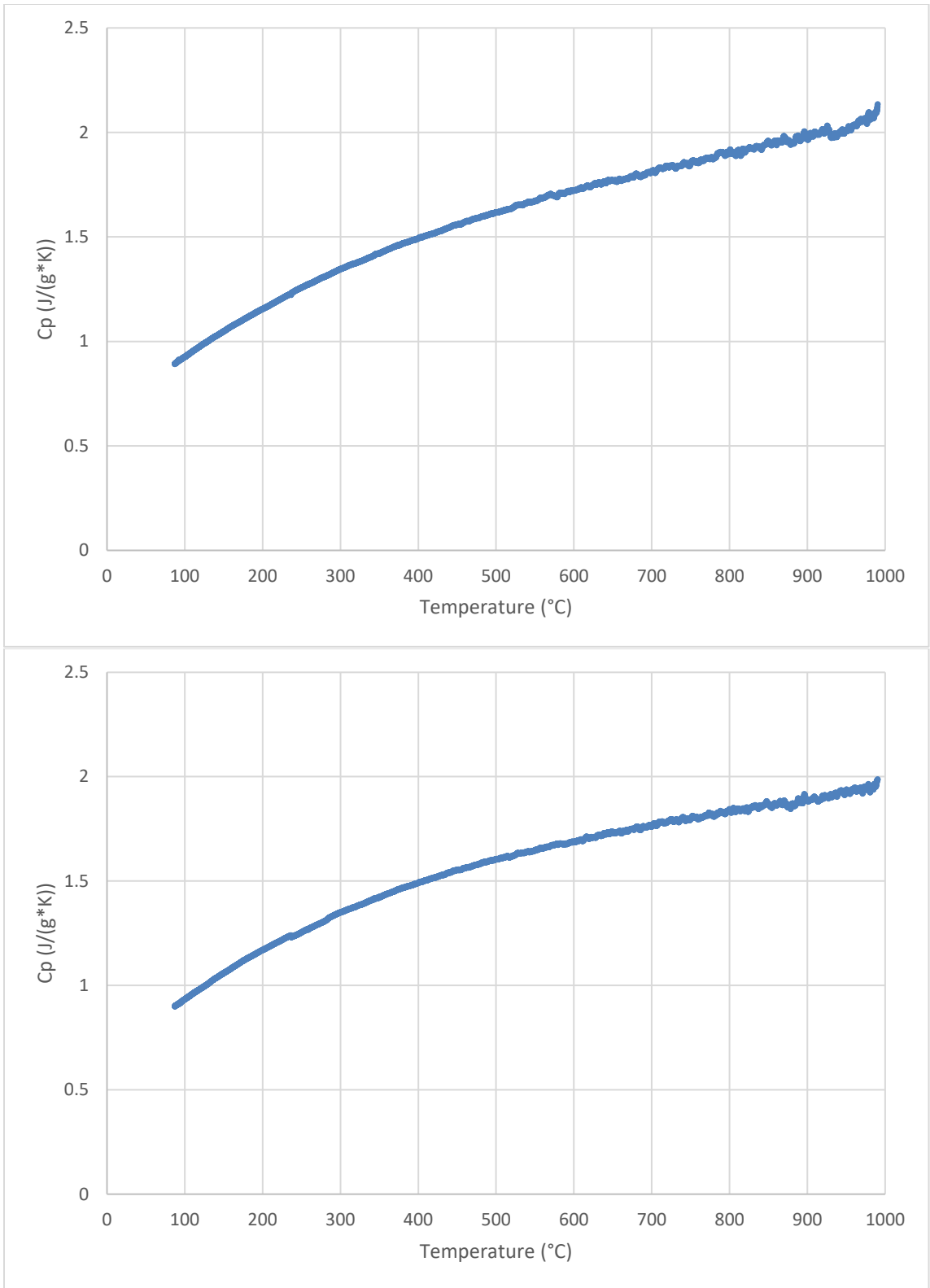


**Figure 50. Plots from Runs 1 (top) and 2 (bottom) of Sample 1, a compact made using the AGR blend of materials for graphite matrix, showing the relationship between temperature and specific heat capacity.**

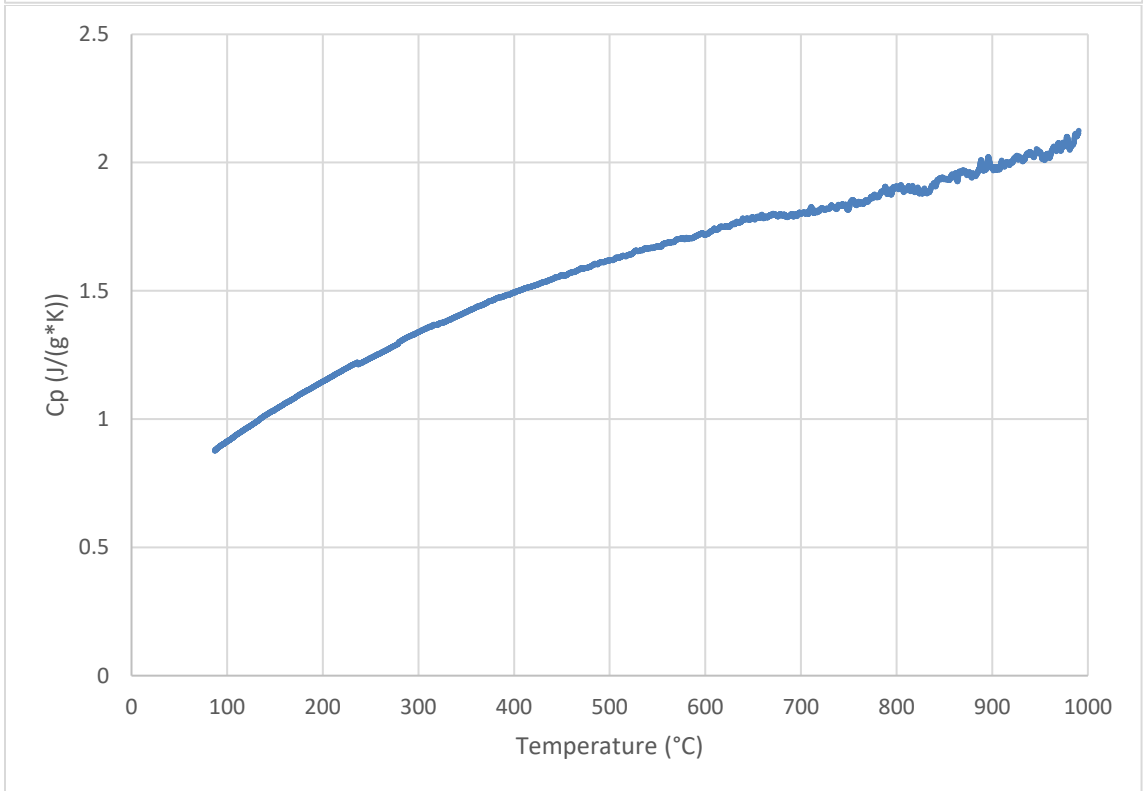
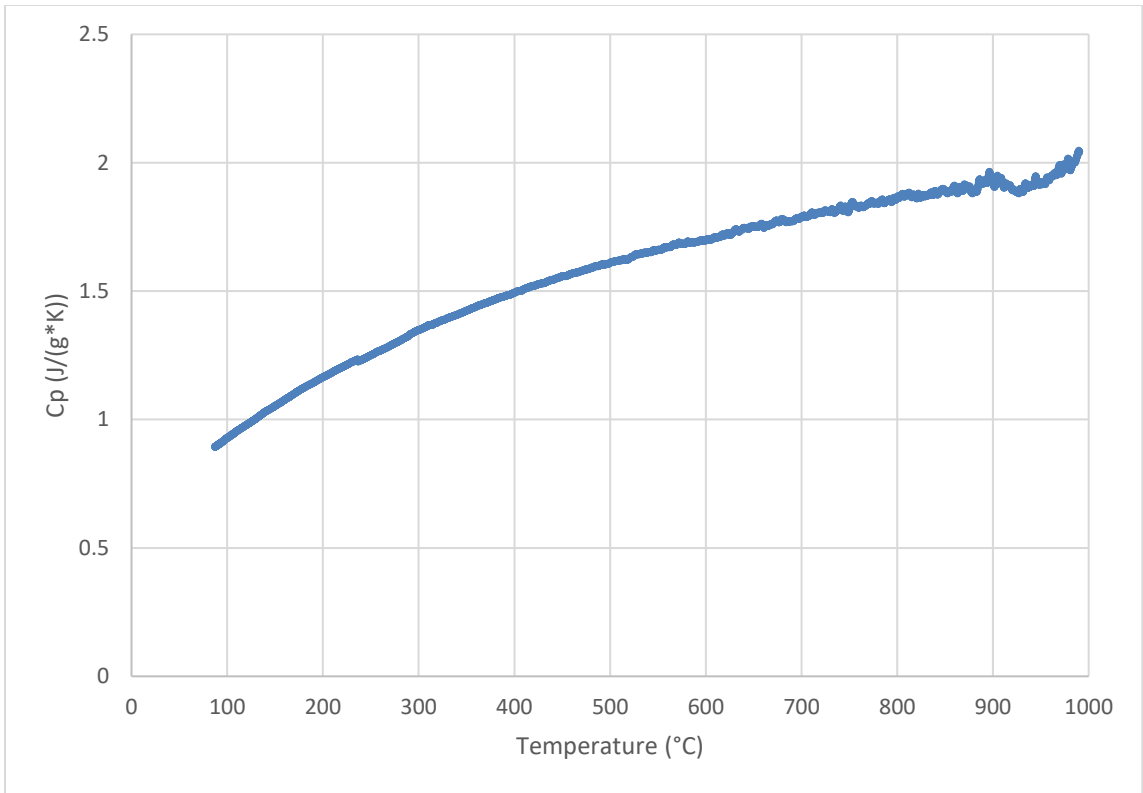


**Figure 51. Plots from Runs 1 (top) and 2 (bottom) of Sample 2 for a compact made using the AGR blend of materials for graphite matrix showing the relationship between temperature and specific heat capacity.**

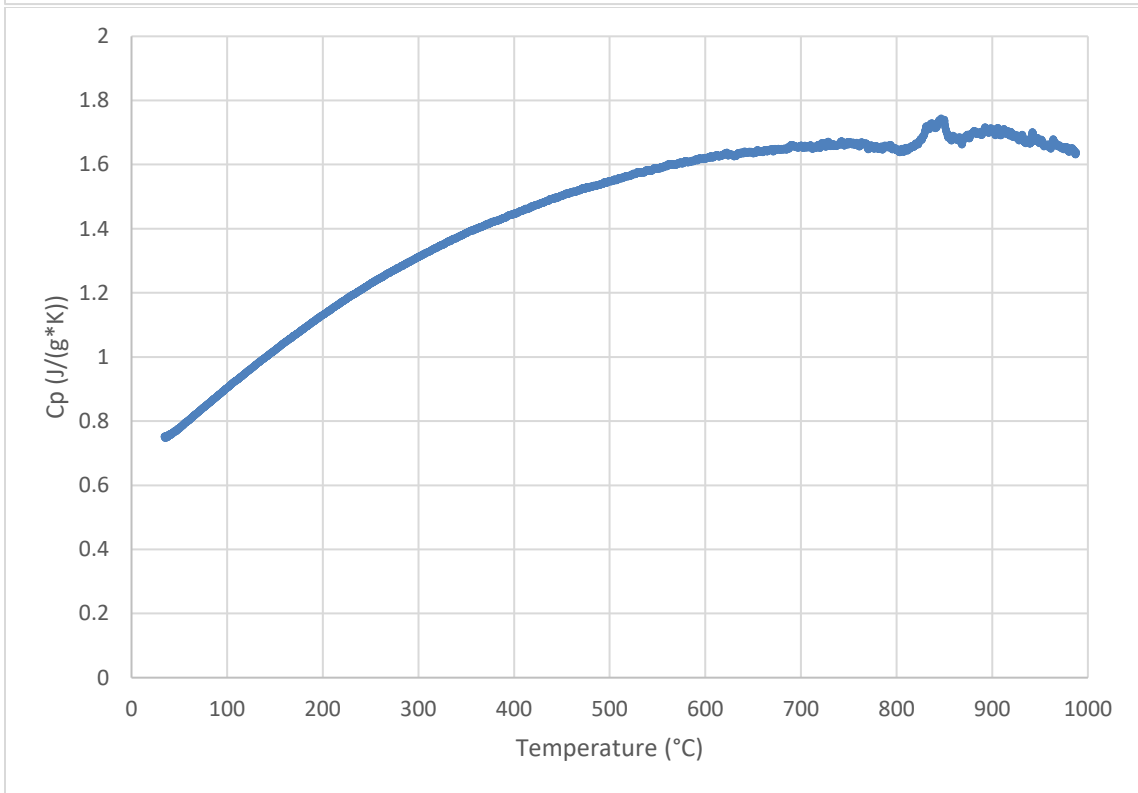
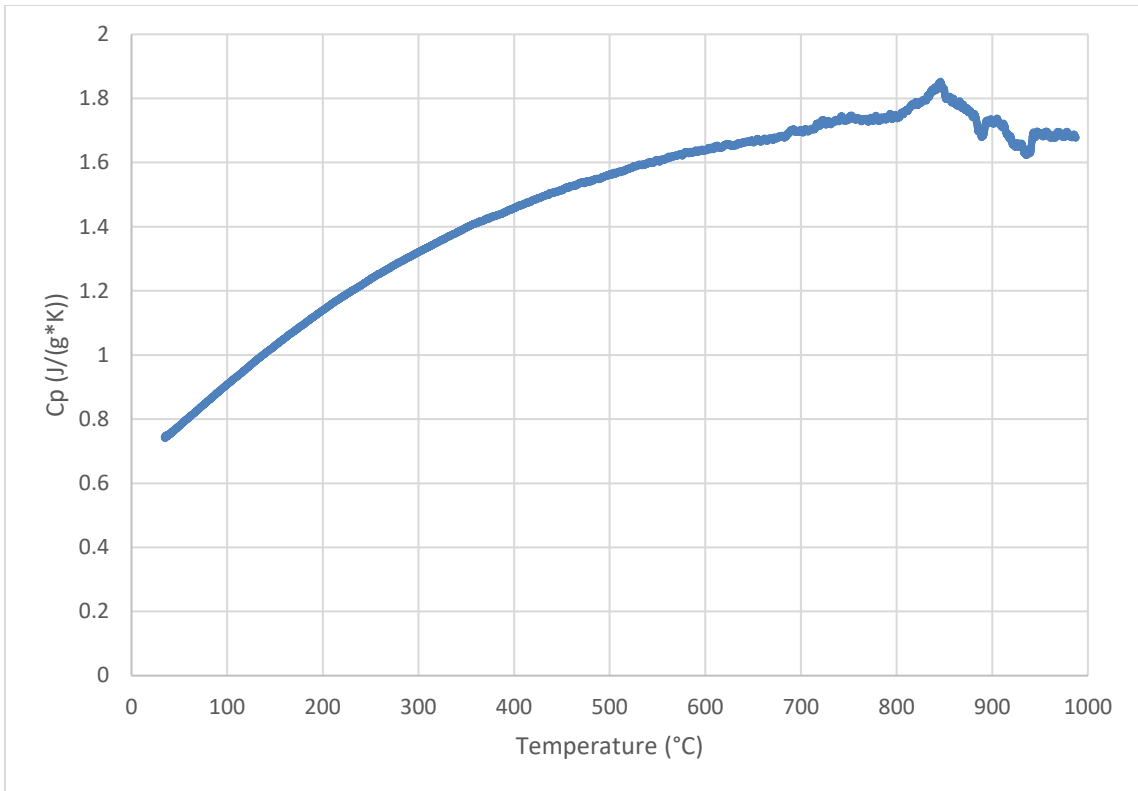


**Figure 52. Plots from Samples 1 (top) and 2 (bottom) for an isostatically pressed Urbix matrix compact showing the relationship between temperature and specific heat capacity.**

**Table 20. Thermal diffusivity results for three uniaxially pressed Urbix matrix specimens; thermal diffusivity was measured three times at each given temperature for each specimen, and temperature and diffusivity results shown are averages of those three readings**

URBIX-UNI Sample #1				URBIX-UNI Sample #2			
Temp. (°C)	Standard deviation	Diffusivity (mm <sup>2</sup> /s)	Standard deviation	Temp. (°C)	Standard deviation	Diffusivity (mm <sup>2</sup> /s)	Standard deviation
25	0	34.479	0.172	27.1	0.1	35.034	0.228
96.4	1.2	25.115	0.144	97	1.2	25.818	0.134
200.4	0.1	17.519	0.061	200.4	0.1	18.081	0.111
300.6	0.2	13.459	0.02	300.7	0.2	13.924	0.01
400.6	0.2	10.982	0.025	400.4	0.1	11.407	0.041
500.5	0.1	9.316	0.026	500.4	0.1	9.676	0.027
600.4	0.1	8.133	0.004	600.3	0.1	8.417	0.015
700.3	0.1	7.306	0.003	700.2	0	7.584	0.014
800.2	0.1	6.628	0.028	800.1	0	6.929	0.008
900.2	0.1	5.767	0.02	900.1	0	6.123	0.017
950.2	0.1	5.407	0.017	950.1	0	5.802	0.038
600	0	5.948	0.002	599.9	0	6.66	0.007
299.3	0.3	8.597	0.019	299.1	0.4	9.959	0.041
98.1	1.4	14.054	0.071				

URBIX-UNI Sample #3			
Temp. (°C)	Standard deviation	Diffusivity (mm <sup>2</sup> /s)	Standard deviation
26.5	0.1	35.825	0.193
100.1	0.1	26.071	0.046
200.3	0.1	18.477	0.035
300.5	0.2	14.226	0.033
400.5	0.2	11.638	0.018
500.4	0.1	9.97	0.043
600.3	0.1	8.761	0.007
700.2	0.1	7.906	0.024
800.2	0.1	7.105	0.018
900.1	0.1	6.006	0.046
950.1	0.1	5.658	0.028
600.1	0	6.191	0.015
300	0	8.668	0.008

**Table 21. Thermal diffusivity results for three uniaxially pressed AGR matrix specimens; thermal diffusivity was measured three times at each given temperature for each specimen, and temperature and diffusivity results shown are averages of those three readings**

AGR Sample #1				AGR Sample #2			
Temp. (°C)	Standard deviation	Diffusivity (mm <sup>2</sup> /s)	Standard deviation	Temp. (°C)	Standard deviation	Diffusivity (mm <sup>2</sup> /s)	Standard deviation
25.4	0.3	23.796	0.118	24.9	0	28.249	0.148
103.2	2.9	18.111	0.144	100	0.2	21.513	0.03
202.4	0.9	13.645	0.03	200.2	0.1	16.129	0.053
302	0.4	10.922	0.027	300.4	0.2	12.875	0.021
401.1	0.2	9.187	0.026	400.4	0.2	10.811	0.024
500.7	0.2	7.887	0.026	500.3	0.1	9.39	0.019
600.5	0.1	7.029	0.017	600.3	0.1	8.403	0.014
700.3	0	6.456	0.007	700.2	0.1	7.637	0.019
800.3	0	6.164	0.027	800.1	0.1	6.949	0.025
900.2	0	6.294	0.034	900.1	0.1	6.38	0.025
950.2	0	6.168	0.043	950.1	0.1	6.49	0.01
599.4	0.2	7.302	0.014	600	0	7.091	0.019
297.4	0.6	10.578	0.005	300	0.1	9.966	0.024
95.5	2.7	17.148	0.135	100.3	0.1	15.329	0.015

AGR Sample #3			
Temp. (°C)	Standard deviation	Diffusivity (mm <sup>2</sup> /s)	Standard deviation
26.7	0.3	25.796	0.16
100.2	3.2	19.868	0.231
202.3	0.9	14.876	0.088
302	0.5	11.922	0.028
401.1	0.3	10.034	0.037
500.8	0.2	8.685	0.023
600.5	0.1	7.728	0.003
700.4	0.1	7.061	0.016
800.3	0.1	6.704	0.022
900.3	0	6.558	0.008
950.2	0	6.374	0.031
599.4	0.2	8.096	0.003
297.5	0.5	12.029	0.047
98.1	1.1	19.663	0.167

**Table 22. Thermal diffusivity results for two isostatically pressed Urbix matrix specimens; thermal diffusivity was measured three times at each given temperature for each specimen, and temperature and diffusivity results shown are averages of those three readings**

URBIX-ISO Sample #1				URBIX-ISO Sample #2			
Temp. (°C)	Standard deviation	Diffusivity (mm <sup>2</sup> /s)	Standard deviation	Temp. (°C)	Standard deviation	Diffusivity (mm <sup>2</sup> /s)	Standard deviation
100	3.2	49.356	0.66	97.5	1.1	48.423	0.167
202.4	0.9	34.603	0.088	200.5	0.1	33.83	0.071
302.1	0.5	26.654	0.147	300.8	0.2	25.936	0.061
401.3	0.4	21.838	0.013	400.5	0.1	21.21	0.053
500.9	0.3	18.506	0.05	500.5	0.1	17.896	0.028
600.6	0.1	16.267	0.034	600.4	0.1	15.579	0.035
700.4	0.1	14.661	0.023	700.3	0.1	13.958	0.021
800.3	0.1	13.45	0.018	800.2	0.1	12.785	0.021
900.3	0	12.424	0.034	900.2	0.1	11.769	0.045
950.2	0	11.838	0.037	950.2	0.1	11.179	0.064
599.4	0.2	15.213	0.01	599.9	0.1	14.374	0.014
297.8	0.4	24.157	0.04	299.2	0.3	23.16	0.043

**Table 23. Values used to calculate thermal conductivity for each type of graphite matrix used in this study (Diffusivity was measured on the average temperature shown; values for heat capacity and CTE were measured to the nearest temperature reading (typically within 0.1 °C of the temperature listed.))**

<b>AGR</b>					
<b>TEMPERATURE (°C)</b>	<b>Diffusivity (mm<sup>2</sup>/s)</b>	<b>Specific Heat (J/(g*K))</b>	<b>CTE (1/K)</b>	<b>Density (g/cm<sup>3</sup>)</b>	<b>Thermal Conductivity (W/(m*K))</b>
25.7	25.947	#N/A	5.40E-06	1.591	#N/A
101.1	19.831	0.92777	5.52E-06	1.589	29.235
201.6	14.883	1.16251	5.71E-06	1.586	27.444
301.5	11.906	1.34830	5.89E-06	1.583	25.416
400.9	10.011	1.49453	6.04E-06	1.580	23.642
500.6	8.654	1.61375	6.21E-06	1.577	22.023
600.4	7.720	1.70746	6.36E-06	1.574	20.743
700.3	7.051	1.79174	6.49E-06	1.570	19.839
800.2	6.606	1.88176	6.61E-06	1.567	19.476
900.2	6.411	1.93916	6.71E-06	1.563	19.434
950.2	6.344	1.97992	6.75E-06	1.562	19.614

<b>URBIX-UNI</b>					
<b>TEMPERATURE (°C)</b>	<b>Diffusivity (mm<sup>2</sup>/s)</b>	<b>Specific Heat (J/(g*K))</b>	<b>CTE (1/K)</b>	<b>Density (g/cm<sup>3</sup>)</b>	<b>Thermal Conductivity (W/(m*K))</b>
26.2	35.113	#N/A	4.54E-06	1.577	#N/A
97.8	25.668	0.91246	4.51E-06	1.575	36.899
200.4	18.026	1.14290	4.63E-06	1.573	32.410
300.6	13.870	1.32717	4.82E-06	1.571	28.913
400.5	11.342	1.47285	5.00E-06	1.568	26.197
500.4	9.654	1.59397	5.18E-06	1.565	24.089
600.3	8.437	1.69761	5.34E-06	1.563	22.380
700.2	7.599	1.78513	5.49E-06	1.560	21.155
800.2	6.887	1.87882	5.62E-06	1.557	20.142
900.1	5.965	1.94374	5.74E-06	1.553	18.013
950.1	5.622	1.99660	5.78E-06	1.552	17.422

<b>URBIX-ISO</b>					
<b>TEMPERATURE (°C)</b>	<b>Diffusivity (mm<sup>2</sup>/s)</b>	<b>Specific Heat (J/(g*K))</b>	<b>CTE (1/K)</b>	<b>Density (g/cm<sup>3</sup>)</b>	<b>Thermal Conductivity (W/(m*K))</b>
98.8	48.8895	0.90305	1.36E-06	1.539	67.926
201.5	34.2165	1.13878	1.44E-06	1.538	59.921
301.5	26.295	1.31933	1.59E-06	1.537	53.320
400.9	21.524	1.45442	1.75E-06	1.536	48.083
500.7	18.201	1.55787	1.91E-06	1.535	43.519
600.5	15.923	1.62944	2.06E-06	1.534	39.788
700.4	14.3095	1.68144	2.21E-06	1.532	36.864
800.3	13.1175	1.69269	2.33E-06	1.531	33.987
900.3	12.0965	1.71418	2.44E-06	1.529	31.708
950.2	11.5085	1.68124	2.48E-06	1.528	29.573